Control over translocation across the lipid bilayer via an engineered channel protein

Mukherjee, Nobina

CONTROL OVER TRANSLOCATION ACROSS THE LIPID BILAYER VIA AN ENGINEERED CHANNEL PROTEIN

Nobina Mukherjee

Cover Front: MscL in the bilayer membrane. MscL is activated by trigger interacting directly with the protein pore.

Cover Back: MscL is activated by trigger, upon it's interaction with the surrounding bilayer membrane.

Cover Design: Randy Wind (randywind@live.nl)

This Ph.D. study was carried out in the Biochemistry Department of the Groningen Biomolecular Sciences and Biotechnology Institute (GBB). The research was financially supported by the European Research Council (ERC), FP6-MediTrans, FP7-BISNES.

The research was carried out according to the requirements of the Graduate School of Science, Faculty of Mathematics and Natural Sciences, University of Groningen, The Netherlands.

Printing of this thesis is financially supported by the University Library, GBB and the Graduate School of Science, Faculty of Mathematics and Natural Sciences, University of Groningen, The Netherlands.

Printed by: Off Page (www.offpage.nl)

ISBN: 978-90-367-6962-4 printed version
978-90-367-6961-7 electronic version

university of groningen

Rijksuniversiteit Groningen

CONTROL OVER TRANSLOCATION ACROSS THE LIPID BILAYER VIA AN ENGINEERED CHANNEL PROTEIN

PhD thesis

to obtain the degree of PhD at the
University of Groningen
on the authority of the
Rector Magnificus Prof. E. Sterken
and in accordance with
the decision by the College of Deans.

This thesis will be defended in public on
Monday 28 April 2014 at 11.00 hours

by

Nobina Mukherjee
born on 19 January 1983
in Allahabad, India

Supervisor

Prof. B. Poolman

Co-supervisor

Prof. A.Koçer

Assessment committee

Prof. S. Cerdan

Prof. A.J. Minnaard

Prof. S.J. Marrink

To all who has been a part of this journey

TABLE OF CONTENTS

CHAPTER 1

General Introduction: Goal and outline of the thesis

Nobina Mukherjee

Department of Biochemistry, Groningen Biomolecular Sciences and Biotechnology Institute, Groningen, The Netherlands

ABSTRACT

In this thesis we explore the potential of a bacterial ion channel protein as a sensory valve for controlled release and uptake of cargo upon being activated by different non-natural triggers. In the first section of the introduction, different ion channels and their engineering is reviewed. Then, a brief overview is given about the mechanosensitive channel of interest for our studies, the Mechanosensitive channel of large conductance (MscL), and the manipulation of the protein. The following section discusses non-natural triggers of MscL, which can activate the channel either by interfering with the surrounding lipid membrane or by directly interacting with the protein. With this knowledge, we explore "how do we control the activation of MscL and utilize it as a sensory valve in drug delivery or hybrid devices?" The last section comprises of the outline of the thesis and the scope of the work.

NATURE'S MODES OF COMMUNICATION

It is amazing how nature has used communication and compartmentalization in a balanced manner to support life. The building block of life, the cell, is enclosed by a cell membrane, which protects the cell from the surrounding environment and acts as a permeability barrier to the passage of ions, solutes, and solvent. The continuous flow of ions and molecules is crucial for the survival of a cell. So, communication is a key not only for a society of people but also for a cell whether a eukaryote or a prokaryote. Nature has devised an elegant solution for this problem by employing various portals or gatekeepers of cell. The integral membrane proteins like ion channels, ion pumps, and ion exchangers allow the passage of specific or non-specific molecules across a membrane upon being stimulated. By facilitating transport across membranes, the membrane proteins play an important role in growth, survival, nutrition, signal transduction, and other biological processes (Hille, 1992b). The energy required by these processes comes from the concentration gradient of the ions across the membrane (in secondary transport) or is provided by the hydrolysis of adenosine triphosphate, ATP (in case of primary transport). Ion channels facilitate the movement of ions down the gradient and dissipate the gradients formed by primary and secondary transporters. Since the focus of this thesis is on ion channels, we first provide a brief review on them.

ION CHANNELS AS NATURE'S SENSORS

Ion channels are integral membrane proteins, which allow the passage of (non-) specific ions down their electrochemical gradient (Hille, 1992a). Another characteristic of ion channels is that the rate of ion transport is usually very high ($\geq 10^5$ ions per second) (Hille, 1992a). The mode of transport is passive as there is no direct expenditure of metabolic energy. Ion channels have diverse functions and are present in high numbers in excitable cells such as neurons, and muscle fibers. In the human genome until now there have been about 400 ion channel genes identified, the majority of which are shown or predicted to be potassium channels (around 170), 58 genes encode chloride channels, 38 encode calcium channels, 29 encode sodium channels and 15 encode glutamate-gated ion channels (Venter, 2001). The remaining of the genes encodes transient receptor potential (TRP) channels, acetyl choline receptors (AChR), inositol triphosphate (IP_3) receptor etc (Drews, 2000).

Ion channels play a significant role in various physiological processes such as osmoregulation, cell signalling, cell volume regulation, activation of nerve and muscle cells like cardiac, skeletal, smooth muscle contraction, insulin release from β cells of Langerhans, and T-cell activation etc (Camerino, 2007 & 2008; Verkman, 2009). Ion channels can sense myriad of stimuli ranging from voltage, ligand, light, to mechanical force and are present ubiquitously in prokaryotes and eukaryotes (Kung, 2005). Most of the ion channels are gated i.e. there are two fundamental functional states for these

membrane proteins, i.e. closed or 'off' state in the absence of the stimulus and open or 'on' state in the presence of the stimulus. Based on the stimuli that trigger the activation of the channels, they can be broadly classified into:

i) Ligand-gated channel- They open in response to binding of specific ligands to a protein domain. Examples: NMDA, $GABA_{A,C}$, Acetylcholine receptor, nAChR (Figure 1).

ii) Voltage-gated channels- These proteins respond to change in the electrical potential across the membrane. Examples: Voltage –dependent calcium channels (VDCC), and primarily the channel proteins that are prevalent in neurons, responsible for generating action potential and transmit signal, such as, potassium (K^+), sodium (Na^+), calcium (Ca^{2+}), chloride (Cl^-) channels (Figure 1).

iii) Mechanosensitive channels- These proteins respond to changes in mechanical forces, either in the membrane or protein-mediated. Example: Transient receptor potential (TRP) family, Mechanosensitive channel of large conductance (MscL), Mechanosensitive channel of small conductance (MscS) (Figure 1).

There are numerous studies where the structure and function of ion channels have been elucidated, through which we now have detailed understanding of their architecture, gating mechanism, and ion selectivity (Doyle, 1998). If represented in a simplified manner, ion channels consist of a pore and in certain cases, a selectivity filter. In response to a stimulus, they undergo conformational changes and opening of the pore for the passage of ions (or neutral solutes). The principle of gating of an ion channel is based on the conformational changes of the protein from the closed to open state, which is coupled to the activation energy provided by the stimuli. Prokaryotic K^+ channel, KcsA is cited as an example to discuss the architecture, gating mechanism, ion selectivity of a ligand-gated ion channel.

Architecture of an ion channel is fundamentally related to its gating mechanism. KcsA consists of multiple transmembrane segments that span the membrane, and create a wide water filled pore which ends at the selectivity filter. The aqueous pore allows rapid diffusion of ions across two-third length of the membrane before reaching the selectivity filter. In potassium channels, a long aqueous pore connected to a short selectivity filter is an important architectural hallmark that allows diffusion of about 10^8 ions per second (Gouaux, 2005). In the closed state, four inner helices of KcsA form a bundle. Upon gating, these helices bend approximately 30 degrees and creates a wide pore (12 Å) (Jiang, 2002). Atomic composition and stereochemistry of the ion-binding site plays an important role in determining the binding site specificity of ligand-gated channels.

Ion selectivity of the binding site of KcsA can be clearly illustrated by comparing selection of K^+ ion over Na^+ ion by its selectivity filter (Zhou, 2001). Na^+ and K^+ are some of the most abundant ions found in biological systems. The selectivity of ligand gated ion channels is determined structurally by providing an oxygen lined binding cavity that has an appropriate size for a particular ion. Tetrameric KcsA has a selectivity filter that can fit

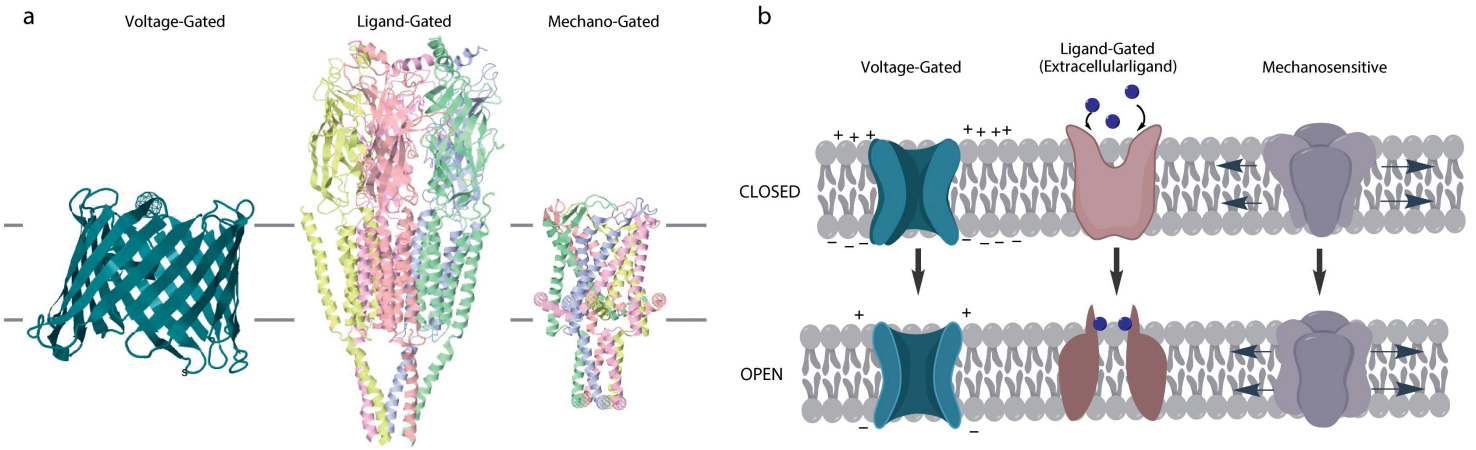

Figure 1. Representation of different types of Ion channels- a) Structure of voltage-gated channel, mouse-Voltage Dependent Anion Channel 1 (mVDAC1, PDB 3EMN), ligand-gated channel, torpedo-Nicotinic Acetylcholine Receptor (nAChR, PDB 2BG9), mechano-gated channel, *Mycobacterium*-Mechanosensitive channel of Large conductance (MscL, PDB 2OAR) in the bilayer membrane. The horizontal lines roughly indicate the boundaries of the lipid bilayer. b) Schematic representation of voltage-gated, ligand-gated and mechanosensitive channels in closed (upper panel) and open (lower panel) states after being stimulated by the respective native triggers.

four dehydrated K+ ions in a row, each interacting with the partially charged surrounding oxygen atom. Eight oxygen atoms can fit in the pore region of KcsA, allowing specific interaction with K^+ ion (Williams, 1970; Dietrich, 1985; Harding, 2002). K^+ has the right size to interact with 8 carbonyls and thereby compensate for the energetic penalty of desolvating the ion. Na is too small and can only interact with a few and, consequently, the process becomes energetically unfavorable. Therefore, the formation of correct coordination sphere, which compensates for the energy cost of desolvating the ion, is an important factor for the selectivity of an ion. In the following section we discuss the importance of ion channels and the motivation for their manipulation.

Since ion channels are crucial for proper functioning of life, dysfunctioning of them may lead to adverse conditions like a multitude of disorders known as channelopathies, for example, cystic fibrosis, epilepsy, long QT syndrome. At the same time many neuro toxins (venom from snake, spider, scorpion etc) work as a modulator of channels and inhibit them. This is the reason why, ion channels have emerged as an important drug target. Naturally, there has been a steady interest in the manipulation of the ion channels for studying their mechanism of action or applying and utilizing them for therapeutics. Thus, it is crucial to gain insight into the mode of action of the ion channels to achieve targeted molecular remedy. Apart from this, it is exciting to control the functioning of ion channels and to engineer entirely new gating mechanisms to natural channels such that they have applications in stochastic sensing or nanotechnology (Hammerstein, 2010; Guan, 2005).

MANIPULATION OF ION CHANNELS

For the manipulation of ion channels, protein engineering combined with synthetic approaches and nanotechnology has proven to be a successful strategy. Ion Channel Engineering (ICE) is a bottom up approach in which channels are modified by genetic methods either or not in combination with labeling with small molecules. Synthetic strategies to chemically modify the natural ion channels consist of methods to introduce chemical modulators to alter the channel's function. Even though, strategies to synthesize total artificial channels also exist, they are beyond the scope of this thesis. Bio-chemical synthetic strategies that will be discussed include: S-alkylation of site-specific cysteines, native chemical ligation (NCL) semi-synthesis and non-sense suppression.

Engineering Ion channels

An important approach for manipulating ion channels is to modify the gating mechanism or selectivity filter by either modulating the path of the ion flow, or changing the pore's specificity, or by making the pore responsive to external stimuli. It is advantageous to have a crystal structure of the protein to guide the engineering.

Modifying the Pore

The pore of a channel protein is a major target for ion channel engineering (ICE) as it allows modification of ion permeation pathway and thus the selectivity of the channel. At first, modification of ion permeation pathway of porins and membrane targeting toxins such as α-hemolysin (αHL), which have a β-barrel structure, will be discussed followed by modification of α-helical ion channel KcsA.

β-barrel proteins usually have a wide pore and are extremely stable structures that remain functional under conditions that are denaturing for most other proteins. For instance, α-hemolysin can tolerate upto 7.2 M urea or 93 ˚C (Pastoriza-Gallego, 2007; Gu, 1999; Jung, 2006). αHL is a membrane toxin from *Staphylococcus aureus* with a heptameric configuration and a long cylindrical conductance pathway, 4nm in length and 1-2 nm in diameter. Bayley and coworkers have extensively engineered αHL by ICE. Engineered αHL was used in a nanoreactor for tracking chemical reactions or as sensors and proteolysis monitors (Bayley, 2001; Hammerstein, 2010; Guan, 2005; Zhao, 2009a, b). It was also applied for DNA nucleotide detection and single nucleotide base discrimination (Howorka, 2001; Ashkenasy, 2005; Clarke, 2009; Stoddart, 2010; Cockroft, 2008). In another fascinating study, it was used as a nanodiode for making connections in lipid droplet networks (Maglia, 2009).

Apart from αHL, porins like OmpG and OmpF have been used for ICE studies (Reitz, 2009; Brenzel, 2009; Grosse, 2010). OmpG is a monomeric protein, so it is an ideal single channel sensor. When a dansyl modulator was attached to OmpG by S-alkylation partial blockage of current was witnessed (Grosse, 2010). On the other hand, OmpF is trimeric and very stable. ICE OmpF variants can be refolded more easily than OmpG and have been modified with chemical modulators like crown ethers to study the channel characteristics (Reitz, 2009; Brenzel, 2009). Upon attaching a crown ether modulator to L16C-OmpF, 18% reduction in specific conductance was observed (Reitz, 2009).

As compared to β-barrel proteins, some α-helical ion channels form a narrow ion transfer pathway. Many α-helical ion channels like the potassium channel KcsA have been engineered by ICE. The majority of studies are concerned with changing the amino acid residues lining the pore and finding the mechanism of gating. For example, the filter region of KcsA has been studied by using truncated versions of the channel (Valiyaveetil, 2004; Valiyaveetil, 2006). MacKinnon *et al* manipulated the filter region of KcsA, which consists of a motif $T^{75}VGYG^{79}$ by changing the amide bond between Y78 and G79 to an ester bond (Valiyaveetil, 2006). This and other studies helped to understand the underlying principle of cation selectivity of KcsA.

S-alkylation of specific cysteines in the target channel protein is an established strategy for attaching modulators to the pore. Cysteines provide the thiol functional group, which can react with a maleimide or haloacetamide groups or form a disulfide, and, consequently, cysteines allow site-specific attachment of a chemical modulator to a protein. There are many examples available in the literature, such as attachment of

a dibenzo crown ether to an OmpF porin mutant via the linkage of a iodoacetamide group to the thiol (Reitz, 2009), a maleimide for the attachment of a photo-switchable azobenzene moiety to E422C residue of K^+(SPARK) channel or the ionotropic glutamate receptor (iGluR-L439C) (Banghart, 2004; Banghart, 2006; Volgraf, 2006; Gorostiza, 2007; Szobota, 2007). Apart from this, S-alkylation of specific cysteines has been frequently used by Bayley and coworkers. For example, Hammerstein *et al* used it to study the thermodynamics of divalent metal ion chelation in the αHL pore (Hammerstein, 2010). They designed 'half-chelator' based on EDTA, consisting of *N*-propyliminodiacetic acid (PIDA) group and an iodoacetamide group to covalently attach to cysteine mutants of αHL. The complex formed by the association of two half-chelators would be comparable to the complex formed by EDTA. A single subunit of αHL was converted to αHL T117C/G143C, which was combined with unmodified WT αHL, giving rise to half-chelator attached to cysteine residues at position 117 and 143 on one of the seven subunits of αHL. Chelation of Zn^{2+} by this engineered complex gave detailed information about the kinetics and thermodynamics of metal-ion complex formation.

Extrinsic control of the Pore

Extrinsic control over ion channels has added a new dimension to their manipulation. Gating of channels stimulated by non-native triggers instead of the natural ones can augment the function of the ion channels and equip them with entirely new 'senses'. This can add a new dimension to the exploration of biological systems and possibly lead to applications in sensory devices. For example, a mechanosensitive channel, which in nature senses the tension in the membrane, can be engineered to sense the changes in the ambient pH or wavelength of the light (Kocer, 2005; Kocer, 2006). This is addressed by tethering a switchable modulator to the channel pore, which makes the channel sensitive to external trigger(s). Light is one of the best triggers for manipulating ion channel properties due to its high spatiotemporal resolution (Szymański, 2013). The basic principle is that a photo-switchable modulator is attached to a sensory part of the channel protein. Upon illumination of the labelled protein with light, the label acquires a different conformation or charged state, and thereby controls the opening or closing of the channel pore. One of the first studies to apply this strategy on voltage gated K^+ channels of the *Shaker* family was done by Trauner, Kramer and coworkers (Banghart, 2004). They used a pore blocker, tetraethyl ammonium (TEA) attached to a photoswitchable azobenzene group to affect the channel gating. When UV light was shone onto the protein, the photosensitive moiety attained condensed configuration, thus unblocking the pore. While with visible light (500 nm), there was an increase in the tether length by 5 Å, which caused TEA to block the pore. From a series of photoswitchable analogues with different linker lengths, MAQ (Maleimide, Azobenzene, Quaternary ammonium) proved to work best. In trans- configuration, MAQ blocked the Shaker channels. These channels were aptly termed by the authors as Synthetic Photoisomerizable Azobenzene Regulated K^+ channels (SPARK). Since the voltage gated potassium channels are

ubiquitously present in the nervous system of vertebrates, optical manipulation of the proteins offers a new perspective to probe their functioning *in situ*.

Another example of pore modification is presented for the nicotinic acetylcholine receptor (nAChR). This is the only ionotropic receptor present at the neuromuscular junction formed by the muscle fibre or sarcolemma and efferent neurone. nAChR plays an important role in muscular contraction by depolarizing the motor end plate of muscle fibre, thereby creating an end plate potential in response to the neurotransmitter acetylcholine. nAChR is a pentameric cationic ligand-gated ion channel and several subtypes of this family of protein have been implicated in nicotine addiction and Alzheimer's disease. A pioneering study by Erlanger, Wasserman, and Lester on nAChR resulted in the first light-gated ion channel (Lester, 1980). A covalently photoswitchable azobenzene isomer, benzylic bromide (Q-Br), was shown to act as a full agonist in the trans-state and reversibly activated the nAChR channel.

In another study, ionotropic glutamate receptors (iGluR) have been modified with light-sensitive probes. These receptors consist of a family of ligand-gated cation channels, classified according to their pharmacological characteristics as NMDA, AMPA (iGluR 1-4) or kainite (iGluR 5-7) receptors. A photoswitchable tethered agonist, MAG (Maleimide, Azobenzene linker, Glutamate), when covalently attached to a cysteine residue in iGluR-6, brought about opening of the channel (Volgraf, 2006). The authors tested the iGluR6-L439C-MAG construct in HEK293 cells. The data from whole cell recordings showed light-induced activation and deactivation of the channel. By illuminating the channel at a wavelength of 380 nm, the tethered agonist attained a cis-configuration with respect to the ligand binding domain (Volgraf, 2006). This led to the opening of the channel and resulted in ion conduction. Visible light (500nm) could reverse the process.

Similarly, α-hemolysin has been rendered light-sensitive (Loudwig, 2006). αHL with its 15 Å pore has been used for stochastic sensing (Bayley, 2001). At first, an irreversible photo-triggered variant of αHL was designed, using caged amino acids (Chang, 1995). The researchers improved the design by attaching a sulfonated azobenzene to a single cysteine mutant of αHL (Loudwig, 2006). Photoisomerization of azobenzene by UV light led to reversible modulation of the channel. This study provided details about the single molecule dynamics of photo switching of azobenzene.

Semi-Synthesis of Ion Channels

One of the major aims of the semi synthetic strategies for manipulation of ion channels is to introduce synthetic modulators at specific sites in the protein.

Native chemical ligation semisynthesis

Native chemical ligation (NCL) is a method for constructing large polypeptides by joining two or more peptide segments of moderate size (200 amino acids) (Figure 2). In NCL, the C-terminal thioester group of the unprotected peptide 1 is attacked by the

thiolate group of an N-terminal cysteine of peptide 2. NCL-based protein engineering has been used for the KcsA channel protein. In one study NCL was applied to alter the selectivity filter of KcsA by changing the amide bond to ester bond between residues Y78 and G79 (Banghart, 2004). The ligation product was obtained from a synthetic and a recombinant protein fragment, and the refolding of KcsA protein was achieved in lipid vesicles (Valiyaveetil, 2004). A three fragment route of NCL was applied to KcsA to modify other functionally important regions (Bayley, 2009; Komarov, 2009). NCL was employed to a bacterial outer membrane pore, OmpF, in order to introduce dansyl-azide functionality. A recombinant C terminal OmpF fragment with the N27C mutation, lacking the first 26 amino acids was ligated to the chemically synthesized N-terminal fragment (1-26 residues) with propargyltyrosine ether at K16 position. The dansyl-azide was used as a reporter group for copper-mediated cycloaddition, producing an N-peptide thiolester (Reitz, 2009). The ligation lead to a successful hybrid OmpF, which was refolded into functional protein in mixed unilamellar vesicles comprising of 1,2-dimyristoyl-*sn*-glycero-3-phosphocholine and *n*-dodecyl-β-D-maltoside.

Protein Trans-splicing

Protein trans-splicing is a special technique for ligation of two protein fragments of interest termed as N- and C-exteins, which are flanked by inteins and eventually spliced off. The ligation of N- and C-exteins via the peptide bond gives rise to the desired product. Brenzel and coworkers applied trans splicing for engineering modified OmpF porin by using Pol inteins (Brenzel, 2009). The N-terminal extein consisted of residues 1-26 (K16C) of OmpF with a benzocrown attached to cysteine at position 16, and the C-terminal extein consisted of residues 27-340 from OmpF. Ligation-mediated by trans splicing of the inteins, formed functional OmpF with benzocrown attached to C16. An advantage of trans-splicing is that the cysteine residue is available for modification even after the reaction takes place.

Nonsense suppression

This biosynthetic method helps to introduce non-natural amino acids in place of natural ones, allows the introduction of special groups and unique properties into a protein. Nonsense suppression requires introduction of a stop codon at the residue of interest in the mRNA of the target protein and the availability of tRNA with the desired unnatural amino acids that recognizes the stop codon. Nonsense suppression was earlier reported to produce nicotinic acetylcholine receptor (nAChR) in *Xenopus* oocytes (Dougherty, 2008). Synthesis of orthogonal aminoacyl-tRNA-synthetase/tRNA pairs has lead to a possible solution (Young, 2010). Conjugation of unnatural amino acids (UAA) containing chemically orthogonal functional groups like ketone, tetrazine, azide, alkyne etc at specific sites in the target protein has revolutionized protein engineering (Liu, 2010). These unnatural amino acids are genetically encoded in response to nonsense or frameshift codons, allowing tight control over the site and stoichiometry of conjugation. Additional tRNA/aminoacyl-tRNA synthetase (aaRS) pairs have been

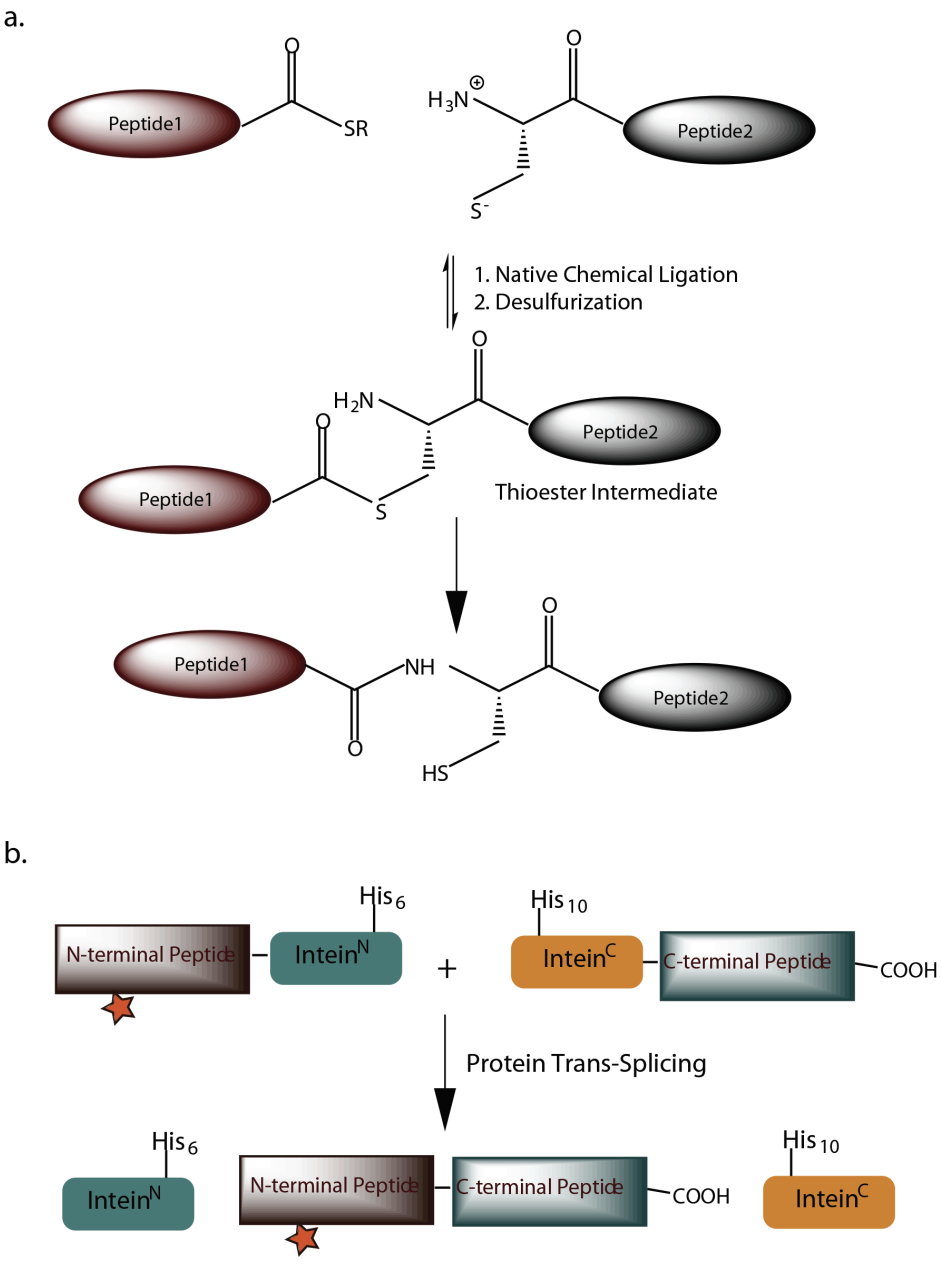

Figure 2. Semi synthesis of ion channel by a) Native chemical ligation (NCL) is a reaction in which, sulphur on the side chain of a cysteine of peptide 2 reacts with peptide 2 (R is usually a phenyl ring), producing a thioester intermediate, which spontaneously rearranges to give peptide bond; b) Protein Trans Splicing is a self-catalytic process where the intervening intein sequence is removed from the precursor protein and the flanking peptide segments are ligated with peptide linkage.

developed that can incorporate UAA successfully. For instance, engineered $tRNA^{Tyr}$/TyrRS pair generated from *M.jannaschii* has been used to incorporate various UAAs into proteins synthesized in *E.coli* (Wang, 2001). Further, new orthogonal ribosomes that recognize quadruplet codons using extended anticodon tRNAs have been evolved from a vast library of ribosomes (Neumann, 2010).

Taken together, all these examples illustrate how chemical modification of channel proteins can trigger their gating by non-native stimuli. In the following sections we will discuss the engineering and chemical modification of the mechanosensitive channel, Mechanosensitive Channel of Large Conductance (MscL), which is the prime topic of this thesis.

ENGINEERING OF THE MECHANOSENSITIVE CHANNEL OF LARGE CONDUCTANCE

Tension generated on the cell membrane by osmotic stress and the accompanying turgor is vital for the functioning of cells. Mechanosensation is an ancient fundamental trait of almost all living cells including microbes. The notion of mechanosensitive channels existed way before they were discovered in mechanosensory neurons (Katz, 1950 a, b; Loewenstein, 1959 a, b). Mechanosensitive channels directly sense force from the lipid bilayer in prokaryotes or through interactions with the cytoskeleton in eukaryotes, and they transduce the mechanical signal into conformational changes, allowing passage of water and small molecules, thereby relieving the tension in the membrane (Hamill, 2001). Though the underlying principles are miscellaneous and intricate, mechanosensitive channels are involved in wide range of sensations, such as touch, hearing, cardiac muscle function, proprioception, and osmoregulation (Kung, 2005). They also act in pressure responsive cells, like neurons, and their occurrence in endothelial and blood cells seems to suggest that they play a role in volume regulation and electrolyte homeostasis (Martinac, 1987).

One of the best-studied bacterial mechanosensitive proteins is the Mechanosensitive Channel of Large Conductance (MscL) (Kung, 2010). Martinac, Kung and coworkers were the first to report the presence of pressure-sensitive bacterial channel proteins (Martinac, 1987). They used the electrophysiological technique, patch clamp, to research pore-forming proteins in the membrane(s) of *E. coli* and discovered a channel that responded to applied pressure rather than voltage. Later, they were characterized as inner membrane proteins, and found to be distinct in structure and gating from the porins in the outer membrane of *E. coli* (Berrier, 1989). MscL plays a vital role in volume regulation of bacterial cells. Since the 1960s it has been known that under hypoosmotic shock conditions bacterial cell fires out osmolites, in order to prevent the cell from lysing. It was discovered more than 30 years later that mechanosensitive channels function as safety valves and release solutes into the environment when the pressure difference and thus the membrane tension gets too high. The *E. coli mscL* gene was identified by reverse genetics and analyzing protein fractions for mechanosensitive activation by patch clamp

electrophysiology (Sukharev, 1994). Sequence analysis and biochemical studies indicated that *E.coli* MscL contains 136 amino acid residues and is a homooligomer with monomeric mass of 17 kDa (Sukharev, 1994; Blount, 1996; Häse, 1997). Eventually, a truncated version of MscL from *Mycobacterium tuberculosis* could be successfully crystallized, and X-ray structural analysis revealed an α-helical, homopentameric structure at 3.5 Å resolution (Chang, 1998). Each of the identical subunits consists of two transmembrane segments (TM1 and TM2) connected by a periplasmic loop (PL) and the N- and C-termini facing the cytoplasmic side of the membrane (Sukharev, 1999).

Part of the TM1 domain makes up the constriction site of the channel, which is lined by hydrophobic residues. In the closed state, the pore region is predicted to be totally dehydrated (Gullingsrud, 2004) and has a diameter of approximately 3 Å. The cross-sectional view of the channel presents a funnel shaped structure with TM2 interacting with the lipid bilayer (Figure 3). Inspite of the availability of detailed structural information, the mechanism of transduction of mechanical force via the lipid bilayer into channel gating is still elusive. Infact, how an increase in membrane tension leads to conformational transition from closed to open is still an open question. In the fully open state, MscL channel forms a large non-selective pore with a diameter of about 40 Å and a conductance of 3nS at -20 mV (Cruickshank, 1997; Blount, 1996). Two different pathways of channel opening have been proposed, namely the '10-helix barrel-stave' and the '5-tilted helix pore' (Yoshimura, 1999; Sukharev, 2001). In the first model, TM1 helices move out of the centre and tilt almost parallel to the TM2 helices and form barrel-like structure. In the second model, tilting of the TM1 helices results in an iris-like expansion. To test these models, random and site-directed mutagenesis studies have been performed. For example, deletion or alteration of the N-terminus of MscL disrupted the channel function, whereas engineering of the C-terminus had comparatively little impact on channel functioning (Blount, 1996; Häse, 1997a, b). In a random mutagenesis study, mutations that lead to slow or no-growth phenotype were selected and analyzed, so-called gain-of-function (GOF) mutants (Ou, 1998). 14 out of 18 mutations were situated in TM1 and the most severe ones were found in the N-terminal half of TM1. Severe mutations resulted from substitutions of valine and glycine residues in TM1 into mostly hydrophilic (charged) amino acids. The mutants not only showed increased sensitivity to tension but also displayed a decrease in open dwell time of the channels. This implies that the energy cost of transition from the closed to open state was lowered. This hypothesis was substantiated by site-directed mutagenesis studies; for instance, the glycine at the 22nd position (G22) was substituted for each of the 19 other α-amino acids (Yoshimura, 1999). The major finding of this study was that the GOF phenotype correlated with the hydrophilicity of the substituted residue rather than size of the amino acid. Further structural studies, using the crystal structure of Tb-Mscl as template showed that G22 in Ec-MscL lies at the constriction site, and, together with a few other residues, forms the hydrophobic gate of MscL. Once there was detailed knowledge about the structure and function of MscL, the next step was to manipulate and gain control over the channel gating by external triggers.

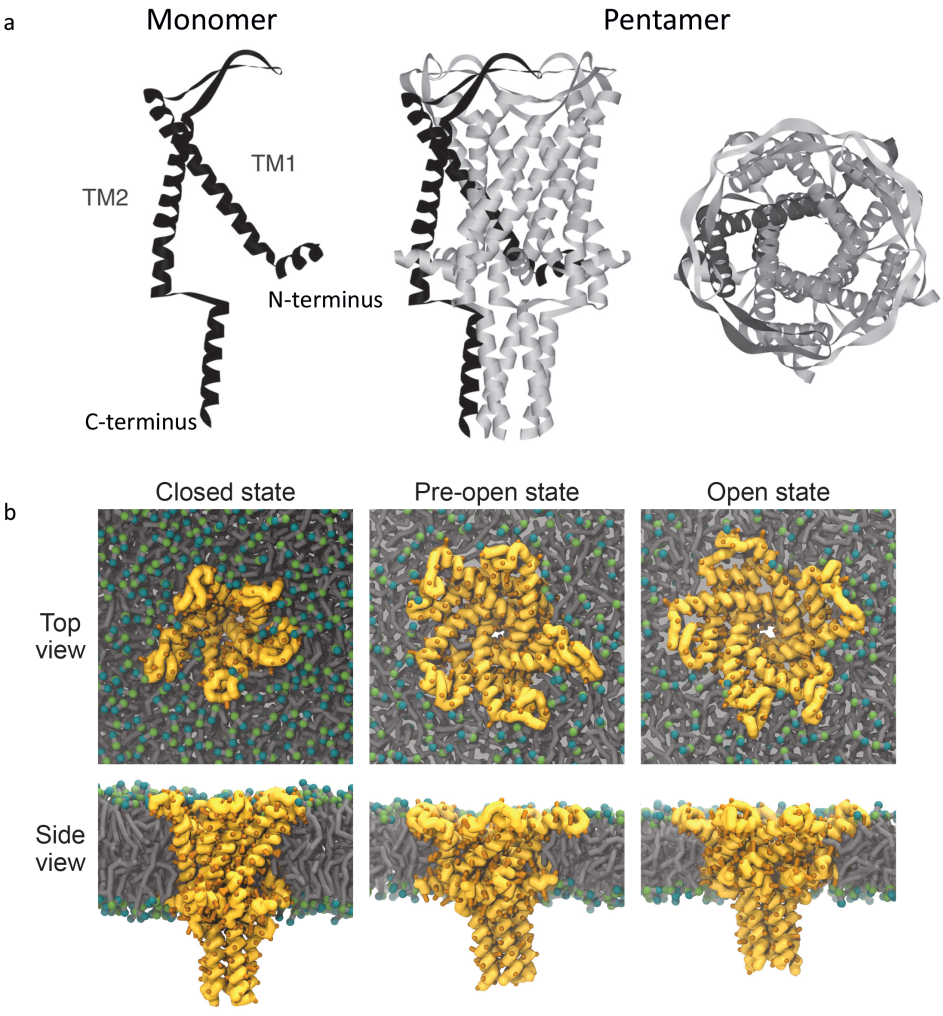

Figure 3. Schematic representation of MscL: a) Based on crystal structure from Mycobacterium tuberculosis (PDB accession code 2OAR). Left: side view of a monomeric MscL. Middle: Side view of pentameric MscL. Right: Top view of pentameric MscL from periplasmic side. The figure is adapted from Li *et al* (Li, 2009). b) Gating of MscL from Martini coarse-grained MD simulations, credits H.I.Ingólfsson. Three states of MscL are depicted: An equilibrated closed state before applying tension (left panel), after applying bilayer tension but before pore opening (middle panel), and after channel opening (right panel).

Chemically charging the MscL Pore

It has been demonstrated that post-translational addition of positive or negative charges to a cysteine at the constriction site of MscL brings about spontaneous gating of the channel (Yoshimura, 2001). Glycine at the 22nd position was substituted with cysteine, which allowed attachment of several available charge bearing compounds via S-S linkage with the

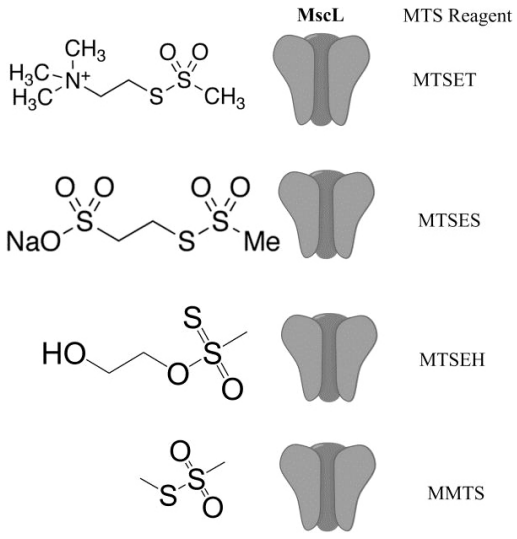

Figure 4. Schematic representation of methanethiosulphonate (MTS) reagents with MscL: MTSET has positive functional group, MTSES has negative functional group, MTSEH is polar and uncharged, MMTS is hydrophobic.

cysteine thiol group. Methanethiosulfonate (MTS) reagents with both positive and negative functional groups (NR_4^+, SO_3^-) opened the channel spontaneously in the absence of applied tension (Figure 4). On the other hand, polar, uncharged MTS reagent, 2-hydroxyethyl methanethiosulfonate (MTSEH) halved the threshold pressure and hydrophobic MTS reagent, methyl methanethiosulfonate increased the threshold pressure to be applied for channel gating. Achieving external control over the gating of MscL opened new possibilities for its manipulation, which is discussed in the following section.

Activation of MscL from the membrane and pore side

Biochemical and biophysical studies of MscL have shown that alterations in the surrounding bilayer membrane affect the channel activity. Lipids of different acyl chain length, single tail amphiphiles and anaesthetics have been used to manipulate MscL (Martinac, 1990; Perozo, 2002). In a similar study, *E.coli* MscL was studied by patch clamp and electron paramagnetic resonance (EPR) and activation of the channel with L-α-lysophosphatidylcholine (LPC), an inverted cone-shaped lipid with a single tail (Perozo, 2002). The study showed that MscL can be activated by asymmetric insertion of LPC in the membrane. Apart from this, light as an external trigger was used, as it offers spatial and temporal control over channel gating. An illustrative example of manipulation of MscL channel activity via the membrane is given by the light-sensitive lipid-mediated activation of MscL (Folgering, 2004). The channels were reconstituted in artificial membranes composed of 80 mol% DOPC and 20 mol% of the light sensitive

lipid, di-(5-{[4-(4-butylphenyl)azo]-phenoxy}-pentyl)phosphate (4-Azo-5P). Light-induced activation of MscL occurred through isomerization of 4-Azo-5P from *trans* to *cis* configuration at 365 nm. There was increase in the channel activity through reversible switching of 4-Azo-5P lipids. The results confirmed that the biophysical properties of the membrane play a very important role in the activity of MscL.

Several studies have employed modification of the pore of MscL by coupling a label to a specific amino acid residue. In one such ingenious study, MscL was labelled with a reversible photochromic spiropyran switch (Kocer, 2005). The actuator was attached to G22C of Ec-MscL. Upon irradiation with UV light (366 nm), the spiropyran actuator formed a zwitterionic merocyanine, which brought about channel opening. Subsequent irradiation with visible light led to reversible closure of the channel. Thus, MscL was turned into a light actuated nano-valve that could be remotely controlled.

In a related study, MscL was converted into a pH-sensitive nanovalve by labelling it with a chemical actuator, which allowed spontaneous activation in a predefined pH range (Kocer, 2006). Glycine-based actuators gave the best results and had advantages in specific and efficient coupling to the protein, pKa tunability, and tight control over the opening of the pore. At pH 7.4, only 5% release calcein was observed. When the pH was lowered to 6.1, the release increased to 45%. Patch clamp analysis supported the data from the efflux assays; the modified channels gated spontaneously in the pH range of 6-7 but at higher pH, they remained tension sensitive. Further, the combination of a light-switch and pH label was used to activate MscL in a two-step activation process. This helped to fine-tune the control over the release of cargo from MscL-liposomes (Kocer, 2006). This is discussed in details in chapter 3.

As a new tool to study how MscL 'senses' membrane tension, a heteropentamer of MscL was generated (Birkner, 2012). This allowed observing the contribution of single subunits of MscL to gating of the channel. This work provided evidence for the presence of a hydrophobic gate as the main energy barrier for permeation of ions through MscL. The hydrophobicity of the MscL pore was altered by assembling the channel from varying ratios WT- and G22C-MscL. By using MTSET and tension as triggers, the results showed that MscL gating is asymmetrical i.e. the gating is initiated by one subunit and followed by the rest. Irrespective of the trigger used, the subconducting states are the same and the channel encounters multiple energy barriers during transition from closed to open.

In vitro synthesis of MscL

In vitro synthesis of MscL was achieved by chemical methods and cell-free expression systems. These approaches have notable advantages over *in cell* expression systems for engineering protein but the yield of functional protein is generally very low. One study reported total chemical synthesis of Ec-MscL and Tb-MscL by ligating synthesized peptide fragments via introduced cysteine residues (Clayton, 2004). The yield of final

synthetic channel for both Ec-Mscl and Tb-MscL was around 15-30%. Functional characterization of the channels was done by reconstituting the synthetic protein in azolectin in a molar ratio of 1: 1000 and studying by patch clamp technique. They observed membrane localization of the channels by fluorescent imaging of N-terminal biotin-tagged Ec-MscL and Tb-MscL using streptavidin-Alexa Fluor 488. Patch results proved that synthetic and recombinant Ec-MscL have similar pressure sensitivity and activation threshold. Synthetic Tb-MscL required two-times more suction to achieve channel opening, as observed in recombinant Tb-MscL. The authors claim that these results imply that the synthetic protein could acquire the native conformation once inserted in the membrane. In a following study, a synthetic strategy was developed to attach a luminescent lanthanide chelate to MscL (Becker, 2004). Distance-dependent luminescence resonance energy transfer (LRET) was observed between the lanthanide donor (Tb^{3+}) and acceptor, methoxycoumarin-lysine. Although the synthetic channel had a comparable conductance as the wild-type MscL, the gating pressure threshold was two-fold higher. The bulky N-terminal DOTA-Mca label was pointed out to be the cause for the decrease in pressure sensitivity. The authors mentioned that N-terminal modification of MscL DOTA-Mca label may affect its pressure sensitivity by stabilizing the closed state or interfering with the transfer of tension from the bilayer to the channel. Ec-Mscl was also synthesized in cell-free expression systems in the presence of detergent instead of a phospholipid membrane (Berrier, 2004). Out of different nonionic and zwitterionic detergents used, Triton X-100 was selected to aid the *in vitro* synthesis of MscL and yielded a high amount of protein (1.3- 3.6 mg per milliliter lysate). The purified protein was reconstituted in liposomes and studied with patch clamp. The tension sensitivity and open probability of the synthetic channel was comparable to that of the recombinant protein.

Contributions of each transmembrane segment (TM1 and TM2) to molecular gating of MscL were addressed by creating N- and C-halves of the protein (Park, 2004). TM1 and TM2 of Ec-MscL were expressed independently in *E.coli* and electrophysiological analysis of assembled channels was done in liposomes. TM1 alone formed channels that spontaneously gated, i.e. in the absence of applied pressure. This result is consistent with a model suggested by Sukharev and coworkers, in which TM1 forms the constriction site of the pore of MscL (Sukharev, 2001). TM2 domain did not show any electrophysiological activity but co-reconstitution of N-and C-halves yielded channel activity, albeit with a lower conductance (1.5 nS) than the full length protein (~3 nS). Taken together, the results imply that TM1 aligns the pore region and has a role in gating, whereas TM2 interacts with the surrounding lipid bilayer, important for pressure sensing and acting as a scaffold for TM1.

Combining all the above studies, we conclude that the synthesis and engineering of MscL, along with the gain of control over its gating, is a cornerstone for possible applications of the channel protein as a nano-biosensor.

Experimental techniques used to study MscL

Functional characterization of an ion channel is usually based on ion conductance measurements. Each channel has certain characteristics like conductance and dwell time, which can be considered as the fingerprint of a channel. Therefore, ion channel activity can be measured in terms of single channel current conductance. In case of MscL, not only ions but also neutral solutes and even small proteins permeate through the pore, for which fluorescence-based methods can be used to probe the bulk flux of molecules. Some commonly used techniques for analysis of ion channels, mainly MscL are discussed here, namely i) patch clamp, ii) fluorescence dequenching assay and iii) dual-color fluorescence burst analysis (DCFBA) (Figure 5). Patch clamp is considered to be gold standard for studying ion channel and gives information about single channel conductance, while the flux assay is an ensemble measurement. DCFBA has been used to probe the size-exclusion limits of the pore and to determine the flux of proteins and reporter molecules.

The invention of patch clamp revolutionized the study of ion channels (Neher, 1976), and resulted in the award of the Noble Prize in medicine to Neher and Sackmann in 1991. The patch clamp technique has spatial and temporal resolution and gives information about unitary conductance, dwell time, sub-conducting states etc of a channel. It has the capacity to resolve ion currents in the pico-ampere range over micro-seconds. In patch clamp, a glass micropipette with electrode is used to make a patch from a whole cell or lipid vesicle. The current flow through the channel in the membrane patch is measured. Since the natural trigger of a mechanosensitive channels is tension in the membrane, suction through the pipette is applied to increase the membrane tension and activate the channels.

Flux assays are usually helpful to study ensemble activity of ion channels. Originally radio-labelled isotopes like ^{22}Na or ^{42}K were used to study sodium or potassium ion channels (Hu, 1995). For channels with large pores and no ion selectivity, like MscL, the flux of a large molecule, e.g. fluorescent dye or protein, can be followed. In one method, fluorescein or derivative [e.g calcein; 2', 7'-bis(N, N-bis(carboxymethyl) aminomethylene) fluorescein] is trapped in the lumen of a vesicle at a self-quenching concentration. The principle of fluorescence self-quenching of calcein is based on collisional quenching at high concentration (around 100 mM), i.e. collision between two excited fluorophores facilitates transition to ground state. Upon release of calcein (e.g. upon gating of MscL), the fluorophore ends up in the external medium where the concentration is low and the fluorescence thus increases or dequenches.

DCFBA allows to study permeation of fluorescently labelled (macro)-molecules from lipid vesicles that are labelled with another, spectrally non-overlapping fluorophore. The fluorescence bursts from the lipid dye of the vesicles diffusing through the focal volume of a confocal microscope will coincide with those from the encapsulated size-marker molecules, the cargo. The internal concentration of cargo is quantitatively

calculated from the fluorescence bursts at a single liposome level (van den Bogaart, 2007). DCFBA has been successfully used to study the effective pore-size of wildtype and heteropentameric MscL (Mika, 2013)

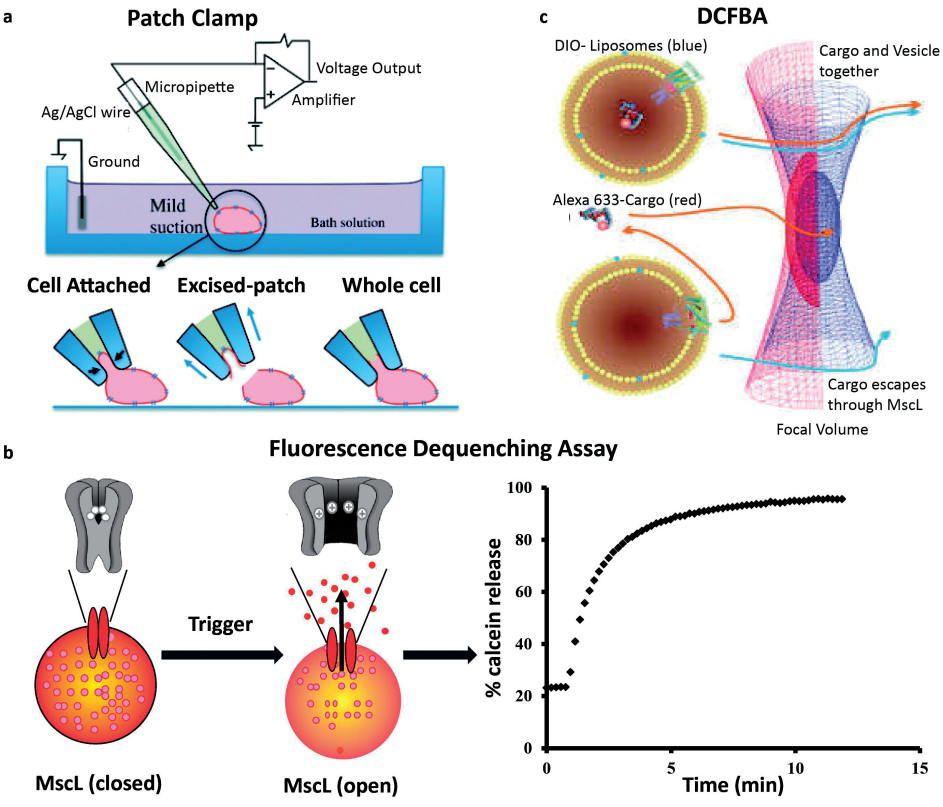

Figure 5. Experimental techniques: a) Patch Clamp- whole cell patch clamps (Clare, 2010). b) Fluorescence Dequenching Assay- upon activation of MscL, calcein is released from the liposomes and undergoes fluorescence dequenching, resulting in increased intensity signal (left panel). A graph of % calcein release as a function of time (right panel). c) Principle of dual-colour-fluorescence-burst analysis (DCFBA) - Showing focal geometry of two-channel confocal microscope. In the upper panel, Alexa 633-labelled cargo (red) cannot escape DiO labelled liposomes (blue) so the diffusion of two fluorophores coincides. In the lower panel, the cargo (red) escapes due to opening of the channel protein, so the diffusion from the fluorophores no longer coincides (van den Bogaart, 2007).

SCOPE AND OUTLINE OF THE THESIS

Communication is key aspect of life, be it a cell or human. Nature has designed ingenious portals to establish communication across the membrane, i.e. membrane transporters and receptors and ion channels. Inspired by nature, we wanted to apply one such portal, an ion channel protein for improving communication across membranes and control the activation of the ion channel by non-natural triggers. As stated in the title, we wanted to gain "Control over translocation across the lipid bilayer using an engineered channel protein."

In Chapter 2 and Chapter 3, I explored the possibilities of gaining control over the opening and closing of the Mechanosensitive Channel of Large Conductance (MscL), using non-native triggers to gate the pore.

Chapter 2 describes the manipulation of gating of MscL using the inverted cone shaped lipid, lyso-phosphatidylcholine (LPC). The potential of LPC in triggering channel opening in a controlled way has been determined. Unlike conventional beliefs that LPC mimics tension (Martinac, 1990; Perozo, 2002), we show that channel activation by LPC is different and cannot simply be equated with tension. The results emphasise the importance of lipid-protein interactions in mechanosensation.

In chapter 3, MscL is modified by attaching a thiol reactive agent to obtain a stable azide side group at the constriction site of the pore. Following the Staudinger reaction, in presence of triphenylphosphine and at a specific pH, the azide group in the pore of MscL gets protonated and activates the channel. In this study, the gating of the channel at physiological conditions is optimized; it is shown that serum does not inhibit Staudinger Reaction but rather facilitates it. Being, a bio-orthogonal reaction, the knowledge about the reaction conditions will benefit physiological applications of the channel protein.

Chapter 4, 5 and 6 presents how Mscl is converted into an extrinsically controlled nanovalve and applied for delivery and sensory applications. Chapter 4 describes the *in vivo* use of stealth liposomes functionalized with a chemically modified pH-sensitive MscL. By using magnetic resonance spectroscopy and imaging, we show that the engineered channels detect the low pH conditions of the tumor microenvironment and release the liposomal luminal cargo into implanted C6 glioma tumors.

In Chapter 5, a nanofabricated biochip platform is successfully employed for studying controlled multiplexed transport events through MscL, embedded in a lipid bilayer (SLB).

Chapter 6 presents an attempt to develop a biomimetic vesicle with inserted MscL acting as a nanovalve for loading and unloading of cargo. The presence of MscL in giant-unilamellar vesicles ensures control over the influx of a model dye, calcein into the giant unilamellar vesicles (GUVs).

REFERENCES

Ashkenasy N, Sanchez-Quesada J, Bayley H, & Ghadiri MR (2005) Recognizing a single base in an individual DNA strand: a step toward DNA sequencing in nanopores. *Angew Chem Int Ed Engl* **44**: 1401-1404

Banghart M, Borges K, Isacoff E, Trauner D, & Kramer RH (2004) Light-activated ion channels for remote control of neuronal firing. *Nat Neurosci* **7**: 1381-1386

Banghart MR, Volgraf M, & Trauner D (2006) Engineering light-gated ion channels. *Biochemistry* **45**: 15129-15141

Bayley H, Cheley S, Harrington L, & Syeda R (2009) Wrestling with native chemical ligation. *ACS Chem Biol* **4**: 983-985

Bayley H & Cremer PS (2001) Stochastic sensors inspired by biology. *Nature* **413**: 226-230

Becker CF, Clayton D, Shapovalov G, Lester HA, & Kochendoerfer GG (2004) On-resin assembly of a linkerless lanthanide(III)-based luminescence label and its application to the total synthesis of site-specifically labeled mechanosensitive channels. *Bioconjug Chem* **15**: 1118-1124

Berrier C, Coulombe A, Houssin C, & Ghazi A (1989) A patch-clamp study of ion channels of inner and outer membranes and of contact zones of E. coli, fused into giant liposomes. Pressure-activated channels are localized in the inner membrane. *FEBS Lett* **259**: 27-32

Berrier C, Park KH, Abes S, Bibonne A, Betton JM, & Ghazi A (2004) Cell-free synthesis of a functional ion channel in the absence of a membrane and in the presence of detergent. *Biochemistry* **43**: 12585-12591

Birkner JP, Poolman B, & Kocer A (2012) Hydrophobic gating of mechanosensitive channel of large conductance evidenced by single-subunit resolution. *Proc Natl Acad Sci U S A* **109**: 12944-12949

Blount P, Sukharev SI, Schroeder MJ, Nagle SK, & Kung C (1996) Single residue substitutions that change the gating properties of a mechanosensitive channel in Escherichia coli. *Proc Natl Acad Sci USA* **93**: 11652-11657

Brenzel S, Cebi M, Reiss P, Koert U, & Mootz HD (2009) Expanding the scope of protein trans-splicing to fragment ligation of an integral membrane protein: towards modulation of porin-based ion channels by chemical modification. *Chembiochem* **10**: 983-986

Camerino DC, Desaphy JF, Tricarico D, Pierno S, & Liantonio A (2008) Therapeutic approaches to ion channel diseases. *Adv Genet* **64**: 81-145

Camerino DC, Tricarico D, & Desaphy JF (2007) Ion channel pharmacology. *Neurotherapeutics* **4**: 184-198

Chang CY, Niblack B, Walker B, & Bayley H (1995) A photogenerated pore-forming protein. *Chem Biol* **2**: 391-400

Chang G, Spencer RH, Lee AT, Barclay MT, & Rees DC (1998) Structure of the MscL homolog from Mycobacterium tuberculosis: a gated mechanosensitive ion channel. *Science* **282**: 2220-2226

Clarke J, Wu HC, Jayasinghe L, Patel A, Reid S, & Bayley H (2009) Continuous base identification for single-molecule nanopore DNA sequencing. *Nat Nanotechnol* **4**: 265-270

Clayton D, Shapovalov G, Maurer JA, Dougherty DA, Lester HA, & Kochendoerfer GG (2004) Total chemical synthesis and electrophysiological characterization of mechanosensitive channels from Escherichia coli and Mycobacterium tuberculosis. *Proc Natl Acad Sci U S A* **101**: 4764-4769

Cockroft SL, Chu J, Amorin M, Bayley H, & Ghadiri MR (2008) A Single-Molecule Nanopore Device Detects DNA Polymerase Activity With Single-Nucleotide Resolution. *J Am Chem Soc* **130**: 818-820

Cruickshank CC, Minchin RF, Le Dain AC, & Martinac B (1997) Estimation of the pore size of the large-conductance mechanosensitive ion channel of Escherichia coli. *Biophys J* **73**: 1925-1931

Dietrich B (1985) Coordination chemistry of alkali and alkaline-earth cations with macrocyclic ligands. *J Chem Educ* **62**: 954

Dougherty DA (2008) Cys-loop neuroreceptors: structure to the rescue? *Chem Rev* **108**: 1642-1653

Doyle DA, Morais Cabral J, Pfuetzner RA, Kuo A, Gulbis JM, Cohen SL, Chait BT, & MacKinnon R (1998) The structure of the potassium channel: molecular basis of K+ conduction and selectivity. *Science* **280**: 69-77

Drews J (2000) Drug discovery: a historical perspective. *Science* **287**: 1960-1964

Folgering JH, Kuiper JM, de Vries AH, Engberts JB, & Poolman B (2004) Lipid-mediated light activation of a mechanosensitive channel of large conductance. *Langmuir* **20**: 6985-6987

Gorostiza P, Volgraf M, Numano R, Szobota S, Trauner D, & Isacoff EY (2007) Mechanisms of photoswitch conjugation and light activation of an ionotropic glutamate receptor. *Proc Natl Acad Sci U S A* **104**: 10865-10870

Gouaux E & Mackinnon R (2005) Principles of selective ion transport in channels and pumps. *Science* **310**: 1461-1465

Grosse W, Reiss P, Reitz S, Cebi M, Lubben W, Koert U, & Essen LO (2010) Structural and functional characterization of a synthetically modified OmpG. *Bioorg Med Chem* **18**: 7716-7723

Gu LQ, Braha O, Conlan S, Cheley S, & Bayley H (1999) Stochastic sensing of organic analytes by a pore-forming protein containing a molecular adapter. *Nature* **398**: 686-690

Guan X, Gu LQ, Cheley S, Braha O, & Bayley H (2005) Stochastic sensing of TNT with a genetically engineered pore. *Chembiochem* **6**: 1875-1881

Gullingsrud J & Schulten K (2004) Lipid bilayer pressure profiles and mechanosensitive channel gating. *Biophys J* **86**: 3496-3509

Hamill OP & Martinac B (2001) Molecular Basis of Mechanotransduction in Living Cells. *Physiol Rev* **81**: 685-740

Hammerstein AF, Shin SH, & Bayley H (2010) Single-molecule kinetics of two-step divalent cation chelation. *Angew Chem Int Ed Engl* **49**: 5085-5090

Harding MM (2002) Metal-ligand geometry relevant to proteins and in proteins: sodium and potassium. *Acta Crystallogr D Biol Crystallogr* **58**: 872-874

Hase CC, Le Dain AC, & Martinac B (1997) Molecular dissection of the large mechanosensitive ion channel (MscL) of E. coli: mutants with altered channel gating and pressure sensitivity. *J Membr Biol* **157**: 17-25

Hase CC, Minchin RF, Kloda A, & Martinac B (1997) Cross-linking studies and membrane localization and assembly of radiolabelled large mechanosensitive ion channel (MscL) of Escherichia coli. *Biochem Biophys Res Commun* **232**: 777-782

Hille B (1992) G protein-coupled mechanisms and nervous signaling. *Neuron* **9**: 187-195

Hille B (1992) Pumping ions. *Science* **255**: 742

Howorka S, Cheley S, & Bayley H (2001) Sequence-specific detection of individual DNA strands using engineered nanopores. *Nat Biotechnol* **19**: 636-639

Hu W, Toral J, Cervoni P, Ziai MR, & Sokol PT (1995) Depolarization-induced 86Rb+ efflux in CHO cells expressing a recombinant potassium channel. *J Pharmacol Toxicol Methods* **34**: 1-7

Jiang Y, Lee A, Chen J, Cadene M, Chait BT, & MacKinnon R (2002) The open pore conformation of potassium channels. *Nature* **417**: 523-526

Jung Y, Bayley H, & Movileanu L (2006) Temperature-responsive protein pores. *J Am Chem Soc* **128**: 15332-15340

Katz B (1950) Action potentials from a sensory nerve ending. *J Physiol* **111**: 248-260

Katz B (1950) Depolarization of sensory terminals and the initiation of impulses in the muscle spindle. *J Physiol* **111**: 261-282

Kocer A, Walko M, Bulten E, Halza E, Feringa BL, & Meijberg W (2006) Rationally designed chemical modulators convert a bacterial channel protein into a pH-sensory valve. *Angew Chem Int Ed Engl* **45**: 3126-3130

Koçer A, Walko M, Meijberg W, & Feringa BL (2005) A light-actuated nanovalve derived from a channel protein. *Science* **309**: 755-758

Komarov AG, Linn KM, Devereaux JJ, & Valiyaveetil FI (2009) Modular strategy for the semisynthesis of a K+ channel: investigating interactions of the pore helix. *ACS Chem Biol* **4**: 1029-1038

Kung C (2005) A possible unifying principle for mechanosensation. *Nature* **436**: 647-654

Kung C, Martinac B, & Sukharev S (2010) Mechanosensitive channels in microbes. *Rev Microbiol* **64**: 483-494

Lester HA, Krouse ME, Nass MM, Wassermann NH, & Erlanger BF (1980) A covalently bound photoisomerizable agonist: comparison with reversibly bound agonists at Electrophorus electroplaques. *J Gen Physiol* **75**: 207-232

Li Y, Wray R, Eaton C, & Blount P (2009) An open-pore structure of the mechanosensitive channel MscL derived by determining transmembrane domain interactions upon gating. *FASEB J* **23**: 2197-2204

Loewenstein WR (1959) The generation of electric activity in a nerve ending. *Ann N Y Acad Sci* **81**: 367-387

Loewenstein WR (1959) Spatial summation of electric activity in a non-myelinated nerve ending. *Nature* **183**: 1724-1725

Loudwig S & Bayley H (2006) Photoisomerization of an individual azobenzene molecule in water: an on-off switch triggered by light at a fixed wavelength. *J Am Chem Soc* **128**: 12404-12405

Maglia G, Heron AJ, Hwang WL, Holden MA, Mikhailova E, Li Q, Cheley S, & Bayley H (2009) Droplet networks with incorporated protein diodes show collective properties. *Nat Nanotechnol* **4**: 437-440

Martinac B, Adler J, & Kung C (1990) Mechanosensitive ion channels of E.coli activated by amphipaths. *Nature* **348**: 261-263

Martinac B, Buechner M, Delcour AH, Adler J, & Kung C (1987) Pressure-sensitive ion channel in Escherichia coli. *Proc Natl Acad Sci U S A* **84**: 2297-2301

Mika JT, Birkner JP, Poolman B, & Kocer A (2013) On the role of individual subunits in MscL gating: "all for one, one for all?" *FASEB J* **27**: 882-892

Neher E & Sakmann B (1976) Single-channel currents recorded from membrane of denervated frog muscle fibres. *Nature* **260**: 799-802

Neumann H, Wang K, Davis L, Garcia-Alai M, & Chin JW (2010) Encoding multiple unnatural amino acids via evolution of a quadruplet-decoding ribosome. *Nature* **464**: 441-444

Ou X, Blount P, Hoffman RJ, & Kung C (1998) One face of a transmembrane helix is crucial in mechanosensitive channel gating. *Proc Natl Acad Sci U S A* **95**: 11471-11475

Park KH, Berrier C, Martinac B, & Ghazi A (2004) Purification and functional reconstitution of N- and C-halves of the MscL channel. *Biophys J* **86**: 2129-2136

Pastoriza-Gallego M, Oukhaled G, Mathe J, Thiebot B, Betton JM, Auvray L, & Pelta J (2007) Urea denaturation of alpha-hemolysin pore inserted in planar lipid bilayer detected by single nanopore recording: loss of structural asymmetry. *FEBS Lett* **581**: 3371-3376

Perozo E, Kloda A, Cortes DM, & Martinac B (2002) Physical principles underlying the transduction of bilayer deformation forces during mechanosensitive channel gating. *Nature* **9**: 696-703

Reitz S, Cebi M, Reiss P, Studnik G, Linne U, Koert U, & Essen LO (2009) On the function and structure of synthetically modified porins. *Angew Chem Int Ed Engl* **48**: 4853-4857

Stoddart D, Maglia G, Mikhailova E, Heron AJ, & Bayley H (2010) Multiple base-recognition sites in a biological nanopore: two heads are better than one. *Angew Chem Int Ed Engl* **49**: 556-559

Sukharev S, Durell SR, & Guy HR (2001) Structural models of the MscL gating mechanism. *Biophys J* **81**: 917-936

Sukharev SI, Blount P, Martinac B, Blattner FR, & Kung C (1994) A large-conductance mechanosensitive channel in E. coli encoded by mscL alone. **368**: 265-268

Sukharev SI, Sigurdson WJ, Kung C, & Sachs F (1999) Energetic and spatial parameters for gating of the bacterial large conductance mechanosensitive channel, MscL. *J Gen Physiol* **113**: 525-540

Szobota S, Gorostiza P, Del Bene F, Wyart C, Fortin DL, Kolstad KD, Tulyathan O, Volgraf M, Numano R, Aaron HL, Scott EK, Kramer RH, Flannery J, Baier H, Trauner D, & Isacoff EY (2007) Remote control of neuronal activity with a light-gated glutamate receptor. *Neuron* **54**: 535-545

Szymanski W, Yilmaz D, Kocer A, & Feringa BL (2013) Bright ion channels and lipid bilayers. *Acc Chem Res* **46**: 2910-2923

Valiyaveetil FI, Sekedat M, MacKinnon R, & Muir TW (2006) Structural and functional consequences of an amide-to-ester substitution in the selectivity filter of a potassium channel. *J Am Chem Soc* **128**: 11591-11599

Valiyaveetil FI, Sekedat M, Muir TW, & MacKinnon R (2004) Semisynthesis of a functional K+ channel. *Angew Chem Int Ed Engl* **43**: 2504-2507

van den Bogaart G, Krasnikov V, & Poolman B (2007) Dual-color fluorescence-burst analysis to probe protein efflux through the mechanosensitive channel MscL. *Biophys J* **92**: 1233-1240

Venter JC, Adams MD, Myers EW, Li PW, Mural RJ, Sutton GG, Smith HO, Yandell M, Evans CA, Holt RA, Gocayne JD, Amanatides P, Ballew RM, Huson DH, Wortman JR, Zhang Q, Kodira CD, Zheng XH, Chen L, Skupski M et al (2001) The sequence of the human genome. *Science* **291**: 1304-1351

Verkman AS & Galietta LJ (2009) Chloride channels as drug targets. *Nat Rev Drug Discov* **8**: 153-171

Volgraf M, Gorostiza P, Numano R, Kramer RH, Isacoff EY, & Trauner D (2006) Allosteric control of an ionotropic glutamate receptor with an optical switch. *Nat Chem Biol* **2**: 47-52

Wang L & Schultz PG (2001) A general approach for the generation of orthogonal tRNAs. *Chem Biol* **8**: 883-890

Williams RJ (1970) Initial steps in oxygen interaction with protein-bound metals. *Biochem J* **117**: 14P-15P

Yoshimura K, Batiza A, & Kung C (2001) Chemically Charging the Pore Constriction Opens the Mechanosensitive Channel, MscL. *Biophys J* **80**: 2198-2206

Yoshimura K, Batiza A, Schroeder M, Blount P, & Kung C (1999) Hydrophilicity of a Single Residue within MscL Correlates with Increased Channel Mechanosensitivity. *Biophys J* **77**: 1960-1972

Young TS & Schultz PG (2010) Beyond the canonical 20 amino acids: expanding the genetic lexicon. *J Biol Chem* **285**: 11039-11044

Zhao Q, de Zoysa RS, Wang D, Jayawardhana DA, & Guan X (2009) Real-time monitoring of peptide cleavage using a nanopore probe. *J Am Chem Soc* **131**: 6324-6325

Zhao Q, Jayawardhana DA, Wang D, & Guan X (2009) Study of peptide transport through engineered protein channels. *J Phys Chem B* **113**: 3572-3578

Zhou Y, Morais-Cabral JH, Kaufman A, & MacKinnon R (2001) Chemistry of ion coordination and hydration revealed by a K+ channel-Fab complex at 2.0 A resolution. *Nature* **414**: 43-48

CHAPTER 2

L-α-lysophosphatidylcholine as an alternative trigger for MS channel activation: how does it compare to tension activation?

Nobina Mukherjee[1], Mac Donald Jose[1], Jan Peter Birkner[1], Martin Walko[1], Helgi I. Ingólfsson[2], Anna Dimitrova[1], Clément Arnarez[2], Siewert J. Marrink[2],Armağan Koçer[1]

[1]Department of Biochemistry, Groningen Biomolecular Sciences and Biotechnology Institute, Zernike Institute for Advanced Materials University of Groningen, Groningen, The Netherlands
[2]Dept of Biophysical Chemistry, University of Groningen, Groningen, The Netherlands

Submitted to FASEB Journal

ABSTRACT

One of the best-studied mechanosensitive ion channels is the Mechanosensitive Channel of Large Conductance (MscL) from *Escherichia coli*. MscL senses tension in the membrane evoked by an osmotic down shock and directly couples it to large conformational change, leading to the opening of the channel and releasing osmolites to the environment. In spite of numerous structural and theoretical studies, the gating mechanism of MscL remains elusive. Spectroscopic techniques would offer unique possibilities to monitor the conformational change if it was possible to perturb the tension in the lipid bilayer during the measurements. Here, the challenge is the activation of MscL with tension, in a controlled manner. To this end, asymmetric insertion of L-α-lysophosphatidylcholine (LPC) into the lipid bilayer has been demonstrated, but the mechanism of this activation is not fully understood. By studying the effects of LPC on tension-sensitive mutants of MscL and homologues from organisms, we report that LPC acts differently from applied tension. We find that LPC shifts the free energy of gating by interfering with MscL-membrane interaction. In addition, we demonstrate that fine-tuned addition of LPC can be used for controlled activation of MscL in spectroscopic studies.

INTRODUCTION

Mechanosensation is the basis for various biological processes including touch, hearing, and osmoregulation. Mechanosensitive ion channels are responsible for detecting mechanical stress and are present in prokaryotes, archae and eukaryotes. These ion channels gate between their open and closed forms upon mechanical stimulation and regulate the flow of ions and small molecules through an otherwise impermeable membrane (Kung *et al*, 2010).

The mechanosensitive channel of large conductance (MscL) is one of the best-studied mechanosensitive channels. It plays an essential role in osmoregulation of bacterial cells. It is composed of five identical subunits (Chang *et al*, 1998). Each subunit has two transmembrane domains (TM1 and TM2), a periplasmic loop, and cytoplasmic N- and C- termini (Blount et al, 1996). The TM1 domains form the narrow pore constriction, which is 2-4 Å in diameter in the closed state of the channel. Upon encountering hypoosmotic shock, a build-up of tension in the bacterial inner membrane occurs, which results in the opening of a water filled, non-selective pore with a diameter of about 30 Å (Cruickshank *et al*, 1997). It jettisons not only ions but also small molecules (Cruickshank *et al*, 1997; van den Boogart *et al*, 2007; Mika *et al*, 2012). Although gating models based on a large body of data are available (Blount *et al*, 1999; Yoshimura *et al*, 1999; Sukharev & Betanzos *et al*, 2001; Sukharev & Durell *et al*, 2001; Perozo *et al*, 2002a; Corry *et al*, 2010), it is not fully understood how MscL senses the mechanical stimulus that leads to protein structural changes and channel opening.

The tension sensation of MscL is directly coupled to large conformational changes in the channel (Sukharev *et al*, 2001; Betanzos *et al*, 2002; Chiang *et al*, 2004 ; Sukharev *et al*, 1999) even before the pore starts conducting (Gullingsrud *et al*, 2001; Gullingsrud *et al*, 2004) (Figure 1). Therefore, spectroscopic techniques are very attractive to follow the changes in protein structure from the very early stages, so as to understand the mechanism of mechanosensation. However, it is challenging to observe these changes due to the lack of suitable methods for activating MscL in a controlled way that is compatible with a spectroscopic setup. Previously, lipids with varying acyl chain length (Perozo *et al*, 2002a) or amphipathic molecules that insert into the lipid bilayer in an asymmetric fashion have been used to activate MscL in Electron Paramagnetic Resonance (EPR) and fluorescence spectroscopic studies (Martinac *et al*, 1990; Perozo *et al*, 2002a). One of these amphipathic molecules, L-α-lysophosphatidylcholine (LPC), an inverted cone-shaped lipid with a single tail, has a dramatic effect on the channel activity (Martinac *et al*, 1990). It has been proposed that LPC can activate *E. coli* MscL by inducing curvature and changing the bilayer lateral pressure profile (Perozo *et al*, 2002a; Martinac *et al*, 1990; Gullingsrud & Schulten, 2004; Vasquez *et al*, 2008). However, despite its substantial effect on the channel activity, the mechanism by which LPC activates MscL is still debated (Yoshimura & Sokabe, 2010).

Here, we systematically studied whether LPC can be used in place of tension for activating MscL in a controlled manner in a lipid bilayer. We investigated the effect of LPC concentration on the degree of opening of MscL, using different tension sensitive

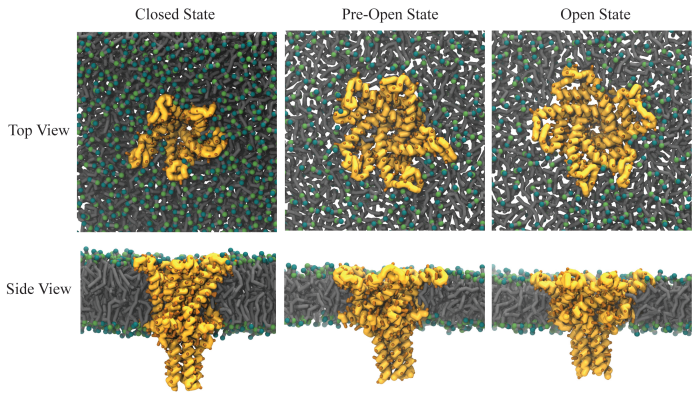

Figure 1. Snapshots of MscL from Martini coarse-grained MD simulations. MscL was embedded in a 1,2-dioleoyl-sn-glycero-3-phosphocholine (DOPC) bilayer and gated using tension as described in Yefimov *et al*, 2008; Louhivuori *et al*, 2010. Three states of MscL are depicted: (**A**) an equilibrated closed state before applying tension, (**B**) after applying bilayer tension but before pore opening, and (**C**) after channel opening.

MscL mutants and MscL homologues from different bacteria. The MscL activity in response to LPC concentration and tension in azolectin liposomes was compared using both ensemble and single molecule measurements. Our results show that i) LPC exerts its effect on MscL with a mechanism different from membrane tension; ii) LPC increases the tension sensitivity of MscL homologues from *L. lactis* and *M. tuberculosis* up to a point of gating with no applied tension; iii) LPC does not affect the mean conductance of MscL homologues but increases the open dwell time; iv) MscL from *L. lactis* and *M. tuberculosis* are more sensitive to the effect of LPC than MscL from *E. coli*; and v) LPC exerts its effect on MscL by altering the protein- membrane interaction. Our results show that LPC can be used to discriminate MscL channels on the basis of their tension sensitivity, and to study loss of function (LOF) mutants or less tension sensitive homologues with electrophysiology and spectroscopy techniques.

MATERIALS AND METHODS

Strains and cell growth

Escherichia coli (*E. coli*) strain PB104 (Blount *et al*, 1996) was used to host *mscl* gene from *E. coli, M. tuberculosis and L. Lactis,* expressed from p1BAD expression constructs (Birkner *et al*, 2012). p1BAD expression constructs were derived from parental pBAD-myc-his B plasmid (pBAD24derivative (Guzman *et al*, 1995); Invitrogen) without myc-his sites. The original Multiple Cloning Site was expanded, and nucleotides encoding for a c-myc epitope and His tag were removed. Chemically ($CaCl_2$)-competent *E. coli* PB104 cells were transformed with p1BAD and were grown in Luria-

Bertani (LB) medium in the presence of ampicillin (100 μg/ml) and chloramphenicol (10 μg/ml) in a shaker-incubator at 37 °C, rotated 250 cycles/min. A single colony of PB104 was used for inoculating an overnight culture in LB media supplemented with ampicillin (100 μg/ml) and chloramphenicol (10 μg/ml). The cells were grown at 37 °C in a 2 L fermentor using a complex medium [12 g/L Bacto-Tryptone (BD), 24 g/L yeast extract (BD), potassium phosphate (17 mM KH_2PO_4 and 72 mM K_2HPO_4) (pH 7), supplemented with the appropriate antibiotics at pH 7.5, and oxygen control (dissolved oxygen >70%). At the late-logarithmic phase, protein expression was initiated by adding 0.1% arabinose. 0.4% glycerol was also added as an additional carbon source. The cells were further grown for another two hours before harvesting.

Synthetic gene design

The MscL amino acid sequences from *L. lactis* (gi 12725155) and *M. tuberculosis* (gi 6016604*)* were used to produce the corresponding codon sequences using the DNA2.0 Bioinformatics Toolbox (www.dna20.com) (Stothard *et al*, 2000). The *FatI* and *SpeI* restriction sites were added to the 5' and 3' termini of the DNA sequence respectively. The DNA sequences were codon optimized for protein expression in *E. coli* and the optimized genes synthesized by Geneart (Germany).

Cloning

The two genes were amplified by PCR from the Geneart plasmid using the following primers:

Ll-MscL optimized for *E. coli*

F:GGCCAGTTAATTAAGAGGTACCAGC

R:GGCCGTCAAGGCCTAGGCGCG

Tb-MscL optimized for *E. coli*

F:GGCCAGTTAATTAAGAGGTACCAGC

R:GGAAGGCCGTCAAGGCCTAGGC

After PCR amplification the product was digested using *Fat*I and *Spe*I restriction enzymes and then ligated into p1BAD vector .The vectors, derivatives of p1BAD, containing the genes of interest were finally used to transform the *E. coli* strain PB104 for functional studies. The cloned gene was confirmed by sequencing (Servicex; Leiden, Netherlands).

Membrane Vesicle Preparation

Cells were harvested by centrifugation and suspended in 25 mM Tris·HCl (pH 8.0) to a final OD_{600} of 100–150. Subsequently, DNAse (0.5 mg/mL, final concentration), RNAse (0.5 mg/mL, final concentration), and 5 mM $MgSO_4$ were added, and cells were broken using a cell disrupter (Type TS/40; Constant Systems) at 1.7 kbar at 4 °C. Cellular

debris was removed by centrifugation for 30 min at 18,460 g at 4 °C. Supernatant was ultra centrifuged at 145,400 g for 90 min at 4 °C. The supernatant was discarded, and the remaining membrane vesicles were re-suspended and homogenized in ice-cold 25 mM Tris·HCl (pH 8.0) to 0.7 g (wet wt)/ml, and stored at −80 °C.

Protein Isolation

His-tagged Ll-MscL, Tb-MscL and Ec-MscL mutants, G22C, G22S, were purified by nickel-nitriloacetic acid (Ni-NTA) affinity chromatography, as described in (Kocer *et al*, 2007). Briefly, membrane vesicles corresponding to about 90 mg of total protein were solubilized at 5 mg/ml in 50 mM sodium phosphate (pH 8.0), 300 mM NaCl, 1% (vol/vol) Triton X-100, and 35 mM imidazole (solubilization buffer) for 30 min at 4 °C. After ultracentrifugation at 267,000 g for 20 min at 4 °C, the supernatant was applied to Ni-NTA agarose resin (Qiagen) [30 mg membrane protein/mL per 50% (wt/vol) slurry], which was pre-equilibrated with 10 column volumes (CV) of solubilization buffer, and incubated under mild agitation for 30 min at 4 °C. Unbound material was collected as flow through and analyzed when appropriate. The column was washed consecutively with 15 CV wash buffer [50 mM sodium phosphate (pH 8.0), 300 mM NaCl, 0.2% (vol/vol) Triton X-100, 35 mM imidazole]. The non-specific proteins were washed off the affinity column with 7.5 CV L-histidine wash buffer [50 mM sodium phosphate (pH 8.0), 300 mM NaCl, 0.2% (vol/vol) Triton X-100, 50 mM histidine]. His-tagged proteins were eluted by the addition of 15× 0.5 CV Ni-NTA elution buffer [50 mM sodium phosphate (pH 8.0), 300 mM NaCl, 0.2% (vol/vol) Triton X-100, 235 mM L-histidine]. The protein content of the fractions was checked with a Bradford assay. The total yield of protein was 3-4 mg at an average concentration of 1 mg/ml MscL.

Ec-MscL WT was Strep-tagged, so a column with StrepTactin resin (IBA) was equilibrated with solubilization buffer as before for 30 min at 4 °C. 80 mg of membrane protein from *E. coli* was incubated with the slurry with gentle agitation at 4 °C to allow binding of *Strep*II-tagged proteins. Unbound material was collected as flow through and the column was washed with 10 CV of wash buffer [50 mM sodium phosphate (pH 8.0), 300 mM NaCl, 0.2% (vol/vol) Triton X-100] to remove non specific membrane proteins and contaminants. The bound protein was eluted with 10 fractions, each 250 µl of biotin buffer [50 mM sodium phosphate (pH 8.0), 300 mM NaCl, 0.2% (vol/vol) Triton X-100 and 10 mM biotin] and analyzed for protein content. Usually, the final concentration of protein isolated from both types of column was around 0.9-1.5 mg/ml. Protein was frozen in liquid nitrogen and stored at −80 °C.

Lipid preparation for reconstitution

Soy PC (20%) (Avanti polar lipids, Cas no:8030-76-0) or better known as azolectin was suspended in 150 mM NaCl, 10 mM sodium phosphate (pH 8.0) buffer to 20 mg/ml final concentration by vortexing and 10 s sonication at room temperature. Subsequently,

seven freeze-thaw cycles were performed with rapid freezing in liquid N_2, and thawing in a waterbath at 50 °C respectively. Aliquots of 1 ml were stored at -80 °C.

Protein reconstitution in Large Unilamellar Vesicles (LUV)

His-tagged MscL was purified by Ni-NTA affinity chromatography and the protein concentration was determined by Bradford assay as described before (Kocer et al, 2007). Briefly, MscL proteins were reconstituted into azolectin liposomes by a detergent mediated reconstitution method, according to (Kocer *et al*, 2007). Azolectin was thawn and extruded eleven times through a 400 nm filter. Thereby LUVs were formed. Subsequently, liposomes were destabilized by addition of 10% Triton X-100. The amount of Triton to be added to lipid was determined by lipid titration method. Protein and lipids were mixed at a 1:50 (wt/wt) and incubated for 30 min at 50 °C. Subsequently, the appropriate buffer (for fluorescence dequenching assay: 200 mM calcein in 10 mM sodium phosphate (pH 8.0); for patch-clamp measurements: 10 mM sodium phosphate (pH 8.0), 150 mM NaCl) was added in 1:1 (vol/vol) and supplemented with 10 mg (wet weight) Biobeads (SM-2 Absorbents) per µl detergent (10% Triton X-100) used in the sample and lipid preparation. For detergent removal, the sample was incubated overnight (~16 h) at 4 °C on a rotating plate.

Determining the Critical Micellar Concentration (CMC) of LPC

The CMC of LPC was determined by fluorescence spectroscopy as described in (Dominguez *et al*, 1997). Briefly, this method is based on changes in vibrational band intensities in the fluorescence spectra of pyrene due to the solvent environment. The solvent environment is different above and below the CMC of surfactants. Below the CMC, pyrene is in a polar environment, and above the CMC of the surfactant, pyrene is solubilized in the core of the micelles. Hence, the vibrational band intensities of pyrene fluorescent spectra are different depending on whether the surfactant is present at concentration below or above its CMC. This is represented by the change in the ratio of the first (373 nm) and third (384 nm) band of pyrene fluorescence spectra. Following this method, we performed assays with LPC and pyrene, and found the CMC of LPC to be ~20 µM (Figure 2).

Fluorescence dequenching assay

L-α-lysophosphatidylcholine (LPC) was purchased from Avanti polar lipids. MTSET ([2-(trimethylammonio) ethyl] methanethiosulfonate and bio-beads (Bio-Beads SM-2 adsorbents) were from Anatrace and Bio-Rad Laboratories B.V., respectively. External calcein was separated from the proteoliposomes on a Sephadex G50 size-exclusion column. Calcein dequenching assay was performed in a Varian Cary Eclipse fluorimeter at a excitation wavelength of 497 nm (slit width 10nm) and emission at 516 nm (slit width 5nm). In a standard assay, 2 µl calcein-filled proteoliposomes were diluted into 2.1 ml of iso-osmotic efflux buffer. At t=2 min, LPC was added into this buffer at varying

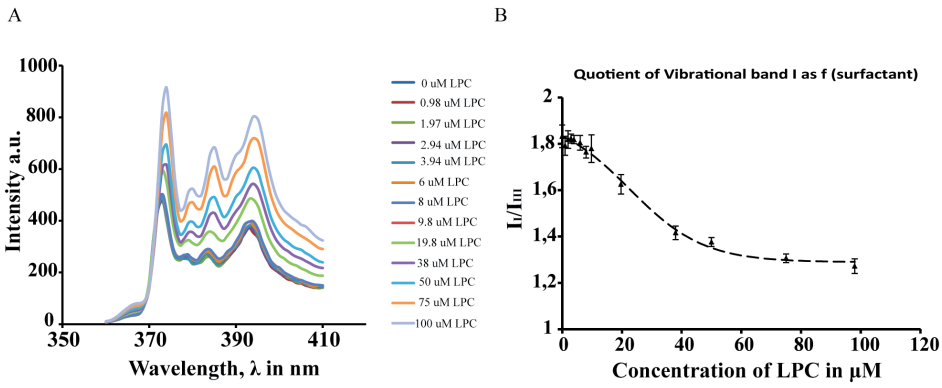

Figure 2. Determining the Critical Micellar Concentration (CMC) of LPC using fluorescence spectroscopy. (**A**) Emission spectra of pyrene showing variation in vibrational band intensities upon LPC addition. (**B**) Ratio of first and third peak intensities from **A**, as a function of LPC concentration. A Boltzmann fit of the data gives a CMC of ~20 µM for LPC.

final concentrations from 0-19.8 µM, and the content was continuously and gently stirred. The fluorescence was measured real-time and the maximum fluorescence of the sample was determined by lysing the proteoliposomes by the addition of 0.5 % (vol/vol) final concentration of Triton X-100 at t=28 min. As a control, background release from liposomes without MscL was recorded upon addition of LPC.

Western blot analysis

Proteoliposome samples were harvested by centrifugation at 26,000 g for 40 min and used for sodium dodecyl sulphate polyacrylamide gel for electrophoresis (SDS-PAGE). Proteins were electrotransferred to a polyvinylidene difluoride membrane and the Western blot analysis was performed using primary antibodies against the MscL C-terminus His- and Strep-tag as previously described (Blount *et al*, 1996). For imaging of the chemiluminescence a Fujifilm, LAS3000 Detection System was used according to the manufacturer's protocol. The developed film was processed using ImageJ (nih.gov) (Schneider *et al*, 2012).

Electron Paramagnetic Resonance (EPR)

EPR is non–destructive method. Together with site–directed spin labelling (SDSL), EPR provides structural information on molecular level by detecting unpaired electrons attached to the amino acid residue in the protein (Hubbell *et al,* 2000; Bordignon *et al,* 2012). To make MscL EPR visible, we specifically labelled the G22C mutant of MscL from *Escherichia coli* with 1– oxyl–2,2,5,5–tetramethylpyrrolin–3–yl)methyl methanethiosulfonate (MTSSL), Toronto Research Chemicals. MscL was

labelled with 1 mM MTSSL after protein isolation from Ni-NTA column for 30 min at 4 °C. The product was then used for EPR studies either in detergent micellar forms or reconstituted in azolectin lipid. Continuous – wave (CW) EPR measurements were performed using a commercially available MiniScope benchtop X-band EPR spectrometer (MS400 Magnettech GmbH, Berlin, Germany) with a rectangular TE102 resonator. Due to heat production in the resonator during operation, the cavity was fluxed with gaseous nitrogen keeping the temperature stable. The microwave power was set to 10mW and the B-field modulation amplitude to 0.20 mT. EPR glass capillaries (0.9 mm inner diameter) were filled with sample volume of 50µL and the final protein concentration was – 285µM. The microwave frequency was 9.41 GHz, the modulation frequency was 100 kHz. Each spectrum corresponds to the accumulation of 36 scans.

Electroformation and patch clamp

Giant Unilamellar Liposomes (GUVs) for patch clamp were prepared as explained before (Girard *et al*, 2004). Briefly, proteoliposomes were recovered as described for calcein efflux procedure. However, for patch clamp experiments, the calcein encapsulation and the size exclusion steps were omitted. Proteoliposomes were diluted to a final lipid concentration of 0.8 mg/ml by addition of an appropriate volume of 2 mM MOPS-Tris (pH 7.5). After dilution, 2 µl aliquots were spotted onto the conducting side of an Indium Tin Oxide (ITO) plate and dried over night in a desiccator under vacuum at 4 °C.

GUVs were prepared by rehydrating the lipid films in 250 mM sorbitol using a Nanion Vesicle Prep Pro instrument. The electroformation protocol was adapted from (Girard *et al*, 2004) with an AC voltage applied across the cell unit for 3 h with stepwise increases from 0.1 to 1.1 V at 12 kHz. At the end, in order to detach glass attached giant unilamellar liposomes, the frequency was lowered to 4 kHz and voltage raised to 2 V for 30 min. Subsequently, GUVs in sorbitol were transferred to a clean tube and assayed by patch clamp.

For patch clamp, the sample chamber of the patch setup was filled with 160 µl of patch buffer [200 mM KCl, 90 mM $MgCl_2$, 10 mM $CaCl_2$, 5 mM HEPES-KOH pH 7.25] and 5 µl GUV sample (lipid concentration ~0.4 mg/ml). Pipettes (Drummond Scientific Calibrated pipettes, 100 µl) with 1 µm tip diameter were pulled by using a Sutter Instrument P-1000. The pipette tip was filled with the same buffer as the bath. All recordings were performed with excised patches under the same conditions (20 mV, gain 10, sampling rate of 20 µs). The data were amplified and filtered at 10 kHz using an Axopatch 1D amplifier, sampled at 33 kHz in a Digidata 1322A digitizer and analyzed with pCLAMP10 software (Molecular Devices, Sunnyvale, California).

Molecular dynamics simulations

MscL simulations were performed using the Martini coarse-grain (CG) model (Marrink *et al*, 2004; Marrink *et al*, 2007; Monticelli *et al*, 2008) and the GROMACS 4.x simulation package (Hess *et al*, 2008) following a similar procedure as described in (Yefimov *et al*,

2008; Louhivuori *et al*, 2010). The topology of MscL was derived from the closed state Tb-MscL crystal structure (PDB ID 2OAR) (Steinbacher *et al*, 2007) using Martini 2.0. The channel was embedded in a 562 CG 1,2-dioleoyl-sn-glycero-3-phosphocholine (DOPC) lipid bilayer and solvated with 20k CG water beads (representing ~80k water molecules) using the insane.py script. In simulations with L-α-lysophosphatidylcholine (LPC) 10 mol% LPC was added on to the upper (periplasmic) leaflet. The temperature and pressure were controlled using the Berendsen thermostat (298 K) and barostat (1 bar semi-isotropic pressure coupling) (Berendsen *et al*, 1984). Initially the system was energy-minimized (steepest descent, 500 steps) and simulated for 10 ns using a short time step (10 fs) and with position restrains on the protein backbone. The restrains were released, and the system simulated for 20 ns with at 20 fs time step. The final time step was 30 fs and the system was simulated for 4 μs. Bilayer tension was incrementally applied in seven short (3 ns) simulations to a value of 60-65 mN/m and then simulated for 3 μs. In the first ~100 ns following the application of the lateral bilayer tension and thinning of the bilayer, the MscL transmembrane helixes tilted, extending the extracellular cavity of the channel (channel pre-open state). The channel hydrophobic gate takes an additional 200-600 ns before expanding and opening. All snapshots were generated using the molecular graphics viewer VMD (Humphrey *et al*, 1996).

RESULTS

Sensitivity of MscL mutants to LPC is directly related to their sensitivity to applied tension in the lipid bilayer

To test whether LPC can activate MscL in a similar manner as tension in the lipid bilayer, we studied its ability to differentiate tension-sensitive mutants of *E. coli* MscL (Ec-MscL). It has been shown that the hydrophilicity of the amino acid at position 22 in MscL affects the threshold of mechanosensitivity (Yoshimura *et al*, 1999). For instance, a mutation of G22 into a more hydrophobic amino acid, such as cysteine (G22C), presents a loss of function (LOF) behavior as this mutant requires higher tension to be activated. On the other hand, mutation of G22 to the hydrophilic amino acid serine (G22S) results in a gain of function (GOF) phenotype and requires less tension than the wild type (WT) channel for activation (Ou *et al*, 1998; Yoshimura *et al*, 1999). Here, we hypothesized that if the mechanism of activation of MscL by LPC is similar to tension, the amount of LPC required for channel activation should be directly related to the magnitude of tension required for activating the LOF or GOF mutants. To test this, we defined the midpoint LPC concentration ($C_{1/2}$) for activating individual mutants using a fluorescence dequenching assay (Kocer *et al*, 2007). We reconstituted individual mutants at the same 1:50 (wt/wt) protein to lipid ratio into azolectin Large Unilamellar Vesicles (LUVs), loaded with a self-quenching fluorescent dye, calcein. We activated the channels with different concentrations of LPC and generated dose-response curves of maximum release from

LUVs as a function of LPC concentration (Figure 3A). The maximum calcein release relative to the LPC concentration was fitted with a Boltzmann distribution and the $C_{1/2}$ and sensitivity (1/α) to LPC were determined as the midpoint and inverse of the slope of the fit, respectively (Figure 3B). We observed a direct correlation between the tension requirement of individual mutants and the concentration of LPC required for activating them. For WT MscL, the LPC concentration for 50% release ($C_{1/2}$) was 2.31 ± 0.15 μM; whereas the GOF mutant G22S, required 2.4 fold less and the LOF mutant G22C required 1.7 fold more LPC than the WT. Furthermore, the slope of the dose-response curves indicated that G22S is more sensitive to LPC addition than the WT and G22C MscL. Overall, the results show that LPC can differentiate Ec-MscL mutants on the basis of their sensitivity to the applied tension. Furthermore, it allows studying LOF mutants, which would be difficult to activate in patch clamp due to the lytic amount of tension required.

A

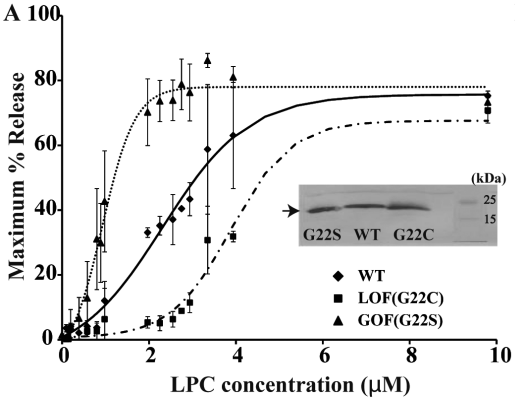

B

Mutant	$C_{1/2}$ ± S.D. (μM)	1/α ± S.D. (μM)
G22S	0.98 ±0.05	0.5 ±0.05
WT	2.31 ±0.15	0.91 ±0.27
G22C	3.88 ±0.12	1.28 ±0.35

Figure 3. Response of *E. coli* MscL mutants to LPC. MscL channels (WT, G22C, and G22S) were reconstituted in azolectin liposomes and tested for their activation by LPC, using calcein dequenching assay. For each channel type, we followed the release of calcein upon addition of different concentrations of LPC to the isoosmotic bulk solution. Maximum calcein released for each LPC concentration tested was collated to give a dose response curve. (**A**) Graph of maximum release vs LPC concentration for *E. coli* WT and mutant MscL. The release of liposomal content was calculated from the relative increase in fluorescence. The background release through the lipid membrane (if any) was accounted for in control experiments with liposomes lacking MscL. Western blot of proteoliposome samples indicates that the amount of protein present is comparable in all samples, see inset. (**B**) The table summarizes the 1/α values, i.e. the amount of LPC required for an e fold change in calcein release, and $C_{1/2}$, i.e. the LPC concentration at which 50% release occurs; the numbers were obtained by fitting the dose response curves with a Boltzmann Z-delta descending function.

LPC activates MscL homologues but the mechanism of activation is dissimilar to tension activation

To further explore the relation between LPC and applied tension in the lipid bilayer, we used LPC to activate MscL homologues from *Mycobacterium tuberculosis* (Tb-MscL)

and *Lactococcus lactis* (Ll-MscL). Both Tb- and Ll-MscL are less tension-sensitive than Ec-MscL and require at least twice as much tension to be activated (Maurer *et al*, 2000; Moe *et al*, 2000; Folgering *et al*, 2005). We reconstituted Tb-, Ll-, and Ec-MscL, 1:50 (wt/wt) protein-to-lipid ratio, into calcein-loaded azolectin LUVs, followed their activation by LPC using a fluorescence dequenching assay and generated dose-response curves as mentioned above (Figure 4A). If the mechanism of activation of MscL of LPC is similar to tension in the lipid bilayer, both Tb- and Ll-MscL channels were expected to behave similar to the G22C LOF mutant of Ec-MscL and be activated at higher LPC concentrations. Surprisingly, both Tb- and Ll-MscL were more sensitive to LPC than Ec-MscL and could be activated with $C_{1/2}$ for LPC of 0.86 ± 0.25 μM and 0.85 ± 0.03 μM, respectively; while Ec-MscL required 2.31 ± 0.15 μM (Figure 4B). When we repeated the experiments in another lipid composition, i.e. *E. coli* total lipids, we observed that all three homologues required more LPC for their activation. However, similar to azolectin lipid, the relative sensitivity of the channels to LPC did not change. Both Tb- and Ll-MscL could be activated at lower LPC concentrations than the Ec-MscL (Figure 5).

To better understand the effect of LPC on individual MscL channels, we studied Tb-, Ll- and Ec-MscL at the single molecule level by patch clamp electrophysiology. If LPC activates MscL channels following exactly the same mechanism as tension in the lipid bilayer, our findings in ensemble measurements on Tb- and Ll-MscL to LPC suggest that these channels are more tension sensitive than Ec-MscL. Alternatively, easy opening with LPC could be caused by a hydrophobic mismatch or an energetically favorable more

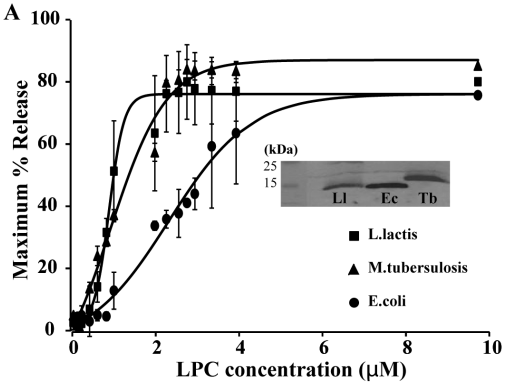

B

Organism	$C_{1/2}$ ± S.D. (μM)	1/α ± S.D. (μM)
L. lactis	0.86 ±0.03	0.21 ±0.04
M. tuberculosis	0.86 ±0.25	0.24 ±0.11
E. coli	2.31 ±0.14	0.68 ±0.19

Figure 4. Response of MscL homologues to LPC. The activation of membrane-reconstituted *E .coli, L. lactis,* and *M. tuberculosis* MscL channels by LPC was tested, using the calcein dequenching assay. For each homologue, the release of calcein upon addition of LPC was followed. (**A**) Graph of maximum release vs LPC concentration; for details see M&M and legend to figure 3. At 3 μM LPC, Tb-MscL has reached the maximum release; Ll- and Ec-MscL require a higher concentration. Western blot of proteoliposome samples used in the fluorimetric assay indicates that the amount of protein present is comparable, see inset. (**B**) The table summarizes the 1/α and $C_{1/2}$ values; the numbers were obtained by fitting the dose response curves with a Boltzmann Z-delta descending function.

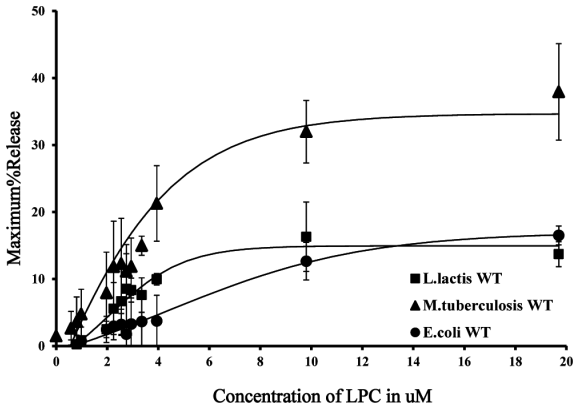

Figure 5. Response to LPC of MscL homologues reconstituted in *E. coli* total lipids. The % Release from Tb MscL is the highest, followed by Ll MscL and Ec MscL, as observed in azolectin lipids. However, more LPC is required to activate the channels in *E. coli* lipids as compared to azolectin, which may relate to the difference in geometry of the most abundant species. *E. coli* total lipids contain around 60% phosphatidylethanolamine (PE) (Charalambous K *et al,* 2008; Avanti Polar Lipids), a cone shaped lipid, as opposed to inverted cone shape of LPC; azolectin contains mostly PC, a bilayer-forming lipids. The release from proteoliposomes is corrected by deducting the release through the lipid membrane.

relaxed conformation of Tb- and Ll-MscL in the lipid bilayer. If any of these assumptions is correct, both Tb- and Ll-MscL should be activated by less applied tension than Ec-MscL in patch clamp experiments. Or in other words, there should be a left shift in their open probability versus tension in the dose-response curves upon activation of the channels with applied tension only. To this end, we generated Giant Unilamellar Vesicles (GUVs) from MscL-reconstituted azolectin LUVs as explained before (Girard *et al*, 2004). First, we tested the tension sensitivity of Tb- and Ll-MscL relative to Ec-MscL in azolectin lipid bilayers by activating the homologues with negative pressure in inside-out patches. The open probability of the individual proteins is represented as a function of applied negative pressure to the lipid bilayer (Figure 6A). The channel's open probability (P_o) follows the Boltzmann distribution function. Unlike their response to LPC in ensemble measurements, in patch clamp both Tb- and Ll-MscL channels required more tension to be activated than Ec-MscL, consistent with previous electrophysiology studies (Moe *et al*, 1998; Moe *et al*, 2000; Folgering *et al,* 2005). The negative pressure at which half of the population of channels is activated ($P_{1/2}$) for Tb- and Ll-MscL was 155.75 ± 0.29 mmHg (mean ± S.E., n=3) and 142.50 ± 1.76 mmHg (mean ± S.E., n=4), respectively; whereas Ec-MscL required 95.17± 0.33 mmHg (mean ± S.E., n=6) (Table I). Since we used pipettes with the same tip radius for all three homologues, the experiments were performed with independent samples, and multiple times for each sample, we assume that the difference in the tension sensitivity is not due to the area of the patched lipid bilayer but it is due to the tension-sensitivity of the channels themselves.

The conductance of Ec-MscL was 3.70 ± 0.23 nS, whereas the conductances of Tb- and Ll-MscL were 3.26 ± 0.10 nS and 1.80 ± 0.27 nS, respectively, in accordance with previous reports (Martinac *et al*, 1987; Sukharev *et al*, 1993; Moe *et al*, 1998; Häse *et al*, 1995; Folgering *et al*, 2005) (Figure 6B and C). The channel kinetics revealed that Ec-MscL has a stable, longer dwell time, whereas Tb- and Ll-MscL showed a flickery behavior (Table I).

Next, we performed patch clamp experiments in the presence of LPC and generated open probability curves as a function of applied negative pressure. After obtaining inside out patches, 9.5 μM final concentration of LPC was added into the bath and negative suction was applied to generate the P_o curves as explained before (Perozo *et al*, 2002a). As shown in Figure 6D, all three channel homologues became more tension-sensitive in the presence of LPC. The most significant shift was observed for Tb-MscL; its midpoint tension sensitivity changed 4.5 fold from $P_{1/2}$ of 155.8 ± 0.3 mmHg (mean ± S.E., n=3), when activated by negative pressure only, to 35.1 ± 0.1 mmHg (mean ± S.E., n=5) in the presence of both negative pressure and LPC (Figure 6D, Table I). In the case of Ll-MscL, the sensitivity to tension in the presence of LPC increased almost two-fold, and the change was 2.8 fold for Ec-MscL (Figure 6D, Table I). If the patches were incubated long enough, i.e. 20 min for Tb- and Ll-MscL and 30 min for Ec-MscL, all three homologues could be activated with no applied tension; which is consistent with previous studies on Ec-MscL (Perozo *et al*, 2002a; Nomura *et al*, 2012). The presence of LPC did not drastically change the unitary conductances of the channels but it affected the channel kinetics. All three channels (Figure 6E and F) had longer open dwell times (Table I), suggesting a more stable open conformation.

Together, the patch clamp results suggest that i) both LPC and applied tension in the bilayer activate the MscL channels. However, their modes of action are not the same because LPC cannot differentiate MscL homologues on the basis of their tension sensitivity as application of membrane tension does; ii) By affecting the bilayer properties, LPC indirectly increases the tension sensitivity of not only Ec-MscL, but also Tb- and Ll-MscL channels; iii) LPC sensitivity of homologous MscL channels is not directly proportional to their tension sensitivities and iv) Tb- and Ll-MscL behave more similar to each other than to Ec-MscL when activated by tension or LPC.

DISCUSSION

In this study we show that the asymmetric insertion of LPC into a lipid bilayer activates mechanosensitive channels from different organisms with a mechanism that is different than that of applied pressure. In patch clamp, the negative pressure applied on a patch pipette generates global tension on the sealed membrane and activates membrane-embedded ion channels on the basis of their tension sensitivity. The effect of LPC, on the other hand is not solely dependent on tension-sensitivity. In the case of *E. coli* mutants, asymmetric insertion of LPC could activate the channel on the basis of their

Table 1. Open Probability and Kinetics of MscL channel from different organism[a]

	Negative pressure				Negative pressure and LPC				
	$P_{1/2}$ ± S.E. (mmHg)	τ_1± S.E (ms)	τ_2±S.E. (ms)	Conductance G (nS)	$P_{1/2}$± S.E. (mmHg)	τ_1± S.E. ms	τ_2± S.E. ms	τ_3± S.E. ms	Conductance G (nS)
Organism	(% normalized population))				(% normalized population				
M. tuberculosis	155 ± 0.3	< 1	< 1	3.3 ± 0.1	35. ± 0.1	< 1	6 ± 1.5 (27%)	17.6 ± 7.4 (28%)	3.2 ± 1.1
L. lactis	142.5 ± 1.8	< 1	1.9 ± 0.2 (38%)	1.8 ± 0.3	78.2 ± 0.5	< 1	2.7 ± 0.2 (37%)	31.2 ± 3.5 (3%)	1.9 ± 0.3
E. coli	95.2 ± 0.3	<1	3.9 ± 0.1 (49%)	3.7 ± 0.2	34.6± 0.5	< 1	8.7 ± 0.2 (41%)	47.8 ± 0.3 (23%)	3.9 ± 0.3

[a]Open probability, dwell time and single channel conductance of MscL homologues—activated by LPC in presence and absence of negative pressure. In the presence of negative pipette pressure, the $P_{1/2}$ of Ec-MscL is lowest followed by Ll- and Tb-MscL. On the other hand, combination of negative pressure and 9.5 μM of LPC have an overall significant impact on the $P_{1/2}$ and dwell times of all MscL homologues. The unitary conductance of all channels from all the homologues remains unaffected.

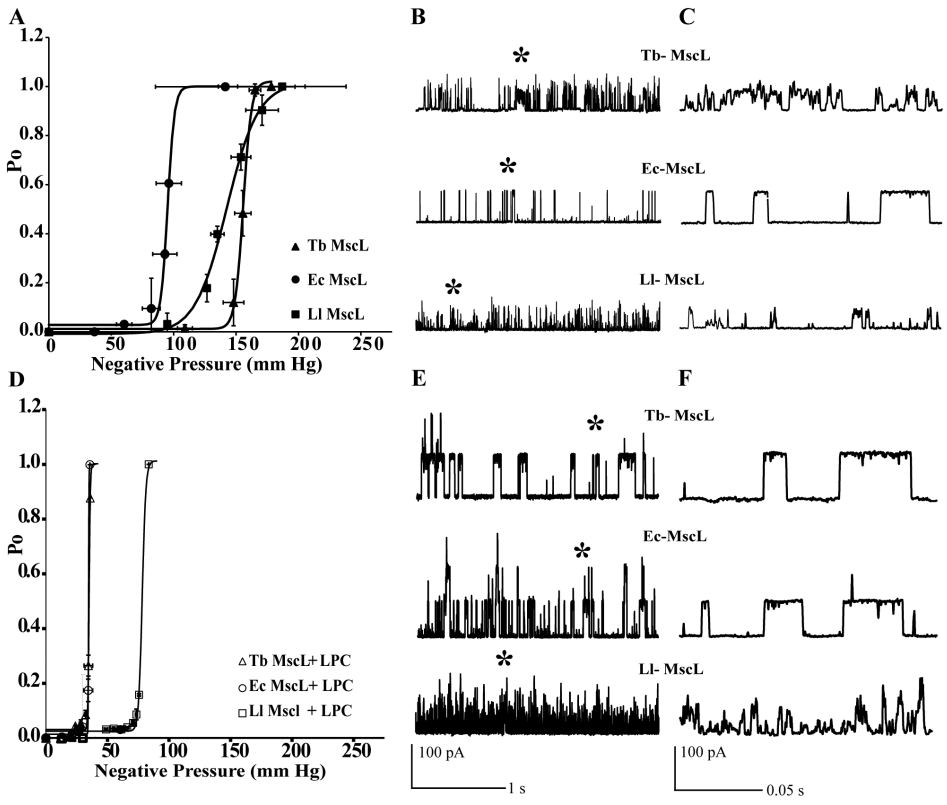

Figure 6. Comparison of open channel probability and single channel conductance of MscL homologues from *E. coli*, *L. lactis*, and *M. tuberculosis*. (**A**) In the presence of applied tension, by creating a pressure difference across the membrane. (**B**) Full opening of MscL channels triggered by tension in patches excised from GUVs at pressures equal to their individual $P_{1/2}$ values . (**C**) Magnified view of the position marked with asterisk (*), highlighting detailed single channel events. (**D**) Ec-, Tb-, and Ll-MscL triggered by tension and 9.5 μM of LPC simultaneously. The open probability of the channels is greatly affected when LPC is present along with tension. The overall trend is that the P_o curve shifts to lower pressures, i.e. the channel requires much less tension for activation, when LPC is present. (**E**) Full opening of MscL channels in patches excised from GUVs. (**F**) Magnified single channel events marked with asterisk (*).

tension sensitivity; the more tension-sensitive the channel was, the less amount of LPC was required for its activation (Figure 3). But, in the case of MscL channels from *M. tuberculosis* and *L. lactis*, that have similar tension sensitivity as the *E. coli* LOF mutant G22C, LPC activation was not proportional to the tension sensitivity of these channels. Both Tb- and Ll-MscL could be activated with significantly less LPC than Ec-MscL (Figure 4). Together, our results show that LPC differentially activates MscL channels and does not exactly mimic the applied tension in the lipid bilayer.

The LPC effect on MscL channels cannot be explained by the influence of LPC on the lipid bilayer only. The addition of LPC changes lipid bilayer properties (e.g. Mandersloot

et al, 1975; Morris *et al*, 1980; Zhelev 1998; Esteban-Martín *et al*, 2009) and some of these changes have been proposed as the mechanism of MscL activation by LPC (Perozo *et al*, 2002a; Yoo *et al*, 2009; Wiggins & Phillips, 2004), such as bending of the membrane (Wiggins & Phillips, 2004), changes in the surface tension (Yoshimura & Sokabe, 2010) or changes in the lateral pressure profile (Perozo *et al*, 2002a; Esteban-Martín *et al*, 2009). However, in our experiments, these physical changes in lipid bilayer properties should be the same because the lipid and LPC amounts were the same in the experiments for all three homologous channels. As the response of these homologs to the effects of LPC varied, the MscL LPC interaction cannot be explained by changes in bilayer properties alone; the protein in the membrane should also be also has a very important contribution. However, being a common activator of structurally different mechanosensitive membrane proteins, LPC is not expected to specifically interact with MscL channels (Machiyama *et al*, 2008; Maingret *et al*, 2000). Indeed, by Electron Paramagnetic Resonance (EPR) spectroscopy, we tested if LPC by itself could activate MscL, (Figure 7). MscL was labelled with a spin probe on one of its mobile amino acid positions as defined before (Perozo *et al*, 2002b) and the mobility of the probe was followed when the protein was embedded in detergent or in liposomes. The probe mobility changed upon addition of LPC only when the channel was in liposomes (Figure 7). Indicating that LPC by itself does not activate MscL.

Additionally, we explored LPC MscL interactions using coarse-grained Martini (Marrink *et al*, 2004; Marrink *et al*, 2007; Monticelli *et al*, 2008) simulations. Using the Martini force field it is possible to gate MscL channels in an unbiased way and in

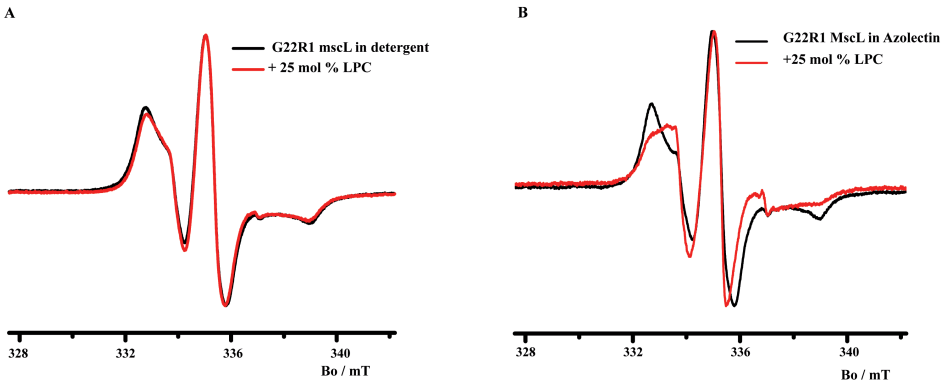

Figure 7. Interaction of spin-labelled Ec-MscL, G22C-R1, with LPC, in azolectin liposomes or detergent, measured with Electron Paramagnetic Resonance (EPR). (**A**) A typical EPR trace accumulated by averaging multiple sweeps, showing that there is no change in EPR probe environment in detergent, with or without LPC. This demonstrates that no interaction takes place between LPC and protein or LPC and detergent micelles; so, LPC does not affect the dynamics of solubilized protein. (**B**) When MscL is inserted in a lipid bilayer, a substantial change in EPR spectra mobility is detected upon addition of 25 mol% LPC. So, EPR result proves that lipid–protein interface is essential for LPC to exert its effects.

tractable computational time by applying lateral bilayer pressure (Figure 1). MscL was embedded in a bilayer and simulated with and without tension, as described in (Yefimov *et al*, 2008; Louhivuori *et al*, 2010) but with an additional 10 mol% LPC inserted on the periplasmic site of the membrane (Figure 8). No specific interactions of LPC with MscL were found. Indeed when the density of LPC relative to the bulk lipid is explored, a small reduction (~15%) in LPC occupancy is observed at the MscL bilayer interface, both with no tension around closed MscL and with tension around open MscL (Figure 8). Taken together, we consider the most plausible explanation for LPC effect on MscL channels to be changes in the interaction between membrane and protein.

In general, changes in lipid composition and/or addition of amphiphiles can indirectly alter membrane protein function through the resulting changes in the protein-membrane coupling (Lee, 2004; Marsh, 2008; Lundbæk *et al*, 2010). The energetic cost of bilayer deformation and packing is often referred to as the bilayer deformation energy or the protein-bilayer line tension. Intuitively, the line tension is the circumferential tension at the perimeter of a channel protein generated as a result of its interaction with the boundary lipids (Markin & Sachs, 2007; Sachs, 2010; Wiggins & Phillips, 2004), and it will be different for every channel in a given lipid composition (Markin & Sachs, 2007). Previously, bilayer-dependent inhibition of mechanosensitive channels by an amphipathic peptide GsMTx4 was shown using gramicidin channels as probes for changes in bilayer properties (Suchyna et al, 2004). It was suggested that the adsorption of the amphipathic peptide may perturb the lipid packing adjacent to the channel protein, and as a result, alter the line tension of the mechanosensitive channel-bilayer interface and hence the channel gating. (Suchyna et al, 2004).

Indeed, our observations could be rationalized by LPC induced changes in protein-bilayer line tension. In the case of *E. coli* MscL tension-sensitive mutants, the channels differ from each other by only a single amino acid residue located at the pore, which is known not to be interacting with the lipid bilayer. Since the rest of the channel is exactly the same, tension-sensitive mutants of Ec-MscL should have the same protein-lipid interactions; hence the same line tension, before LPC addition, unless the point mutation changes the conformation of the channel. Upon addition of a given concentration of LPC, the magnitude of the change in line tension should again be the same for each mutant; as the only difference among these channels is the strength of the forces in the pore that keeps the channel in its closed form i.e. the hydrophobicity of the pore (Yoshimura *et al*, 1999; Ou *et al*, 1998). The pore of the GOF mutant is more hydrophilic, therefore it requires less energy for activation. Indeed $C_{1/2}$ for LPC was the lowest for G22S, the GOF mutant. Similarly, LOF mutants have more hydrophobic pores, and therefore they are tightly closed and require higher energy for activation. This explains the higher $C_{1/2}$ for LPC activation of G22C in our experiments (Figure 3).

In case of MscL homologues, on the other hand, the protein-bilayer line tension could be different for each homologue even in the absence of LPC. Even though all three

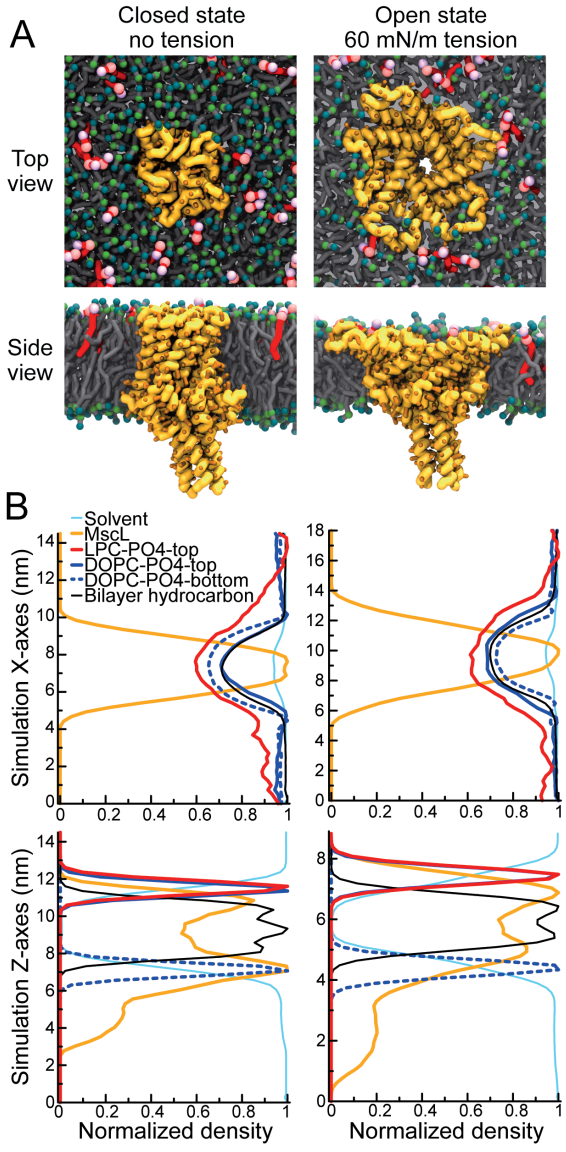

Figure 8. Coarse-grained Martini simulations of MscL in the presence of LPC. MscL was embedded in a DOPC and 10 mol% LPC was added to the outer (top) leaflet. The channel was simulated for 4 μs (left column) and then tension was applied up to 60 mN/m (right column). (**A**) Snapshots from the simulations showing MscL (orange), DOPC (dark gray) and LPC (light red). (**B**) Coarse-grained particle density profiles along the simulations Z-axes (normal to the bilayer) and X-axes (bottom and top panels, respectively. The density of the LPC phosphate beads show that the LPC head groups sit at the same level as DOPC (bottom panels) and the LPC is well distributed throughout the outer leaflet of the bilayer but with a slight exclusion away from the MscL channel, both the open and closed conformation (top panels). For the density calculations the first 100 ns from each simulation was excluded from the analysis. During the 3-4 μs long simulations LPC molecules diffused throughout the bilayer and can be considered to have reach equilibrium.

homologues share the same functionality, they share only 40% sequence identity (Moe *et al*, 2000; Maurer *et al*, 2000). The pore forming half of these channels is well conserved, however, the upper part of the TM1 (highlighted in the Figure 9) and TM2 helices, which interact with the lipid bilayer (Chang *et al*, 2004), differ. Therefore, Tb-, Ll-, and Ec-MscL can have different line tensions. As a result of this, independent of how strong or weak the hydrophobic interactions in their pore region are, these homologous MscLs already have different free-energy requirements for their gating. Since the channels differ from each other on their lipid-interacting face, the contribution of the effect of LPC to the deformation energy for each homologous channel is most likely different. The patch clamp experiments, in which we activated MscL channels with applied tension in the absence and presence of LPC, allowed us to define the contribution of the line tension to the overall bilayer deformation energy relative to the applied tension; the biggest change in activity was for Tb-MscL, which was followed by Ll-MscL, and finally by Ec-MscL (Table I). The amount of tension required to activate each channel reduced 2-5 times in the presence of 9.5 μM of LPC. Since Tb- and Ll-MscL reacted to LPC in a similar fashion, we compared their amino acid sequences (Figure 9). Interestingly, the upper half of the TM1 and TM2 helices are more alike in Tb- and Ll-MscL than in Ec-MscL, which might explain the similar behavior of Tb- and Ll-MscL in response to LPC.

Instead of invoking protein-lipid deformation energy or line tension as the primary driving force for LPC induced channel gating, our results could also be explained through coupling of the bilayer pressure profile and shape changes of the channels

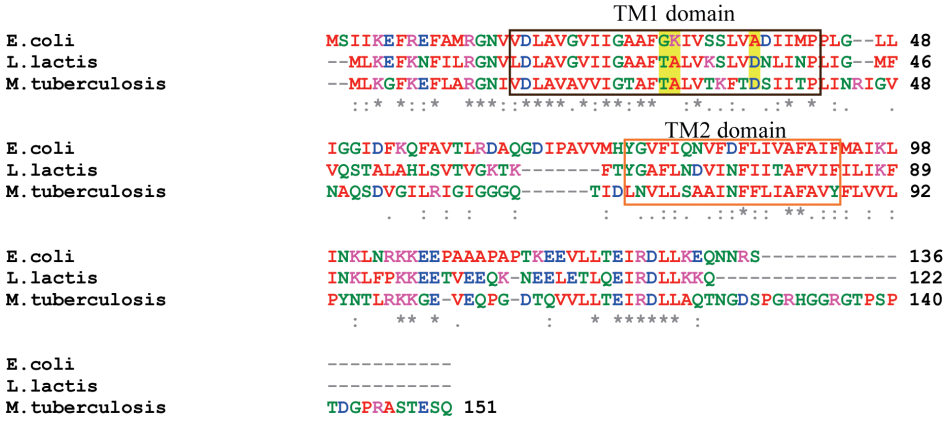

Figure 9. Alignment of amino acid sequence of *E. coli, L. lactis,* and *M. tuberculosis* MscL. Comparison of the total protein sequences using ClustalW version 2.0. The colour codes represent: Red- Small and hydrophobic residues (aromatic-Y) (AVFPMILW); Blue- Acidic (DE); Magenta- Basic-H (RK); Green- Hydroxyl+ Sulfhydryl+ Amine+ G (STYHCNGQ). An asterisk (*) indicates residues which are fully conserved; a colon (:) indicates conservation between strongly similar amino acids; a period (.) indicates conservation between weakly similar amino acids

during gating. A recent computational study on MscL channel gating found protein shape change to be a major contributor to its free energy of gating (Ollila *et al*, 2011), in particular through shape changes occurring at the lipid/water interface, which is characterized by a large negative lateral pressure component. For MscL, the protein area change upon gating is estimated to be over 5 nm^2 at the interface. If LPC affects the lateral pressure in this region, the gating free energy of the channel changes depending on the adapted shape of the protein. Indeed, in another computational study it has been found that asymmetric addition of LPC caused a considerable asymmetric shift in the bilayer lateral pressure profile (Esteban-Martín *et al*, 2009), about 100 bar at the interface. Taking these studies together, as a rough estimate, LPC's effect on the pressure profile would contribute $\Delta A.\Delta p.l$ = 15 kJ mol^{-1} to MscL gating (assuming an interfacial width l = 0.5 nm). Depending on the details of the shape differences, which are currently unknown, the exact contribution will vary between different MscL homologues and account for the observed changes in their sensitivity to LPC.

CONCLUSION

In conclusion, we have shown that LPC can be used to activate individual MscL channels in a controlled fashion in the absence of imposed membrane tension. Furthermore, our results indicate that the effect of LPC may strongly depend on the properties of the protein-membrane interaction. The addition of LPC changes lipid bilayer properties and may affect the interfacial line tension between the protein and the bilayer. These changes will alter the free energy required to open the channel, but the amplitude of this change will depend on the exact conformational preference of the channel in question. LPC can be used to study more tension-insensitive MscL or other channels at lower applied tension. Finally, even though Tb- and Ll-MscL are less tension-sensitive than Ec-MscL, they become more sensitive in the presence of LPC. It is then intriguing to consider whether these channels may have other activators in their native environment.

REFERENCES

Berendsen HJC, Postma JPM, van Gunsteren WF, DiNola A, Haak JR (1984) Molecular dynamics with coupling to an external bath. *J Chem Phys* **81**: 3684–3690

Betanzos M, Chiang CS, Guy HR, Sukharev S (2002) A large iris-like expansion of a mechanosensitive channel protein induced by membrane tension. *Nat Struct Biol* **9**: 704-710

Birkner JP, Poolman B, Kocer A (2012) Hydrophobic gating of mechanosensitive channel of large conductance evidenced by single-subunit resolution. *Proc Natl Acad Sci U S A* **109**: 12944-12949

Blount P, Moe PC (1999) Bacterial mechanosensitive channels: Integrating physiology, structure and function. *Trends Microbiol* **7**: 420-424

Blount P, Sukharev SI, Schroeder MJ, Nagle SK, Kung C (1996) Single residue substitutions that change the gating properties of a mechanosensitive channel in *Escherichia coli*. *Proc Natl Acad Sci U S A* **93**: 11652-11657

Bordignon E (2012) Site-directed spin labeling of membrane proteins. *Top Curr Chem* **321**:121–57

Chang G, Spencer RH, Lee AT, Barclay MT, Rees DC (1998) Structure of the MscL homolog from mycobacterium tuberculosis: A gated mechanosensitive ion channel. *Science* **282**: 2220-2226

Chiang CS, Anishkin A, Sukharev S (2004) Gating of the large mechanosensitive channel in situ: Estimation of the spatial scale of the transition from channel population responses. *Biophys J* **86**: 2846-2861

Corry B, Hurst AC, Pal P, Nomura T, Rigby P, Martinac B (2010) An improved open-channel structure of MscL determined from FRET confocal microscopy and simulation. *J Gen Physiol* **136**: 483-494

Cruickshank CC, Minchin RF, Le Dain AC, Martinac B (1997) Estimation of the pore size of the large-conductance mechanosensitive ion channel of *Escherichia coli*. *Biophys J* **73**: 1925-1931

Dominguez A, Fernandez A, Gonzalez N, Iglesias E, Montenegro L (1997) Determination of Critical Micelle Concentration of some surfactants by three techniques. *J Chem Edu* **74**: 1227-1231

Esteban-Martin S, Risselada HJ, Salgado J, Marrink SJ (2009) Stability of asymmetric lipid bilayers assessed by molecular dynamics simulations. *J Am Chem Soc* **131**:15194-15202

Folgering JH, Moe PC, Schuurman-Wolters GK, Blount P, & Poolman B (2005) Lactococcus lactis uses MscL as its principal mechanosensitive channel. *J Biol Chem* **280**: 8784-8792

Girard P, Pecreaux J, Lenoir G, Falson P, Rigaud JL, Bassereau P (2004) A new method for the reconstitution of membrane proteins into giant unilamellar vesicles. *Biophys J* **87**: 419-429

Gullingsrud J, Kosztin D, Schulten K (2001) Structural determinants of MscL gating studied by molecular dynamics simulations. *Biophys J* **80**: 2074-2081

Gullingsrud J, Schulten K (2004) Lipid bilayer pressure profiles and mechanosensitive channel gating. *Biophys J* **86**: 3496-3509

Guzman LM, Belin D, Carson MJ, Beckwith J (1995) Tight regulation, modulation, and high-level expression by vectors containing the arabinose PBAD promoter. *J Bacteriol* **177**: 4121-4130

Häse CC, Le Dain AC, Martinac B (1995) Purification and functional reconstitution of the recombinant large mechanosensitive ion channel (MscL) of *Escherichia coli*. *J Biol Chem* **270**: 18329-18334

Hess B, Kutzner C, van der Spoel D, Lindahl E (2008) GROMACS 4: Algorithms for highly efficient, load-balanced, and scalable molecular simulation. *J Chem Theory Comput* **4**: 435–447

Hubbell WL, Cafiso DS, Altenbach C (2000) Identifying conformational changes with site-directed spin labeling. *Nat Struct Biol* **7**:735–739

Humphrey W, Dalke A, Schulten K (1996) VMD: Visual molecular dynamics. *J Mol Graph* **14**: 33–38

Kocer A, Walko M, Feringa BL (2007) Synthesis and utilization of reversible and irreversible light-activated nanovalves derived from the channel protein MscL. *Nat Protoc* **2**: 1426-1437

Kung C, Martinac B, Sukharev S (2010) Mechanosensitive channels in microbes. *Annu Rev Microbiol* **64**: 313-329

Larkin MA, Blackshields G, Brown NP, Chenna R, McGettigan PA, McWilliam H, Valentin F, Wallace IM, Wilm A, Lopez R, Thompson JD, Gibson TJ, Higgins DG (2007) Clustal W and clustal X version 2.0. *Bioinformatics* **23**: 2947-2948

Lee AG (2004) How lipids affect the activities of integral membrane proteins. *Biochim Biophys Acta* **1666**: 62–87

Louhivuori M, Risselada HJ, van der Giessen E, Marrink SJ (2010) Release of content through mechano-sensitive gates in pressurized liposomes. *Proc Natl Acad Sci U S A* **107**: 19856-19860

Lundbæk JA, Collingwood SA, Ingólfsson HI, Kapoor R, Andersen OS (2010) Lipid bilayer regulation of membrane protein function: gramicidin channels as molecular force probes. *J R Soc Interface* **7**: 373–395

Machiyama H, Tatsumi H, Sokabe M (2009) Structural changes in the cytoplasmic domain of the mechanosensitive channel MscS during opening. *Biophys J* **97**: 1048-1057

Maingret F, Patel AJ, Lesage F, Lazdunski M, Honore E (2000) Lysophospholipids open the two-pore domain mechano-gated K(+) channels TREK-1 and TRAAK. *J Biol Chem* **275**: 10128-10133

Mandersloot JG, Reman FC, Van Deenen LL, De Gier J (1975) Barrier properties of lecithin/lysolecithin mixtures. *Biochim Biophys Acta* **382**: 22–26

Markin VS, Sachs F (2004) Thermodynamics of mechanosensitivity. *Phys Biol* **1**: 110-124

Marrink SJ, de Vries AH, Mark AE (2004) Coarse grained model for semiquantitative lipid simulations. *J Phys Chem B* **108**: 750–760

Marrink SJ, Risselada HJ, Yefimov S, Tieleman DP, de Vries AH (2007) The MARTINI force field: coarse grained model for biomolecular simulations. *J Phys Chem B* **111**: 7812–7824

Marsh D (2008) Protein modulation of lipids, and vice-versa, in membranes. *Biochim Biophys Acta* **1778**: 1545–1575

Martinac B, Adler J, Kung C (1990) Mechanosensitive ion channels of *E. coli* activated by amphipaths. *Nature* **348**: 261-263

Martinac B, Buechner M, Delcour AH, Adler J, & Kung C (1987) Pressure-sensitive ion channel in Escherichia coli. *Proc Natl Acad Sci U S A* 84: 2297-2301

Maurer JA, Elmore DE, Lester HA, Dougherty DA (2000) Comparing and contrasting *Escherichia coli* and *Mycobacterium tuberculosis* mechanosensitive channels (MscL). New gain of function mutations in the loop region. *J Biol Chem* **275**: 22238-22244

Mika JT, Birkner JP, Poolman B, Kocer A (2013) On the role of individual subunits in MscL gating: "all for one, one for all?" *FASEB J* **27**: 882-892

Moe PC, Blount P, & Kung C (1998) Functional and structural conservation in the mechanosensitive channel MscL implicates elements crucial for mechanosensation. *Mol Microbiol* **28**: 583-592

Moe PC, Levin G, Blount P (2000) Correlating a protein structure with function of a bacterial mechanosensitive channel. *J Biol Chem* **275**: 31121-31127

Monticelli L, Kandasamy SK, Periole X, Larson RG, Tieleman DP, Marrink SJ (2008) The MARTINI coarse-grained force field: extension to proteins. *J Chem Theory Comput* **4**: 819–834

Morris DA, McNeil R, Castellino FJ, Thomas JK (1980) Interaction of lysophosphatidylcholine with phosphatidylcholine bilayers. A photophysical and NMR study. *Biochim Biophys Acta* **599**: 380–390

Nomura T, Cranfield CG, Deplazes E, Owen DM, Macmillan A, Battle AR, Constantine M, Sokabe M, Martinac B (2012) Differential effects of lipids and lyso-lipids on the mechanosensitivity of the mechanosensitive channels MscL and MscS. *Proc Natl Acad Sci U S A* **109**: 8770-8775

Ollila OHS, Louhivuori M, Marrink SJ, Vattulainen I (2011) Protein shape change has a major effect on the gating energy of a mechanosensitive channel. *Biophys J* **100**: 1651–1659

Ou X, Blount P, Hoffman RJ, Kung C (1998) One face of a transmembrane helix is crucial in mechanosensitive channel gating. *Proc Natl Acad Sci U S A* **95**: 11471-11475

Perozo E, Cortes DM, Sompornpisut P, Kloda A, Martinac B (2002) Open channel structure of MscL and the gating mechanism of mechanosensitive channels. *Nature* **418**: 942-948

Perozo E, Kloda A, Cortes DM, Martinac B (2002) Physical principles underlying the transduction of bilayer deformation forces during mechanosensitive channel gating. *Nature* **9**: 696-703

Sachs F (2010) Stretch-activated ion channels: What are they? *Physiology (Bethesda)* **25**: 50-56

Schneider CA, Rasband WS, Eliceiri KW (2012) NIH image to ImageJ: 25 years of image analysis. *Nat Methods* **9**: 671-675

Steinbacher S, Bass R, Strop P, Rees DC (2007) Structures of the Prokaryotic Mechanosensitive Channels MscL and MscS. In *Current Topics in Membranes,* Hamill OP (ed) vol 58 pp 1-24. Academic Press, New York, USA

Stothard P (2000) The sequence manipulation suite: JavaScript programs for analyzing and formatting protein and DNA sequences. *BioTechniques* **28**: 1102-1104

Suchyna TM, Tape SE, Koeppe RE, Andersen OS, Sachs F, Gottlieb PA (2004) Bilayer-dependent inhibition of mechanosensitive channels by neuroactive peptide enantiomers. *Nature* **430**: 235-240

Sukharev S, Betanzos M, Chiang CS, Guy HR (2001) The gating mechanism of the large mechanosensitive channel MscL. *Nature* **409**: 720-724

Sukharev S, Durell SR, Guy HR (2001) Structural models of the MscL gating mechanism. *Biophys J* **81**: 917-936

Sukharev SI, Martinac B, Arshavsky VY, Kung C (1993) Two types of mechanosensitive channels in the *Escherichia coli* cell envelope: Solubilization and functional reconstitution. *Biophys J* **65**: 177-183

Sukharev SI, Sigurdson WJ, Kung C, Sachs F (1999) Energetic and spatial parameters for gating of the bacterial large conductance mechanosensitive channel, MscL. *J Gen Physiol* **113**: 525-540

van den Bogaart G, Krasnikov V, Poolman B (2007) Dual-color fluorescence-burst analysis to probe protein efflux through the mechanosensitive channel MscL. *Biophys J* **92**: 1233-1240

Vasquez V, Sotomayor M, Cordero-Morales J, Schulten K, Perozo E (2008) A structural mechanism for MscS gating in lipid bilayers. *Science* **321**: 1210-1214

Wiggins P, Phillips R (2005) Membrane-protein interactions in mechanosensitive channels *Biophys J* **88**: 880-902

Wiggins P, Phillips R (2004) Analytic models for mechanotransduction: Gating a mechanosensitive channel. *Proc Natl Acad Sci U S A* **101**: 4071-4076

Yefimov S, van der Giessen E, Onck PR, Marrink SJ (2008) Mechanosensitive membrane channels in action. *Biophys J* **94**: 2994-3002

Yoo J, Cui Q (2009) Curvature generation and pressure profile modulation in membrane by lysolipids: Insights from coarse-grained simulations. *Biophys J* **97**: 2267-2276

Yoshimura K, Batiza A, Schroeder M, Blount P, Kung C (1999) Hydrophilicity of a single residue within MscL correlates with increased channel mechanosensitivity. *Biophys J* **77**: 1960-1972

Yoshimura K, Sokabe M (2010) Mechanosensitivity of ion channels based on protein-lipid interactions. *J R Soc Interface* **7** Suppl 3: S307-20

Zhelev DV (1998) Material property characteristics for lipid bilayers containing lysolipid. *Biophys J* **75**: 321–330

CHAPTER 3

Triggered activation of MscL by Staudinger's Approach: Bio-Orthogonality *in Vitro*

Nobina Mukherjee[1], Marc Robillard[2], George Robillard, Armağan Koçer[1]

[1]Department of Biochemistry, Groningen Biomolecular Sciences and Biotechnology Institute, Zernike Institute for Advanced Materials University of Groningen, Groningen, The Netherlands
[2]Philips Research, High Tech Campus 11, 5656AE Eindhoven

ABSTRACT

This chapter describes the application of a bio-orthogonal reaction, i.e., the Staudinger reaction to command the gating of a mechanosensitive ion channel. To accomplish this, the channel protein, MscL, reconstituted in liposomes was modified with an azide label that could react with a phosphine moiety. Here, we optimized the system and explored the efficiency of the Staudinger reaction for activating MscL-liposomes under physiologically relevant conditions.

INTRODUCTION

Lipid- or polymer-based drug delivery systems have ameliorated the chemotherapy of cancer such as, hepatocelluar carcinoma, sarcoma, immensely by improving the pharmacological properties of free drug (Torchillin, 2005; Schmidinger, 2001; Skubitz, 2003). For example, encapsulation of drugs in lipid vesicles (liposomes) enhances the efficacy of the treatment by increasing the stability of the encapsulated drug and/or inhibiting premature degradation (Allen, 2004). Furthermore, encapsulation of drugs increases the half-life of circulation and lowers side-effects arising from damage of normal tissue by cytotoxic drugs (Allen, 2004). Although liposomal delivery systems have many advantages, they lack the specificity for the target site and an efficient drug release strategy at this site. There have been notable advances in liposomes-based delivery in the form of long-circulating (PEGylated) vesicles and ligand-targeting of the liposomes (Allen, 2013). However, the need for a "triggered drug release" at the target site for more potent treatment and fewer side-effects has not yet been fully satisfied. There are instances where remote triggers such as heat, ultrasound or light are used for releasing the liposomal load (Bibi, 2012). But for applying the above mentioned triggers, external intervention in the form of a microwave device to apply hyperthermia or ultrasound apparatus is required to activate the liposomes (Huang, 1994; Ning, 1994). An alternative is to utilize the endogenous conditions, which are unique to the target site (e.g. a low pH in the vicinity of tumors), to trigger liposomal release. One approach is to incorporate ion channels as sensory-valves in the liposomal delivery system, which renders the liposomes sensitive to the environment and brings about controlled release of the cargo. The ions channels can be modified by attaching chemical labels, such that ion channel becomes responsive to changes in the target environment. In order to tightly regulate the opening of the liposomes, it is necessary to have fine-tuned control over the sensitivity of the liposomes. This can be done by a two-step activation process, i.e. the activation of the liposomes is done in two steps. The first trigger primes the system for activation by the second trigger. The two-step activation process has been applied to the ion channel, MscL, where activation was achieved by light and pH (Kocer, 2006). In the first step, a caged pH actuator was attached to the ion channel. Caging the pH modulator with a photoactive group disabled the protonation of the pH actuator and the channel remained closed irrespective of the pH. Upon removal of the protecting group by illumination (second step), the ion channel became responsive to the ambient pH and the channel opened when the pH dropped below the pK_a of the modulator.

Although light as a second trigger is an ingenious solution for 'triggered release", the depth of penetration of ultraviolet light poses a limitation. A better option is to use a bio-orthogonal reaction as second trigger where a chemical probe primes the channels in the liposomes to be opened by the primary trigger. Several chemical reactions, well established *in vitro,* cannot be used *in vivo* due to the presence of competing nucleophiles

and electrophiles in cells (van Berkel, 2011). For example, Bertozzi et al cited that ketone ligation reactions have limited cellular applications because of the presence of various ketone metabolites in the cells like pyruvate and oxaloacetate (Saxon & Bertozzi, 2000). Therefore, it is necessary to be able to modify liposomes for triggered release with a bio-orthogonal chemical functionality that is not affected by the conditions in the cell. In chemistry there are a few bio-orthogonal chemical reactions such as the Staudinger and the Diels Alder reaction that can serve this goal. Here, we evaluate the Staudinger reaction for controlled release from a liposomal delivery system, comprising of an ion channel as the environment sensitive nanovalve. The Staudinger reaction takes place between a phosphine and an organic azide that leads to the formation of an azaylide intermediate (Staudinger, 1919; Kohn & Breinbauer, 2004; Sletten, 2011). The hydrolysis of the azaylide produces a primary amine and phosphine oxide (Figure 1). This reaction is a mild way of reducing an azide, which is physiologically inert, stable, and rarely present in biological systems, to an amine. Further, both azide and phosphine do not react with bio-molecules and cause no toxicity. Triphenylphosphine is commonly used as a reducing agent, yielding triphenylphosphine oxide as the side product in addition to the amine. A variation of the Staudinger reaction, the Staudinger ligation has been

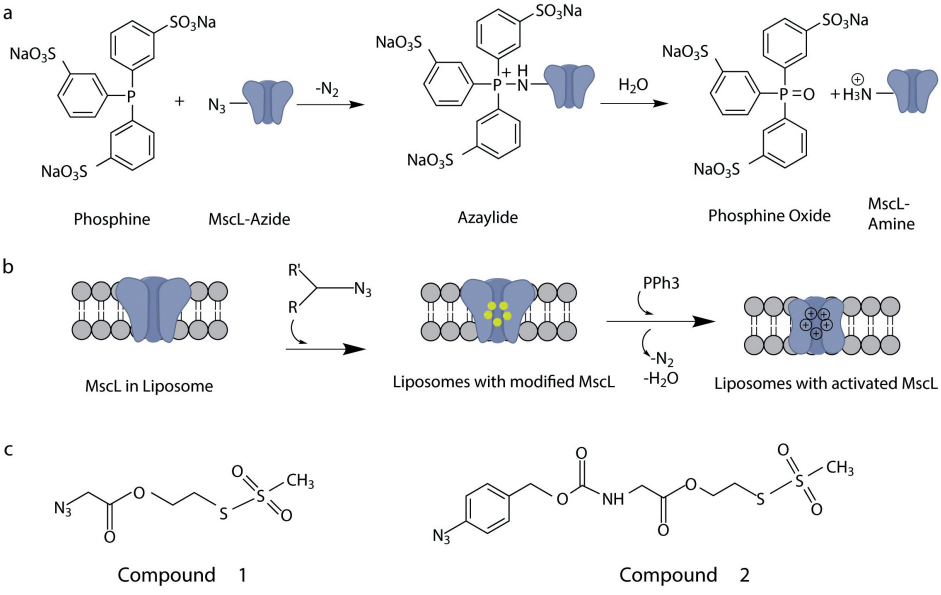

Figure 1. The principle of Staudinger's reaction. a) Staudinger reaction is a mild method of reducing an azide to an amine. Triphenylphosphine is used as a reducing agent, yielding triphenylphosphine oxide as the side product in addition to the primary product, amine. b) Azide-labelled MscL is activated by triphenylphosphine to induce opening of the channel. c) Two different azide variants, compound **1** and compound **2**, were used to label MscL.

extensively used in bioconjugation for labelling proteins or antibodies with dyes and imaging agents (Dube, 2006; van Dongen, 2009; Liu, 2010; Lemieux, 2003).

In this work, we design the azide functionality on the basis of a previously used pH-sensitive molecule (**Compound 1**, see Fig.1) (Kocer, 2006). **Compound 1** is attached to the pore of MscL. When the modified channel is embedded in the drug-loaded liposomes, the drug is released upon a decrease in the ambient pH. The working principle is as follows: if the liposomes encounter an acidic environment, i.e. a pH lower than the pKa of the chemical actuator, the group gets protonated and the protein pore acquires positive charges and opens. By using an azide variant and using the Staudinger reaction to command the pH sensitivity, we gain two-step control over the release of cargo from liposomes. Labelled MscL will not be pH-sensitive until the Staudinger reaction generates the amine group from an azide. Upon entering a low pH environment, MscL will release the internal cargo at the therapeutic site.

In this study, azide-labelled MscL is reconstituted in PEGylated-liposomes and the controlled release of a model compound through the channel is studied by fluorescence dequenching at 37 ˚C. We test the release at different pH's and in the presence and absence of fetal bovine serum. Our results show that- (i) the Staudinger reaction is compatible with MscL-liposome system under physiological conditions (serum in the buffer, temperature of 37 ˚C); and ii) Staudinger reaction is more efficient in the presence of serum than in the buffer.

MATERIALS AND METHODS

Synthesis of Compound 1

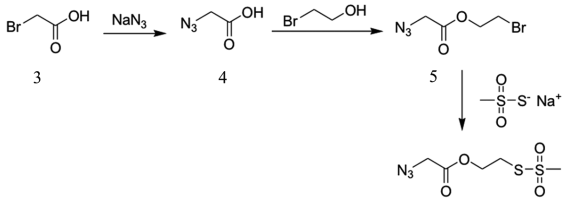

Compound 1 was prepared following a published procedure disclosed in Banaszynski et al. (2005). Compound 5 was prepared by adding bromoethanol (7.3 mL, 102 mmol) to azide 4 (1.03 gram, 10.2 mmol). The pink solution was cooled to 0°C and thionylchloride (0.94 ml, 13 mmol) was added drop-wise over a period of 10 min, keeping the reaction mixture below 10 °C. The reaction mixture was stirred at RT for 1h and subsequently toluene (150 ml) was added and the solution was evaporated. To the resulting light brown liquid dichloromethane (100 ml) was added and the solution was washed with water (3 x 100 ml), brine, dried over $MgSO_4$, filtered and evaporated.

Column chromatography (silica gel, dichloromethane) afforded 5 as a colourless liquid (1.60 gram, 7.7 mmol, 75 %). 1H NMR (300 MHz, CDCl3) δ 4.52 (t, 2H, J = 6.0 Hz), 3.95 (s, 2H), 3.55 (t, 2H, J = 6.0 Hz). 13C NMR (75 MHz, CDCl3) δ 155.9, 65.5, 65.3, 50.6, 28.5. GCMS: m/z: 208 [M + H]+. The azide 1 was obtained by adding sodium MTS (1.14 gram, 8.5 mmol) to a solution of 5 (1.60 gram, 7.7 mmol) in DMF (8 ml). The mixture was stirred at 70°C for 5 h. A white precipitate formed, which was filtered off, and the yellow solution was evaporated, affording a yellow liquid mixed with a white solid. Addition of chloroform to the mixture resulted in more white precipitate, which was again filtered off. The yellow solution was evaporated and the resulting liquid purified by column chromatography (silica gel, chloroform/ethylacetate, 9/1) yielding 1 as a slightly tanned liquid (1.18 gram, 4.9 mmol, 64 %). [1]H NMR (300 MHz, CDCl3) δ 4.52 (t, 2H, J = 6.1 Hz), 3.94 (s, 2H), 3.45 (t, 2H, J = 6.1 Hz), 3.38 (s, 3H). [13]C NMR (75 MHz, CDCl3) δ 155.9, 64.0, 51.4, 50.6, 35.1. GCMS: m/z: 240 [M + H]+, 257 [M + NH4]+. IR: 2130 cm-1 (azide). Anal. Calcd for C5H9N3O4S2: C, 25.10; H, 3.79; N, 17.56; S, 26.80; O, 26.80. Found: C, 25.3; H, 3.8; N, 17.3; S, 27.1, O, 26.8.

Synthesis of Compound 2

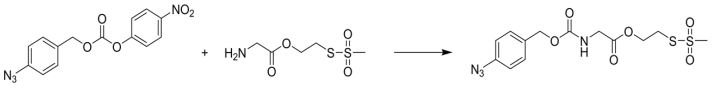

6 7 **Compound 2**

Compound 6 was prepared following a published procedure as in Robillard 2008. Compound 7 was prepared following a published procedure in Kocer et al.. 2006. Compound 7 (132.5 mg, 0.62 mmol) and azide derivative 6 (576 mg, 1.83 mmol) were dissolved in DMF (45 mL). Triethylamine (0.5 mL) was added and the resulting bright yellow solution was stirred in the dark at RT overnight. The reaction mixture was evaporated under reduced pressure and the resulting yellow oil was purified by silica column chromatography with diethylether. Pure compound 2 was collected as orange oil in a yield of 50 % (121.5 mg, 0.313 mmol). [1]H NMR (300 MHz, CDCl3) δ 7.29 (d, 2H, J = 8.3 Hz), 6.9 (d, 2H, J = 8.3 Hz), 5.2 (br t, 1H), 5.1 (s, 2H), 4.4 (t, 2H, J = 6.1 Hz), 4.0 (d, 2H, J = 5.9 Hz), 3.4 (t, 2H, J = 6.1 Hz), 3.3 (s, 3H). [13]C NMR (75 MHz, CDCl3) δ 170.1 (C), 156.6 (C), 140.5 (C), 133.3 (C), 130.3 (CH), 119.6 (CH), 67.0 (CH2), 63.7 (CH2), 51.3 (CH3), 43.1 (CH2), 35.2 (CH2). Anal calcd for C13H16N4O6S2: C 40.20, H 4.15, N 14.42, S 16.51; found: C 40.51, H 4.16, N 13.99, S 16.15. HPLC (A: 0.1% formic acid in H2O; B: 0.1% formic acid in ACN; 5 to 95 % B in 25 min): 14.7 min.

Strains and cell growth

E. coli PB104 (ΔmscL::Cm) (Blount, 1996a) was used to host the p1BAD expression constructs (Birkner, 2012), containing *mscl* from *E. coli*. A single colony of PB104

was used for inoculating an overnight culture in TY (Tryptone-Yeast extract) media supplemented with ampicillin (100 µg/ml) and chloramphenicol (10 µg/ml). Subsequent cultures were routinely grown in TY media containing ampicillin (100 µg/ml) in a shaker-incubator at 37 °C, rotated at 250 cycles/min. Alternatively, the cells were grown in a 2 L bioreactor using TY media supplemented with the appropriate antibiotics. Protein expression was initiated by adding 0.1% (w/v) L-arabinose and 0.4% (v/v) glycerol as an alternative carbon source. The cells were further grown for another two hours before harvesting. Cell disruption was done in a Constant Cell Disruptor (Constant Systems Ltd.), at 25,000 psi. This step was followed by differential centrifugation at 30 min at 18,460 g and 145,400 g for 90 min at 4 °C to obtain membrane vesicles.

Lipid preparation for reconstitution

In this study two types of lipid compositions were used: Azolectin or Soy PC (20%) (Avanti polar lipids, Cas no: 8030-76-0) and DOPC: cholesterol: DSPE-PEG2000 (Avanti polar lipids). A chloroform solution of DOPC, cholesterol plus DSPE-PEG 2000 at a molar ratio 70:20:10 was dried (rotary evaporator) and rehydrated in 150 mM NaCl, 10 mM sodium-phosphate pH 8.0 to yield a final lipid concentration of 20 mg/ml final. Subsequently, seven freeze-thaw cycles were performed with rapid freezing in liquid N_2, and thawing in a waterbath at 60 °C. Aliquots of 1 ml were stored at -80 °C.

Protein Isolation and Labelling

His-tagged G22C-MscL was purified by nickel-nitriloacetic acid (Ni-NTA) affinity chromatography, as described in (Kocer, 2007). Briefly, membrane vesicles were solubilized at 5 mg/ml in 50 mM sodium phosphate (pH 8.0), 300 mM NaCl, 1% (vol/vol) Triton X-100, and 35 mM imidazole (solubilization buffer) for 30 min at 4 °C. After ultracentrifugation at 267,000 g for 20 min at 4 °C, the supernatant was applied to Ni-NTA agarose resin (Qiagen) [30 mg membrane protein/mL per 50% (wt/vol) slurry], which was pre-equilibrated with 10 column volumes (CV) of solubilization buffer, and incubated under mild agitation for 30 min at 4 °C. Unbound material was collected as a flow through. The column was washed consecutively with 15 CV wash buffer [50 mM sodium phosphate (pH 8.0), 300 mM NaCl, 0.2% (vol/vol) Triton X-100]. Then, 1 mg/ml final concentration of the azide label was added to the slurry and mixed with G22C-MscL; incubation for 30 min at room temperature. The non-specific proteins were washed off the affinity column with 7.5 CV L-histidine wash buffer [50 mM sodium phosphate (pH 8.0), 300 mM NaCl, 0.2% (vol/vol) Triton X-100, 50 mM histidine]. His-tagged proteins were eluted by the addition of 15× 0.5 CV Ni-NTA elution buffer [50 mM sodium phosphate (pH 8.0), 300 mM NaCl, 0.2% (vol/vol) Triton X-100, 235 mM L-histidine]. The protein content of the fractions was checked with a Bradford assay. The average concentration of labelled protein was around 0.42 mg/ml.

Protein reconstitution in LUVs

The concentration of MscL-his tagged proteins was determined with the Bradford assay. MscL was reconstituted into liposomes by a detergent-mediated reconstitution method, as described before (Kocer, 2006). The liposomes that were prepared as explained above were thawed and extruded through a 400 nm filter (11 times). Liposomes were destabilized by the addition of 10% Triton X-100 in detergent:lipid volume ratio of 1:10. The amount of Triton X-100 for liposome destabilization was determined by the lipid titration method. Next, protein and detergent-destabilized liposomes were mixed at a 1:50 weight ratio of protein and lipid, and incubated for 30 minutes at 50 °C. Subsequently, the appropriate buffer (for fluorescence dequenching assay: 200 mM calcein in 10 mM sodium-phosphate pH 8.0) was added in 1:1 volume ratio and supplemented with 10mg (wet weight) Biobeads (SM-2 Absorbents) for 100 µl liposomes. For detergent removal, the sample was incubated overnight (~16 hours) at 4 °C on a rotating plate. The resulting proteoliposomes were used for dequenching experiments as explained below.

Fluorescence dequenching assay

The free calcein in the bulk solution after protein reconstitution was removed by passing the liposomes through a Sephadex-G50 size exclusion column. Calcein-containing proteoliposome fractions were tested for MscL activity. In a standard assay, 2 µl of calcein-filled proteoliposomes were diluted into 2100 µl of iso-osmotic efflux buffer. In order to mimic the biologically relevant media, this buffer was substituted with 5, 10, 15, 20% Fetal Bovine serum mixed with 10 mM sodium phosphate (pH 8.0), 150 mM NaCl. The channel was activated by triphenylphosphine following the Staudinger reaction; two other channel activators were used as controls; i.e. MTSET ([2-(Trimethylammonium) ethyl] methanethiosulfonate) and LPC (Lysophosphatidylcholine). The activity of the channel was represented by the increase in the fluorescence signal due to release of calcein. We follow the time course of release of calcein through MscL *in situ* upon addition of 100 µM of triphenylphosphine, 2 mM MTSET or 4 µM LPC. LPC was purchased from Avanti polar lipids. MTSET and bio-beads (Bio-Beads SM-2 adsorbents) were from Anatrace and Bio-Rad Laboratories B.V., respectively. The calcein dequenching assay was done in Varian Cary Eclipse Fluorimeter at an excitation wavelength of 497 nm and emission at 516 nm. After the base reading, different triggers were added and the calcein release was measured continuously under gentle stirring at 37°C. The maximum fluorescence of the sample was determined by bursting the proteoliposomes by the addition of 0.5 % (v/v) final concentration of Triton X-100. As a control, the background release from liposomes without MscL was recorded.

RESULTS

Staudinger reaction activates MscL-liposomes

For the modification of MscL, we first used compound **1**. We followed the progression of the Staudinger reaction on MscL protein by ESI-MS (Fig 2). The azide-labelled MscL channel in detergent was incubated with 5 mM triphenylphosphine at 37 ˚C and samples were taken at time points 0, 2, 8, and 20 h. At time zero, all MscL subunits were labelled with the azide and had a mass to charge ratio of 15,856 amu. We did not detect unlabelled MscL with a mass/charge (m/z) ratio of 15,697 amu. However, within 2 hr, even though the product of the Staudinger reaction (amine labelled MscL) already started to appear at the expected m/z of 15,830 amu, unlabelled MscL also appeared in the mixture due to reduction of disulphide bond between azide and MscL by triphenylphosphine. Finally, only unlabelled protein was left. After testing different triphenylphosphine concentrations, 100 µM was found to be optimal.

Next, the activity of compound **1**-labelled protein reconstituted in model liposomes, triggered by the triphenylphosphine (PPh3), was studied by an *in vitro* fluorescence dequenching assay (Fig 3a). Even though the channel was fully labelled, as evidenced by ESI-MS (electron spray-ionization mass spectrometry) measurements, the liposomal

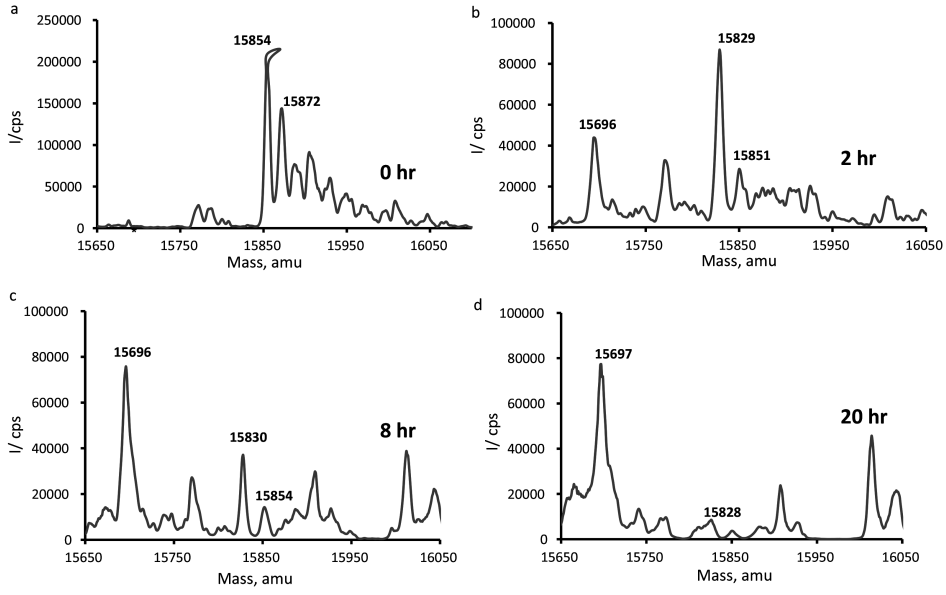

Figure 2. ESI-MS spectra of azide labelled MscL in detergent, showing the gradual formation of amine-labelled MscL, mass in atomic mass unit (amu) in X-axis and intensity in counts per second (cps) in Y-axis: (a) at 0h, a prominent peak of azide labelled MscL at 15,854 amu; (b) formation of amine-MscL at 15,830 amu at 2h; (c) at 8h, along with amine-MscL peak, native MscL appears at 15,696 amu; (d) Native MscL peak at 20h.

release was very low. In order to optimize the system towards getting higher and faster release, the more reactive compound **2** (refer Fig. 1) was synthesized.

MscL was successfully labelled with compound **2**. Triggered liposomal release from compound **2**-labelled MscL liposomes was performed at pH 7.4 and pH 6 at 37 ˚C (Fig 2b). 100 μM PPh3 was enough and sufficient to open MscL in proteoliposomes. Full release of liposomal content was completed within 3 hrs. In another experiment, proteoliposomes were activated by hourly addition of 100 μM phosphine during 3 hr incubation; however, the additional phosphine did not increase the amount of release.

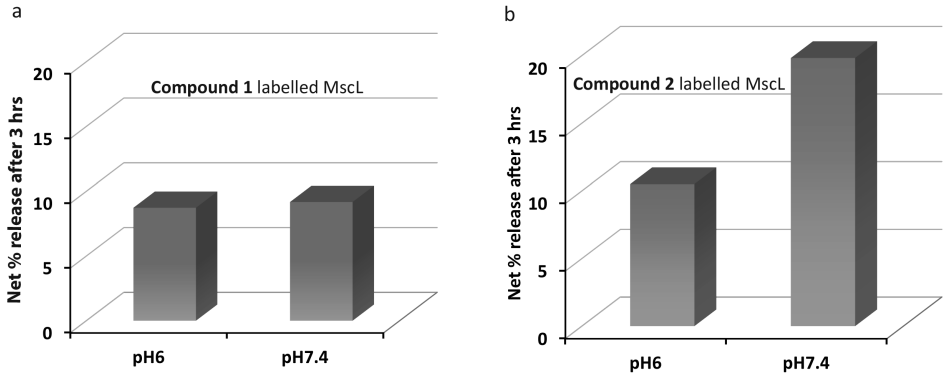

Figure 3. Net release of calcein from proteoliposomes in buffer of pH 6 and pH 7.4 by using the Staudinger's reaction. a) MscL is labelled with compound 1. b) MscL is labelled with compound 2. 100uM of triphenylphosphine was used to trigger opening of the channels.

PEGylation of liposomes does not inhibit activation of MscL by the Staudinger reaction

After showing that the Staudinger reaction works *in vitro*, using conventional liposomes, we next tested the sensitivity and selectivity of this reaction in stealth liposomes. A common approach in the drug delivery field is to reduce the recognition of nanocarriers by the reticuloendothelial system (RES), which is done by covering their surface with polyethylene glycol groups (Caliceti and Veronese, 2003; Alexis, 2008). In our study, coating of the surface was achieved by having pegylated lipids in the reconstitution mixture and the resulting liposomes are named "stealth liposomes". PEG-coating significantly reduces the clearance of liposomes by the innate immune system of the body and increases the circulation time of the liposomes. The liposomes consisted of DOPC, cholesterol and DSPE.PEG-2000 in molar ratio of 70:20:10. Azide-labelled MscL was reconstituted in the stealth liposomes and the activity, triggered by 100 μM triphenylphosphine (PPh3), was measured by fluorescence dequenching of calcein (Fig.4 a). Two other triggers were also used in the assay, namely LPC and MTSET, which

served as controls for channel functionality and labelling efficiency, respectively. LPC has been previously shown to activate the MscL upon insertion into the membrane (Perozo, 2002), whereas MTSET brings positive charge to the constriction site of the pore (Yoshimura, 2001). When triphenylphosphine was applied, 60% release of calcein was observed from azide-labelled MscL liposomes after 22 h, in buffers of pH 6.0 and pH7.0 and at 37˚C. Activation with LPC, gave 80% release of calcein after 22 h. Addition of MTSET led to 34% release, implying that some of the cysteine residue are not modified with the azide label and are available for reaction with MTSET. As a negative control, liposomes without any channel were used, and only background leakage of 20% was seen after 22h. In summary, we show that Staudinger's reaction is also taking place in stealth liposomes. Triphenylphosphine can penetrate the mesh formed by the PEG layer and find its partner, azide moiety, in the pore of the channel and convert it into an amine, thereby triggering the channel gating and efflux of the dye from the liposomes.

ESI-MS was performed to monitor the activation of azide-labelled MscL by triphenylphosphine. When azide-labelled MscL in detergent (m/z: 15,856 amu) was allowed to react with 100 μM of triphenylphosphine, at 37°C, we could follow the gradual conversion of azide to amine. The ESI-MS result showed that the Staudinger's reaction is taking place in the pore of the channel, leading to the appearance of a peak at the expected m/z ratio of 15,830 amu. The ratio of amine labelled MscL to azide labelled MscL at 30 min was 4.25, which doubled to 7.6 in 2.5 h, (Fig. 4b). There were some unlabelled MscL channels (m/z: 15,697 amu) at 30 min. Further, it was also seen from the MS data that triphenylphosphine reduced the disulphide bond between the protein and the azide/amine, giving rise to a higher unlabelled protein peak at 15,697 amu. The longer the duration of the reaction with triphenylphosphine, the higher amount of native protein was produced. The ratio of amine-labelled MscL to native MscL at 30 min was 5.6, which decreased to 1.8 after 2.5 h. Even after 5 h of incubation with triphenylphosphine, unlabelled G22C sample, gave no peak at 15,830 amu. This implies that no product was formed and that the azide label is necessary for the Staudinger reaction to take place (Fig. 4c).

Bio-orthogonality in vitro: Staudinger's Reaction at physiological conditions can trigger opening of pH-sensitive MscL inserted in stealth liposomes

To address the general usefulness and application of the Staudinger reaction in biologically compatible media, we supplemented the buffer with serum (Arigony, 2013). The buffer composed of 10mM sodium phosphate, 150mM NaCl of pH 6.0 and pH 7.0 was supplemented with 5%, 10%, 15% or 20% total Fetal Bovine Serum (FBS). In order to activate azide-labelled MscL in the stealth liposomes, we used 100 μM triphenylphosphine. As controls, stealth-liposomes with unlabelled MscL or without MscL were tested in the presence of triphenylphosphine. Figure 5 shows that the azide-labelled liposomes and triphenylphosphine are stable in the presence of 20% of serum. In fact, serum up to 5%

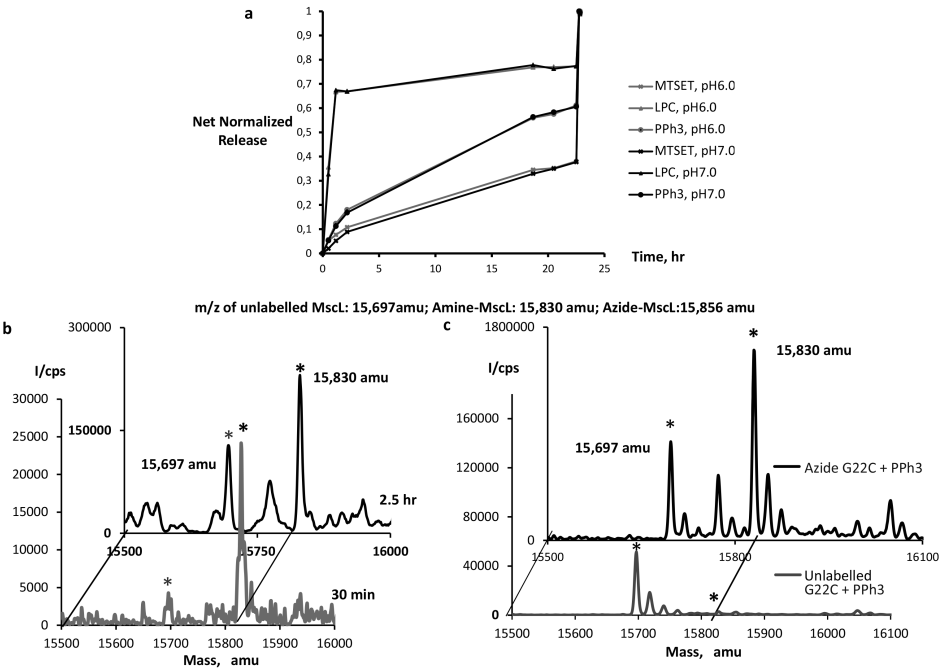

Figure 4. (a) Normalised calcein release from Stealth Liposomes. Release from azide-labelled MscL reconstituted in liposomes upon addition of triphenylphosphine, LPC or MTSET as triggers. (b) ESI-MS spectra of MscL in detergent, showing the gradual formation of amine-labelled MscL: a prominent peak of azide-labelled MscL is visible at 15,830 amu (c) ESI-MS spectra showing the effect of PPh3 on labelled and unlabelled MscL in detergent. Unlabelled MscL is visible at 15,830 amu.

even enhanced the release of calcein from azide-labelled liposomes. (Fig.5). The pH also had a prominent effect on the release, which was higher at pH 6.0, as expected because the higher level of protonation of the protein-attached amine opens the MscL channel further. The release was between 45% to 50% at pH 6.0 for 5% to 20% serum. At pH 7.0, a maximum release of 35% was seen in 20% serum (Fig.5b).

Serum or pH differences in the buffers did not have visible effect on the release of calcein from liposomes without MscL. Overall, our results show that serum boosts the release of dye via azide-labelled MscL and activation of the channel by triphenylphosphine.

To investigate whether there was any interaction between serum and azide of the protein, or serum and triphenylphosphine, ESI-MS was done with azide-labelled and unlabelled MscL proteoliposomes in the presence of 20% serum and 100 μM triphenylphosphine at 37°C (Fig. 6). The data show that the ratio of amine-labelled Mscl to azide-labelled MscL is 1.9 after 5 h of reaction, whereas the ratio of amine-labelled MscL to native MscL is 3.5. This suggests that there was less back conversion to native protein in the presence of serum when MscL was reconstituted in liposomes as compared to MscL dispersed in detergent.

ESI-MS data showed that no additional compounds were formed when serum, triphenylphosphine and azide-labelled protein were present together. The labelled peak of the product appeared at the expected mass (15830 amu) and the native protein gave a peak at 15697 amu. However, serum had some indirect effects on the reaction: (i) the progression of the Staudinger reaction was slowed down in presence of serum compared to that in the absence of serum, as is evident from the ratio of amine- to azide-labelled MscL peaks in ESI-MS; and (ii) the re-conversion of amine-labelled MscL to native MscL was decreased. These observations suggest that serum may sequester triphenylphosphine.

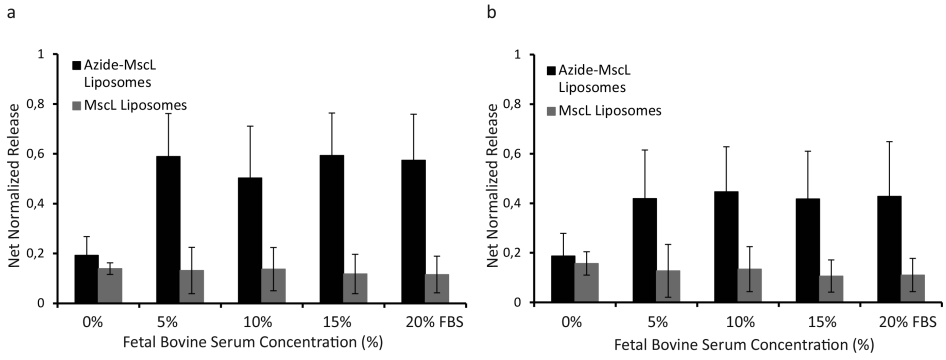

Figure 5. Net release of calcein via azide-labelled and unlabelled MscL in stealth-liposomes at pH6.0 (n=5) (a) and pH 7.0 (n=5) (b) Serum. Triphenylphosphine is added at a concentration of 100μM and the release is followed for 3.5 h at 37°C.

DISCUSSION

Here, we describe the performance of a bio-orthogonal reaction in a biologically relevant medium at physiological conditions carried out *in vitro*. We show that the Staudinger reaction elicited the release of liposomal cargo via MscL modified with azide at the constriction site of the pore. The method involves a two-step triggering mechanism: (i) the protein is pre-labelled with a caged azide modulator (compound **2**), and (ii) secondary activation via a bio-orthogonal and biocompatible, Staudinger reaction, creates the pH-responsive functionality in the pore. Moreover, the size of the azide group is small, so that it can be attached to a protein without much effect on the local conformation (van Berkel, 2011).

MscL protein does not contain any cysteine in its amino acid sequence (Sukharev, 1999). However, the protein was engineered such that it contains a cysteine residue at the 22nd position, where the azide group was linked via a disulfide bond. The azide group also does not carry any charge. Upon reaction with a phosphine, the azide group is converted into a primary amine, which gets protonated below its pKa. Thus, the primary amine charges the pore of MscL when the ambient pH becomes lower than

its pK_a, which brings about opening of the channel. We also show that serum did not interfere with the Staudinger reaction. Our work indicates that azide-labelled MscL-liposomes are effectively triggered by the triphenylphosphine in presence of serum, at acidic (pH 6.0) to neutral pH. The enhanced release of the cargo may be due to sequestering of triphenylphosphine by serum, which decreases the rate of oxidation of triphenylphosphine and in turn increases its availability over time. Further, sequestering of triphenylphosphine also lowers the cleavage of the disulphide bond in the labelled protein. This, in turn, ensures that more labelled MscL is present over longer periods of time. Another important observation is that substitution of buffer with serum leads to stabilization of liposomes and lowers the non-specific leakage from unlabelled proteoliposomes. In the literature, there are claims that the presence of serum in the media stabilizes liposomes (Mercadal, 1995).

Further, due to the bio-compatibility and selectivity of the Staudinger reaction, this system can be translated to *in vivo* drug delivery systems for controlled release of cargo.

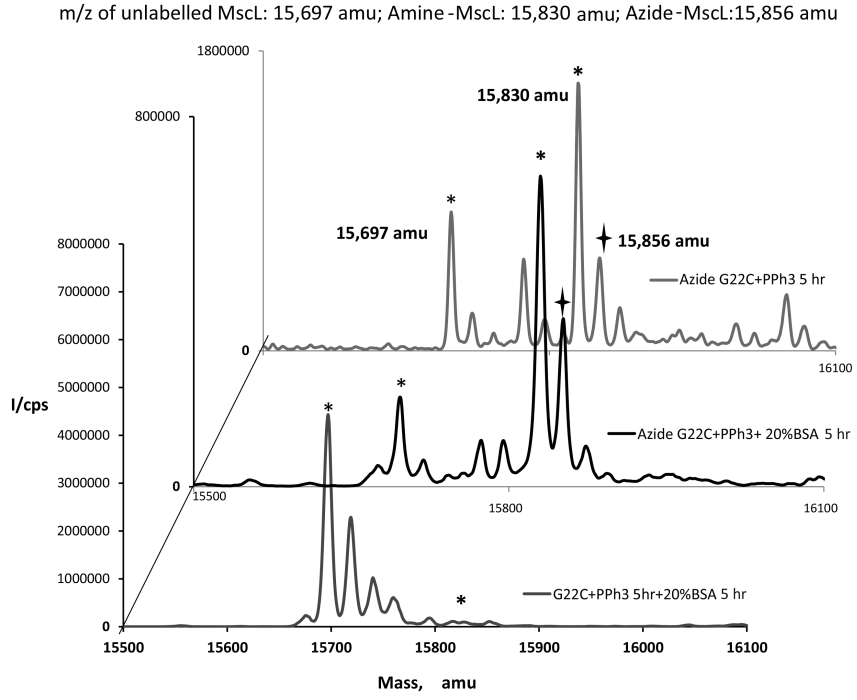

Figure 6. ESI-MS of azide-labelled and unlabelled MscL treated with triphenylphosphine in proteoliposomes at 37°C: The effect of Fetal Bovine Serum on labelled and unlabelled MscL in proteoliposomes in the presence and absence of triphenylphosphine. Fetal Bovine Serum does not interfere with the product formation but sequesters triphenylphosphine and retards its oxidation, which indirectly boosts activation of MscL.

The first step would involve administration of drug-loaded liposomes containing an azide-labelled MscL, which is followed by administration of a phosphine to trigger the opening of MscL and release of the drug. A study on doxorubicin-azide prodrug activated by the Staudinger reaction showed that only upon addition of triphenylphosphine the prodrug was converted to active doxorubicin and had an antiproliferative effect on human vulvar skin squamous carcinoma cells (van Brakel, 2008). It was also shown that triphenylphosphine alone did not inhibit any cell growth.

There are very few chemical reactions that can be applied *in vivo* due to issues regarding toxicity, bio-compatibility and selectivity. For example, an adaptation of Staudinger reaction is the Staudinger ligation method, which has found wide application in biology over the last decades. This ligation method employs a phosphine and an azide, which forms non-toxic components as shown *in vivo* in a rat model (Prescher, 2004). For *in vivo* applications, another important aspect is the lipid composition of the liposomes. In order to have a physiologically relevant formulation, the liposomes are derived from a lipid composition that is mainly neutral in nature. Thus, when the system is applied for *in vivo* delivery purposes, the liposomes should not be removed easily from the blood stream by the Mononuclear Phagocytic System (MPS) or the reticuloendothelial system (RES) in the kidney, liver or spleen. Coating of liposomes with polyethylene glycol (PEG) ensures that they are not taken up by the innate immune system, and this increases the half-life of the liposomes in circulation (Blume, 1990; Klibanov, 1990; Senior, 1991). PEGylation provides a protective layer and slows down liposomal recognition by opsonins, making them "stealth" (Klibanov, 1990). Controlled release of drugs or other small molecules ensures that the local bio-availability is enhanced, whereas systemically there will be hardly any release. This will enhance the therapeutic efficiency and decrease the toxic side effects at the same time.

CONCLUSION

Control over cargo release via the Staudinger reaction ensures that we do not have to rely on disease-specific markers to design customized therapy. Recent advances in design of multifunctional delivery systems have lead to increased complexity, which poses problems in their production. It is necessary to develop simple and generic delivery systems, which can be effectively controlled to release their cargo by bio-compatible triggers. Our findings will find application in the further development of advanced drug delivery systems and their use *in vivo*.

REFERENCES

Alexis F, Pridgen E, Molnar LK, & Farokhzad OC (2008) Factors affecting the clearance and biodistribution of polymeric nanoparticles. *Mol Pharm* **5**: 505-515

Allen TM & Cullis PR (2013) Liposomal drug delivery systems: from concept to clinical applications. *Adv Drug Deliv Rev* **65**: 36-48

Allen TM & Cullis PR (2004) Drug delivery systems: entering the mainstream *Science* **303**: 1818-1822

Arigony AL, de Oliveira IM, Machado M, Bordin DL, Bergter L, Pra D, & Henriques JA (2013) The influence of micronutrients in cell culture: a reflection on viability and genomic stability. *Biomed Res Int* **2013**: 597282

Bibi S, Lattmann E, Mohammed AR, & Perrie Y (2012) Trigger release liposome systems: local and remote controlled delivery? *J Microencapsul* **29**: 262-276

Birkner JP, Poolman B, & Kocer A (2012) Hydrophobic gating of mechanosensitive channel of large conductance evidenced by single-subunit resolution. *Proc Natl Acad Sci U S A* **109**: 12944-12949

Blount P, Sukharev SI, Moe PC, Schroeder MJ, Guy HR, & Kung C (1996) Membrane topology and multimeric structure of a mechanosensitive channel protein of Escherichia coli. *EMBO J* **15**: 4798-4805

Blume G & Cevc G (1990) Liposomes for the sustained drug release in vivo. *Biochim Biophys Acta* **1029**: 91-97

Caliceti P & Veronese FM (2003) Pharmacokinetic and biodistribution properties of poly(ethylene glycol)-protein conjugates. *Adv Drug Deliv Rev* **55**: 1261-1277

Dube DH, Prescher JA, Quang CN, & Bertozzi CR (2006) Probing mucin-type O-linked glycosylation in living animals. *Proc Natl Acad Sci U S A* **103**: 4819-4824

Huang SK, Stauffer PR, Hong K, Guo JW, Phillips TL, Huang A, & Papahadjopoulos D (1994) Liposomes and hyperthermia in mice: increased tumor uptake and therapeutic efficacy of doxorubicin in sterically stabilized liposomes. *Cancer Res* **54**: 2186-2191

Klibanov AL, Maruyama K, Torchilin VP, & Huang L (1990) Amphipathic polyethyleneglycols effectively prolong the circulation time of liposomes. *FEBS Lett* **268**: 235-237

Kocer A, Walko M, Bulten E, Halza E, Feringa BL, & Meijberg W (2006) Rationally designed chemical modulators convert a bacterial channel protein into a pH-sensory valve. *Angew Chem Int Ed Engl* **45**: 3126-3130

Kocer A, Walko M, & Feringa BL (2007) Synthesis and utilization of reversible and irreversible light-activated nanovalves derived from the channel protein MscL. *Nat Protoc* **2**: 1426-1437

Kohn M & Breinbauer R (2004) The Staudinger ligation-a gift to chemical biology. *Angew Chem Int Ed Engl* **43**: 3106-3116

Lemieux GA, De Graffenried CL, & Bertozzi CR (2003) A fluorogenic dye activated by the staudinger ligation. *J Am Chem Soc* **125**: 4708-4709

Liu CC & Schultz PG (2010) Adding new chemistries to the genetic code. *Annu Rev Biochem* **79**: 413-444

Mercadal M, Domingo JC, Bermudez M, Mora M, & De Madariaga MA (1995) N-palmitoylphosphatidylethanolamine stabilizes liposomes in the presence of human serum: effect of lipidic composition and system characterization. *Biochim Biophys Acta* **1235**: 281-288

Ning S, Macleod K, Abra RM, Huang AH, & Hahn GM (1994) Hyperthermia induces doxorubicin release from long-circulating liposomes and enhances their anti-tumor efficacy. *Int J Radiat Oncol Biol Phys* **29**: 827-834

Perozo E, Kloda A, Cortes DM, & Martinac B (2002) Physical principles underlying the transduction of bilayer deformation forces during mechanosensitive channel gating. *Nature* **9**: 696-703

Saxon E & Bertozzi CR (2000) Cell surface engineering by a modified Staudinger reaction. *Science* **287**: 2007-2010

Schmidinger M, Wenzel C, Locker GJ, Muehlbacher F, Steininger R, Gnant M, Crevenna R, & Budinsky AC (2001) Pilot study with pegylated liposomal doxorubicin for advanced or unresectable hepatocellular carcinoma. *Br J Cancer* **85**: 1850-1852

Senior J, Delgado C, Fisher D, Tilcock C, & Gregoriadis G (1991) Influence of surface hydrophilicity of liposomes on their interaction with plasma protein and clearance from the circulation: studies with poly(ethylene glycol)-coated vesicles. *Biochim Biophys Acta* **1062**: 77-82

Skubitz KM (2003) Phase II trial of pegylated-liposomal doxorubicin (Doxil) in sarcoma. *Cancer Invest* **21**: 167-176

Sletten EM & Bertozzi CR (2011) From mechanism to mouse: a tale of two bioorthogonal reactions. *Acc Chem Res* **44**: 666-676

Staudinger H & Meyer J (1919) Uber neue organische phosphoverbindungen III. Phosphinmethlenderivate und phosphimimine. *Helv. Chim. Acta.* **2**: 635-646

Sukharev S (1999) Mechanosensitive channels in bacteria as membrane tension reporters. *FASEB J* **13 Suppl**: S55-61

Torchilin VP (2005) Recent advances with liposomes as pharmaceutical carriers. *Nat Rev Drug Discov* **4**: 145-160

van Berkel SS, van Eldijk MB, & van Hest JC (2011) Staudinger ligation as a method for bioconjugation. *Angew Chem Int Ed Engl* **50**: 8806-8827

van Brakel R, Vulders RC, Bokdam RJ, Grull H, & Robillard MS (2008) A doxorubicin prodrug activated by the staudinger reaction. *Bioconjug Chem* **19**: 714-718

van Dongen SF, Teeuwen RL, Nallani M, van Berkel SS, Cornelissen JJ, Nolte RJ, & van Hest JC (2009) Single-step azide introduction in proteins via an aqueous diazo transfer. *Bioconjug Chem* **20**: 20-23

Yoshimura K, Batiza A, & Kung C (2001) Chemically charging the pore constriction opens the mechanosensitive channel MscL. *Biophys J* **80**: 2198-2206

CHAPTER 4

Image guided drug release from pH-sensitive ion channel-functionalized stealth liposomes into an *in vivo* glioblastoma model

Nobina Mukherjee [1, †], Jesus Pacheco-Torres [2, †], Martin Walko[3], Pilar Lopez[2], Paloma Ballesteros[4], Sebastian Cerdan[2] and Armagan Kocer[1]

[1] Groningen Biomolecular Sciences and Biotechnology Institute, University of Groningen, Nijenborgh 4, 9747 AG Groningen, The Netherlands
[2] Instituto de Investigaciones Biomédicas "Alberto Sols" CSIC/UAM, Arturo Duperier 4, Madrid 28029, Spain
[3] Institute of Chemistry, Faculty of Science, P.J. Safarik University in Kosice, Moyzesova 11, 040 01, Kosice, Slovakia
[4] Laboratory of Organic Synthesis and Molecular Imaging by MRI, CSIC Associated Unit, Paseo Senda del Rey 9, Madrid 28040, Spain

[†] Contributed equally to this work

Submitted for publication

ABSTRACT

Liposomal drug delivery is one of the most promising tools for bringing cytotoxic drugs to cancerous tissue. Despite of the ongoing efforts to improve their performance, the triggered release of cargo from liposomes in response to a target-specific stimulus has remained elusive. Here, we report on the *in vivo* use of stealth liposomes functionalized with a chemically modified pH-sensitive ion channel. The engineered ion channel is reconstituted in the lipid bilayer of the liposomes and senses changes in the environmental pH. If the ambient pH drops below a threshold value, the channel undergoes conformational changes and generates temporary pores on the liposomal surface, thus allowing leakage of the drug. We loaded such proteo-liposomes with an imaging agent and programmed them via the ion channel to respond to pH values below 7.0. By using magnetic resonance spectroscopy and imaging, we show that the engineered channels detect the mildly acidic pH conditions of the tumor microenvironment, which allows the release of the liposomal luminal content into implanted C6 glioma tumors, *in vivo*. In contrast, proteo-liposomes with non-modified ion channels did not show any pH-dependent release. A drug delivery system with this level of sensitivity and selectivity to environmental stimuli could well serve as an optimal tool not only for environmentally-triggered but also for image-guided drug release.

Abbreviations: CSI: Chemical Shift Imaging, DTPA: Diethylene triamino-pentaacetic acid, i.p.: intraperitoneal, i.v. : intravascular, MRI: Magnetic Resonance Imaging, MRSI; Magnetic Resonance Spectroscopic Imaging, MscL; Mechanosensitive channel of large Conductance, pH_e: extracellular pH, RARE: Rapid Acquisition Relaxation Enhancement, SI: Signal Intensity, SNR: Signal to Noise Ratio, TE: Echo Time, TR: Repetition Time, VAPOR: Variable Pulse Power and Optimized Relaxation Delays.

INTRODUCTION

Chemotherapy is one of the major treatments of cancer. Over the last decades systemic chemotherapeutic interventions have witnessed increased efficacy, decreasing significantly the pathological and socioeconomic repercussions of cancer and improving the outcome of surgically inaccessible tumors and multifocal neoplastic disease (Pinedo, 1997; Stewart, 2002). However, these treatments are often shadowed by a plethora of deleterious effects mostly derived from the secondary impact of the therapeutic drug on the healthy tissues (Park, 2010). Furthermore, limited bioavailability of drugs to the cancer cells demands for larger doses, increasing the risk of multiple drug resistance (Egusquiaguirre, 2012; Fojo, 2007; Higgins, 2007; O'Connor, 2007; Wojtkowiak, 2011). On these grounds, it has become mandatory to be able to deliver the cytotoxic drug more selectively to the tumor under *in vivo* conditions (Egusquiaguirre, 2012). To this end, the selection of robust and specific tumoral targets as well as improvements towards more selective drug delivery strategies entail a vital importance to the advancement of efficacy of chemotherapy and decrease in its side effects.

The acidic extracellular pH (pH_e) microenvironment of tumors is an aberrant pathophysiological circumstance underlying vital events of cancer biology including malignancy, invasion or metastasis (Garcia-Martin, 2001; Gatenby, 2006; Gatenby, 2008; Kallinowski, 1988; Stubbs, 1999; Vaupel, 1997; Wike-Hooley, 1984a, Wike-Hooley, 1984b). It represents a distinct property of tumors, thus providing an inherently robust discriminant for targeted drug delivery to cancers (Gerweck, 1999 Raghunand, 1999; Yatvin, 1980). In fact, the acid extracellular environment of tumors has been previously utilized for the most appropriate, systemically administered, free chemotherapeutic drugs (Wike-Hooley, 1984a; Wike-Hooley, 1984b). However, this therapeutic approach does not preclude significant amounts of the administered cytotoxic drug to reach other healthy tissues, does not hamper the development of resistance, and consequently does not restrict satisfactorily the undesired secondary effects.

The use of liposomes loaded with anticancer drugs has demonstrated improved sensitivity and specificity when compared to the direct administration of the free drug (Gabizon, 2001; Northfelt, 1998; Torchilin, 2005). These preparations are known to accumulate in the tumoral lesions because of the increased capillary permeability of the angiogenic neovasculature and the reduced clearance capacity of the tumor, decreasing significantly the undesired delivery of the cytotoxic drug to non tumoral tissues (Allen, 2004; Bae, 2011; Drummond, 2000). However, the use of liposomes in pH-triggered drug delivery has been limited mainly due to the absence of a sensory component in liposomes that is sufficiently sensitive to detect the mild pH differences between healthy and neoplastic tissue, and in response, trigger the drug release (Drummond, 2008; Egusquiaguirre, 2012; Lee, 2008).

In our previous work, we converted one of nature's sensory ion channels into a pH-sensitive nanovalve by interfering with its gating mechanism. We engineered the mechanosensitive channel of large conductance (MscL) from *Escherichia coli* into a pH-sensitive nano-valve

by specifically and selectively modifying its pore region with tailor-made pH-responsive chemical modulators (Kocer, 2006). The modulators were designed such that at pH's lower than the pK_a of the modulator, they acquire charge through protonation. These charges in the pore of the channel interfere with the gating mechanism of the channel and open its pore (Birkner, 2012; Ou, 1998; Yoshimura, 2001). We have reconstituted these engineered ion channels into physiologically relevant stealth liposomes, i.e. sterically-stabilised liposomes. These proteo-liposomes could sense the ambient pH and, in response to acidic pH conditions the channel protein gates and they were shown to release *in vitro* their intraluminal content. Furthermore, it was possible to fine tune the pH sensitivity of the proteo-liposomes with an unprecedented precision by manipulating the pK_a of the chemical modulators attached to MscL, such that the proteo-liposomes were able to respond to a physiologically relevant narrow pH range (Kocer, 2006).

Here, we demonstrate *in vivo,* the pH-triggered release of intraluminal content from these pH-sensitive proteo-liposomes into a tumor model. To this end, we loaded the proteo-liposomes with a paramagnetic imaging agent detectable non-invasively by Magnetic Resonance Imaging (MRI). After constructing the extracellular pH map of individual brain tumors, we delivered intravenously the pH-sensitive proteo-liposomes and could follow the liposomal release by MRI in every voxel of the tumor by the local increase in the MRI signal intensity. Comparison of the pH maps and the release profiles in the tumor showed that liposomes functionalized with the ion-channel pH sensor are sensitive enough to detect the mildly acidic extracellular pH range (pH 6.6-7.0) occurring in implanted C6 glioma tumors in mice, releasing selectively their intraluminal content in these areas.

MATERIALS AND METHODS

Strains and cell growth

Escherichia coli (E. coli) strain PB104 (*mscL::CmR*; Ara) (Blount, 1996) was used to host the pBAD-myc-his B plasmid (pBAD24derivative; Invitrogen) (Guzman, 1995) containing *mscl* from *Escherichia coli*. The original vector is modified by expanding the original multiple cloning site and removing the sequences for the c-myc epitope and His tag. Chemically ($CaCl_2$)-competent *E. coli* PB104 cells were transformed with P1BAD G22C-His and were grown in LB medium in the presence of 10 μg/mL chloramphenicol and 100 μg/mL ampicillin. Cells were grown in a bioreactor at pH 7.5, temperature of 37 °C, and oxygen control (dissolved oxygen >70%), using a complex medium [12 g/L Bacto-Tryptone (BD), 24 g/L yeast extract (BD), potassium phosphate (17 mM KH_2PO_4 and 72 mM K_2HPO_4), pH 7]. The medium was supplemented with chloramphenicol and ampicillin. At the early and mid-log phases, 10 ml of 40% (vol/vol) glycerol per liter was added as an additional carbon and energy source. The protein expression was induced in the late logarithmic phase by adding L-arabinose at 0.1% (wt/vol). Upon induction, another 10 ml 40% (vol/vol) glycerol was added per liter of medium, and cultivation was continued for 90 min.

Membrane vesicle preparation

Cells were harvested by centrifugation and suspended in ice-cold 25 mM Tris·HCl, pH 8.0, to a final OD_{600} of 100–150. Subsequently, DNAse (0.5 mg/mL, final concentration), RNAse (0.5 mg/mL, final concentration), and 5 mM $MgSO_4$ were added, and cells were broken using a cell disrupter (Type TS/40; Constant Systems) at 1.7 kbar and 4 °C. Cellular debris was removed by centrifugation for 30 min at 18,460 x g and 4°C. Supernatant was ultra centrifuged at 145,400 x g for 90 min at 4 °C. The supernatant was discarded, and the remaining membrane vesicles were re-suspended and homogenized in ice-cold 25 mM Tris·HCl (pH 8.0) to 0.7 g (wet weight)/ml. Membrane vesicles were frozen in liquid nitrogen and stored at −80 °C.

Protein isolation

MscL-his tagged proteins were purified by nickel-nitriloacetic acid (Ni-NTA) affinity column chromatography, as described before (Kocer, 2007). Briefly, membrane vesicles corresponding to about 90 mg of total protein were solubilized at 5 mg/ml in 50 mM sodium phosphate (pH 8.0), 300 mM NaCl, 1% (vol/vol) Triton X-100, and 35 mM imidazole (solubilization buffer) for 30 min at 4 °C. After ultracentrifugation at 267,000 x g for 20 min at 4 °C, the supernatant was applied to Ni-NTA agarose resin (Qiagen) [30 mg membrane protein/mL per 50% (wt/vol) slurry], which was pre-equilibrated with 10 column volumes (CV) of solubilization buffer, and incubated under mild agitation for 30 min at 4 °C, enabling binding of his-tagged proteins to the matrix. Unbound material was collected as flow through and analyzed when appropriate. The column was washed consecutively with 15 CV wash buffer [50 mM sodium phosphate (pH 8.0), 300 mM NaCl, 0.2% (vol/vol) Triton X-100, 35 mM imidazole] and 10 CV of wash buffer without Imidazol. At this stage, MscL protein was labeled with pH modulator at Cys-22. It was labeled with 1 mg/ml final concentration of the pH-sensitive probe in DMSO for 45 min at room temperature. The unbound label was washed off the affinity column with 7.5 CV L-histidine wash buffer [50 mM sodium-phosphate (pH 8.0), 300 mM NaCl, 0.2% (vol/vol) Triton X-100, 50 mM histidine]. His-tagged proteins were eluted by addition of 15× 0.5 CV Ni-NTA elution buffer [50 mM sodium phosphate (pH 8.0), 300 mM NaCl, 0.2% (vol/vol) Triton X-100, 235 mM L-histidine]. The protein content of the fractions was checked with the Bradford assay. The total yield of protein was 3-4 mg at an average concentration of 0.5 mg/ml MscL. Protein was frozen in liquid nitrogen and stored at −80°C.

Chemical synthesis

The pH modulator, dimethylamino-acetic acid 2-methanesulfonylsulfonyl-ethyl ester; hydrochloride, was synthesized as described before (Kocer, 2006) by esterification of N,N-dimethylglycine with 2-bromoethanol and subsequent exchange of bromide for the methanethiosulfonate group.

Preparation of drug loaded stealth liposomes

A chloroform solution of DOPC, cholesterol, DSPE-PEG 2000 (Avanti polar lipids) in the molar ratio 70:20:10 was prepared. After removal of chloroform in rotary evaporator at 25˚C, the lipid mixture was rehydrated for 40 min with 0.5 M Gd(III) DTPA (Magnevist, Bayer, DE) solution at 50˚C to 20 mg/ml final concentration. Subsequently, seven freeze-thaw cycles were performed with rapid freezing in liquid N_2, and thawing in a water bath at 60 °C. Aliquots of 1 ml were stored at -80 °C.

Protein reconstitution in stealth proteo-liposomes

The labeled MscL was reconstituted into Gd(III) DTPA-containing liposomes by a detergent mediated reconstitution method, according to Kocer *et al* (Kocer, 2007). Briefly, the Gd(III) DTPA-containing liposome mixture was thawed and extruded through a 400 nm filter (11 times). Liposomes were destabilized by the addition of 0.25% (weight/volume) Triton X-100. MscL and detergent-saturated liposomes were mixed at a 1:50 weight ratio, respectively, and incubated for 30 minutes at 50 °C. Subsequently, the appropriate buffer (for fluorescence dequenching assay: 200 mM calcein in 10 mM sodium-phosphate pH 8.0, 150 mM NaCl, 0.125 M Gd(III) DTPA; for animal experiment formulation: only 0.125 M Gd(III) DTPA) was added in 1:1 volume ratio and supplemented with 10mg (wet weight) Biobeads (SM-2 Absorbents) per µl detergent (10 % Triton X-100) used in the sample and lipid preparation. For detergent removal, the sample was incubated overnight (~16 hours) at 4 °C on a rotating plate. Proteoliposomes with an average diameter of 100nm were formed (as determined by Dynamic Light Scattering). Calcein encapsulated proteo-liposomes were used in fluorescence dequenching assay. For animal experiment: proteoliposomes (without calcein) containing 0.1875 M final (GdIII)DTPA concentration were centrifuged at 202,500 x g for 45 min at 4˚C, and the supernatant containing external (GdIII)DTPA was removed by pipetting. For administering to the animals, the proteo-liposomes were resuspended in sterile iso-osmotic buffer containing 10 mM sodium phosphate, 150 mM NaCl at pH 8.0.

Fluorescence dequenching assay

In this ensemble measurement, pH-induced release was followed by a fluorescence dequenching assay (Kocer, 2007). A self quenching fluorescent dye, calcein, was co-encapsulated together with Gd(III) DTPA in the proteo-liposomes. The proteo-liposomes were applied onto a Sephadex G50 size-exclusion column to remove the unencapsulated, external dye and Gd(III)DTPA. Then, the release from proteo-liposomes was measured by fluorescence spectrometry (Cary Eclipse Fluorimeter) at excitation and emission wavelengths of 497 nm and 516 nm (slit width: 5nm, 10 nm), respectively, in isoosmotic buffers of different pH value. The pH-induced activity of the channels is represented as an increase in the fluorescent signal due to the release of calcein. In a standard assay, 2 µl calcein-filled proteo-liposomes were diluted into 2100

µl of iso-osmotic efflux buffer at pH 6.2, 6.5, 7.2, and 7.8. The maximum fluorescence of the sample was determined by lysing the proteo-liposomes upon addition of 0.5 % (v/v) of Triton X-100. As a control, background release from control liposomes with unmodified MscL was recorded under identical conditions.

C6 glioma model

The experimental protocols used in these experiments were approved by the appropriate institutional committees; all efforts being made to minimize animal suffering. C57BL6 adult male mice (25-30g) were housed in a humidity- and temperature-controlled room on a 12h light/dark cycle, receiving water and food ad libitum. The C6 glioma model was implemented essentially as described previously (33). C6 cells (ATCC CCL-107, LGC Standards, Barcelona, ES) were grown to confluence (10-cm Petri dishes, 37 ºC, 5% CO_2/95% O_2) in DMEM supplemented with 5% Fetal Bovine Serum (w/v), 100 µg/mL streptomycin, 25 µg/mL gentamycin, 100 units/mL penicillin and 1 % fungizone, harvested and kept on ice until injection. Animals were anesthetized intraperitoneally with ketamine and xylazine hydrochlorides (8% Ketolar®, 0.5 ml Rompun®/100 g of body weight), secured with a stereotaxic holder (Kopf, Tujunga, CA). Then, an intracerebral injection of C6 cells (approx. 10^6) were administered to the left caudate nucleus of the animals. The development of intracranial C6 tumors was followed acquiring consecutive Magnetic Resonance Images; 1, 5, 7, 10 and 15 days after implantation in every animal.

When the tumor reached proper size (approx. 1cm diameter), animals were anesthetized by inhalation with 3 % of isofluorane in 99.9% O_2 (1 L min^{-1}) in an induction chamber and maintained with 1.5 % of isofluorane in 99,9% O_2 (1 L min^{-1}), delivered through a nose mask. The tail vein and the peritoneum were cannulated. Tail cannula was filled with saline whereas the intraperitoneal cannula was filled with [(±)2-(Imidazol-1-yl) succinic acid] ISUCA solution. Body temperature was monitored with a rectal probe (Panlab, Barcelona, Spain) and maintained at approximately 37 ºC during the experiment, using a thermostatic blanket and a temperature-regulated circulating water bath.

Preparation of solutions for intravascular injection

In order to remove external Gd(III) DTPA from the preparations, pH-sensitive and insensitive proteoliposomes were purified as follows. The liposome solution (4 ml) was centrifuged (26,600 x g, 40 min, 4 °C) and the supernatant removed completely, leaving and almost transparent, small, hard pellet, kept at 4 °C. Proteoliposome pellets were resuspended gently in 0.4 ml of 10mM sodium phosphate and 150 mM sodium chloride buffer of pH 8.0, just before tail vain injection.

[(±)2-(Imidazol-1-yl) succinic acid] ISUCA solution (SOIREM Res. S.L., Madrid, ES) was prepared in water at 1M concentration and pH adjusted to 7.2 with sodium bicarbonate and filtered through an Acrodisck Syringe filter (PALL Corp, PNN4612,

Port Washington, NY 11050, US), yielding a transparent solution with yellowish colour. This solution was stored at 4 °C no more than 4 days before use.

In vivo magnetic resonance imaging and spectroscopic imaging

MR studies were performed *in vivo* during tumor development, using a 7.0 T/16 cm Bruker Pharmascan system equipped with a 90 mm diameter gradient insert (360 mT/m). The transmit/receive arrangements included a ^{1}H rat brain receive-only surface coil (38 mm, circularly polarized) used as receiver and an actively detuned transmit-only resonator (Bruker BioSpin MRI GmbH, Rimpar, DE). Data were acquired with a Hewlett-Packard console running Paravision software (Bruker Medical GmbH, Ettlingen, DE) operating on a Linux platform.

Anesthetized animals were fixed with tape to the plexiglass animal-holder to minimize breathing-related motion, and placed in a water-heated probe that kept the body temperature at 37 °C. The physiological state of the animal was monitored throughout the MRI experiment with a Biotrig physiological monitor (Bruker Medical, Ettlingen, DE), recording the respiratory rate and rectal temperature. This setup was then positioned in the isocenter of the magnet.

In the experiments following up tumor development, anatomical T_2 weighted spin-echo images were acquired using Rapid Acquisition Relaxation Enhancement (RARE) sequence (Hennig, 1986; Hennig, 1988). The following parameters were used: repetition time (TR) = 3000 ms, echo time (TE) = 60 ms, RARE factor = 8, 3 averages, field of view (FOV) = 38 x 38 mm, acquisition matrix (Mtx) = 256 × 256; 148 × 148 μm^2 in plane resolution, slice thickness = 1 mm and 16 slices.

For the MRSI and MRI experiments, animals were prepared as previously described. ^{1}H Magnetic Resonance Spectroscopic Images were acquired using a PRESS-CSI sequence (Provent, 2007). Briefly, the tumor was localized with a coronal T_2 weighted RARE sequence, and first- and second-order shims adjusted with FASTMAP through a sufficiently large voxel containing tumor and some surrounding healthy tissue. Basal Chemical Shift Imaging (CSI) was performed in two spatial dimensions, exciting a PRESS selected volume of 8 × 8 × 4 mm. Acquisition conditions were: FOV = 22 × 22 mm, CSI matrix = 8 × 8 zero-filled to 32 × 32, (final in-plane resolution 687 x 687 μm^2), TR = 1500 ms, TE = 19.3 ms and 500 transients acquired during 12.7 min. Water suppression was performed with a Variable Pulse Power and Optimized Relaxation Delays (VAPOR) sequence.

The changes in signal intensity, SI induced by the injected proteo-liposomes were monitored successively in the anesthetized animals using T_1 weighted images. Two types of T_1 weighted images, with the same geometry, were acquired, under "high" and "low" resolution conditions, respectively. The "high" resolution images were acquired using: TR = 350 ms, TE = 10.6 ms, 3 averages, FOV = 22 x 22 mm (the same for MRSI), matrix = 256 x 256, 86 × 86 μm^2 in plane resolution, slice thickness = 1 mm and 5 slices, total acquisition time = 4.4 min. In addition, "low" resolution images

were acquired to obtain by MRI the same voxel size and voxel grid implemented for the MRSI. Conditions were: TR = 350 ms, TE = 10.6 ms, 3 averages, FOV = 22 x 22 mm (the same for MRSI), matrix = 32 x 32, 687 × 687 μm^2 in plane resolution, slice thickness = 1 mm and 5 slices, total acquisition time = 0.5 min.

Image analysis

Spectroscopic images were reconstructed using 3DiCSI 1.9.9 software (Hatch Centre for MR Research, Columbia University, New York, NY). pH maps were obtained as previously described (Provent, 2007). Briefly, the basal spectroscopic images, acquired before administration of ISUCA, allowed us to check the spectrometer settings and to verify that there were no endogenous resonances overlapping the aromatic ISUCA peaks. In the presence of ISUCA, Lorentzian line shapes were fitted to the H2 peaks to obtain the H2 chemical shifts using the endogenous creatine resonance as reference. Only those voxels with signal to noise ratio (SNR) higher than two were processed. The extracellular pH was then determined in each voxel from the chemical shift of the H2 peak, using the Henderson-Hasselbalch equation:

$$pH = pk_a - \log\frac{\delta_1 - \delta}{\delta - \delta_2} \quad [1]$$

where pK_a = 7.07, δ is the measured ISUCA H2 chemical shift and δ_1 (8.75) and δ_2 (7.68) are the alkaline and acidic asymptotic values.

T_1 weighted images were analyzed using Image J (W. S. Rasband, U.S. National Institutes of Health, Bethesda, MD, USA, http://rsb.info.nih.gov/ij/,19972005). Briefly, SI in the initial two (i= 1,2) T_1 weighted images were averaged to obtain an average baseline. Normalized image SI values were then calculated on a voxel-by-voxel basis using the expression:

$$\Delta SI(\%)_{i,m,n} = \frac{SI_{i,m,n}}{\left(\sum_{i=1}^{2} SI_{i,m,n} \Big/ 2\right)} * 100 - 100 \quad [2]$$

where *i* is the image number, *m* and *n* are the image matrix sizes, and *SI* is the voxel intensity. Mean ΔSI values were calculated averaging the changes occurring in SI 60 min after liposome administration. pH and mean ΔSI(%) maps were generated using a MATLAB (2008a, The Mathworks Inc., Natick, Massachusetts , USA) based home made software.

The spatial distributions of pairs of quantities (e.g., mean ΔSI and pH) were compared by calculating the linear regression and the Pearson correlation coefficient as implemented in the SPSS Statistical Package (18.0, SPSS Inc., Chicago, Illinois, USA).

RESULTS

Proteo-liposomes are functional in vitro

In order to test if the encapsulation of an imaging agent will affect the functioning of the engineered ion channel, we first tested the pH-induced release from proteo-liposomes *in vitro,* using fluorescence dequenching. Briefly, we prepared stealth liposomes containing MscL with or without pH-modulator (Kocer, 2006). In liposomes with pH-sensitive MscL, the channel was covalently modified in its pore region with the pH modulator (**Fig. 1A** and **1D**). pH-insensitive proteo-liposomes embedded with the unmodified MscL were used as a control for any nonspecific release either through the lipid bilayer or through the channel itself (**Fig. 1B**). The two types of proteo-liposomal formulations were loaded with both, a MRI contrast agent (Gd(III) DTPA), and a self-quenching fluorescent dye (calcein). The pH-triggered release was followed as an increase in the fluorescence intensity due to the dilution of the fluorescent dye that was released from the liposomes along with the paramagnetic contrast agent. **Fig. 1B** shows the pH dependence of the release of intraluminal content from pH-sensitive and -insensitive proteo-liposomes. The pH-insensitive proteo-liposomes displayed less than 10 % variation of basal fluorescence level, throughout the investigated pH range, i.e. pH 6.15-7.8. However, the pH-sensitive liposomes showed a clear release of their intraluminal content in a pH-dependent manner; the lower the pH, the higher the release (**Fig. 1C**).

Liposomal release could be localized to defined regions of the tumor by Magnetic Resonance Spectroscopy and Imaging

In order to define the pH-dependence of the liposomal release in tumors, we used the classical C6 glioblastoma model, obtained after implanting C6 cells in the left hemisphere of C57BL6 mice (n=11) (Garcia-Martin, 2001). We loaded the pH-sensitive or insensitive proteo-liposomes with Gd(III) DTPA and followed its release from proteo-liposomes *in vivo* by MRI. We chose Gd(III) DTPA as the imaging agent because of its extended use in clinical facilities and its ability to enhance the MRI signal selectively only in those areas where it is released from the proteo-liposomes.

We first generated the pH map of the tumor *in vivo* using our extracellular pH-sensitive probe [(+/-)2-(imidazol-1-yl)succinic acid disodium salt], ISUCA (Provent, 2007). We began by acquiring anatomical MRI images of the cerebral tumor and injecting intraperitoneally 0.4 ml, 1 M of ISUCA to create the extracellular pH map of the tumor (**Fig. 2A**). This diamagnetic probe depicts a characteristic magnetic resonance spectrum that depends on the tumoral pH and can be resolved spatially *in vivo*, in all tumor voxels, using Magnetic Resonance Spectroscopic Imaging (MRSI) (**Fig. 2B**) (Garcia-Martin, 2001; Provent, 2007). The multivoxel spectroscopic grid acquired *in vivo* can then be converted into a regional pH map of the tumor (**Fig. 2C-D**). Once the pH map was acquired and ISUCA was cleared from the tumor, we recorded the

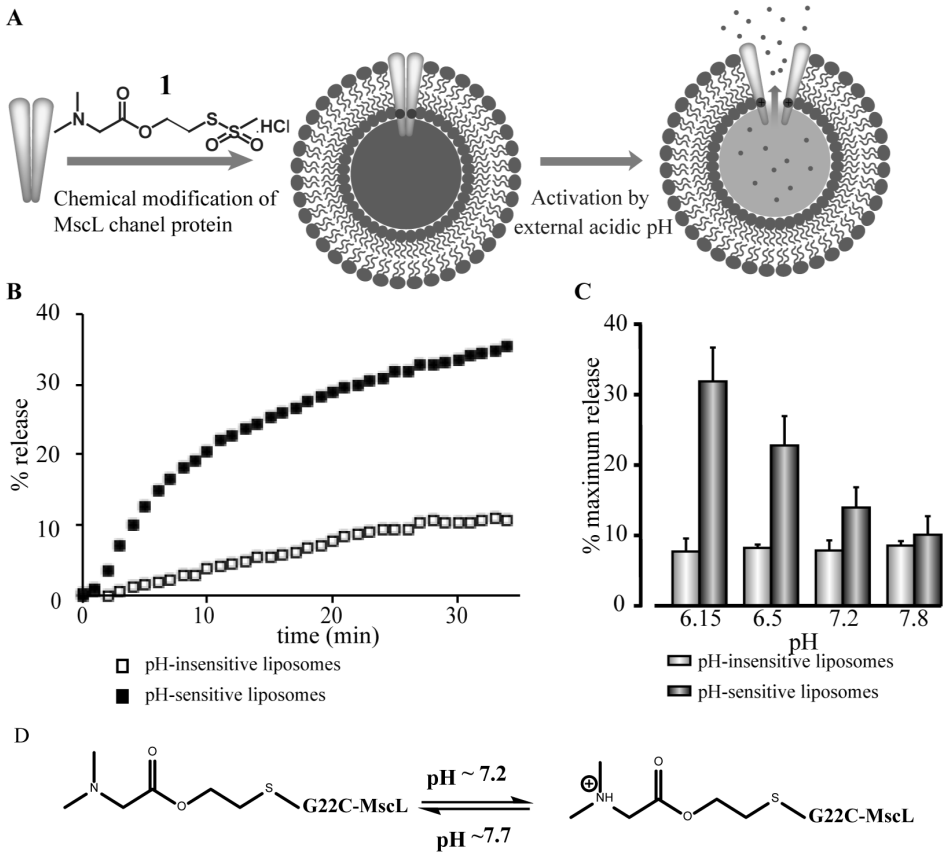

Figure 1. Extracellular pH triggered drug release from pH-sensitive and pH-insensitive proteo-liposomes *in vitro*. A) MscL channels are labeled with a pH-sensitive modulator **1** and reconstituted into stealth liposomes (DOPC:Cholesterol:DSPE-PEG200, 70:20:10 M ratio). Proteoliposomes are loaded with self quenching dye, calcein and contrast agent, Gd(III) DTPA for *in vitro* and *in vivo* experiments, respectively. The drug release is triggered by the opening of the liposome-embedded MscL channels through the protonation of the chemical modulator on the channel pore. B) In an *in vitro* assay, extracellular pH-triggered drug release from pH-sensitive and pH- insensitive liposomes is followed by fluorescence dequenching, in which the release of self-quenching calcein is followed as an increase in fluorescence. Exemplary release kinetics of liposomes at pH 6.15 is shown. Open and filled squares refer to liposomes with unmodified MscL (i.e., pH-insensitive) and modified MscL (i.e., pH-sensitive), respectively. C) The % release in efflux assay, i.e. fluorescence at t=20 min, from liposomes is shown as a function of pH. Light and dark gray bars refer to liposomes with unmodified and modified MscL, respectively. D) Protonation of the amine moiety in the pH sensitive label attached to G22C-MscL upon decrease in pH below its pK_a.

background T_1 weighted image of every tumor before injecting the pH-sensitive (n=4) or pH-insensitive (n=7) proteo-liposomes through the tail vein (**Fig. 2E-F**).

After injection of liposomal preparations, we followed kinetically by MRI the *in vivo* release of Gd(III) DTPA from the liposomal lumen, as the local increase in water SI in

T_1 weighted MR images acquired from the same voxels where the extracellular pH of the tumor was measured by MRSI (**Fig. 2G**). Finally, we obtained the statistical correlation between the extracellular pH value, determined by ^{1}H MRSI, and the average SI change (ΔSI) detected by T_1 weighted MRI of every voxel of the tumor (**Fig. 2H**).

pH-sensitive proteo-liposomes release the cargo at low pH voxels of the tumor

Both pH-sensitive and -insensitive proteo-liposomal formulations were tested *in vivo* for the release of their intraluminal content in the C6 glioblastoma model using MRSI and MRI techniques (Garcia-Martin, 2001; Provent, 2007). **Fig. 3** shows representative results obtained *in vivo* for the release of intraluminal content of (GdIII) DTPA from pH-sensitive (top panels) and pH-insensitive proteo-liposomes (bottom panels) in two representative mice carrying implanted C6 glioblastoma. The extracellular pH within these tumors varied between 6.6 and 7.0 (**Fig. 3A** and **3E**). The release of the paramagnetic imaging agent from the pH-sensitive proteo-liposomes into the acidic

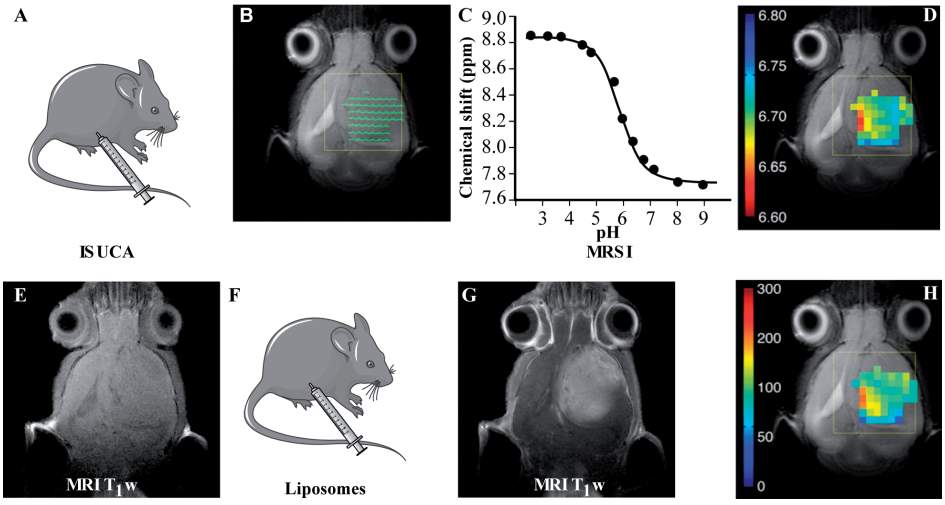

Figure 2. Experimental design. A) The C6 tumour-bearing animal was anesthetized and positioned in the magnet isocenter, and a basal multivoxel spectroscopy grid was acquired as described in **Materials and Methods**. A single bolus of 0.4 ml of ISUCA 1M was then injected intraperitoneal. B) Successive multivoxel spectroscopy grids were acquired. C) The dependence of chemical shift on pH was fitted with the Henderson-Hasselbach equation to obtain a calibration curve for the analysis of the pH *in vivo* (33). D) The measured ISUCA chemical shift in every voxel was transformed into an extracellular pH map. E) When ISUCA was cleared from the tumor and its resonances became no longer detectable, T_1 weighted baseline images were acquired. F) Then, the pH-sensitive or pH-insensitive proteo-liposomes containing Gd(III) DTPA were injected in the tail vein. G) T_1 weighted images acquired for the next 60 minutes or different time period when the analysis showed signs of animal discomfort. With the complete series of T_1 weighted images, the relative changes in signal intensity (SI) were calculated in a pixel by pixel manner using the baseline images as reference. H) Then, maps representing the mean change in signal intensity (ΔSI_{mean}) were calculated and overlaid with the anatomical T_1 image.

voxels of the tumor started within the first ten minutes after intravascular injection and lasted for approximately sixty minutes, as estimated from the relative mean changes in voxel signal intensity (ΔSI_{mean}) (**Fig. 3B** and **3F**). Panels **3C** and **3G** depict maps of relative ΔSI_{mean} measured in the same voxels during 60 minutes after the injection. In case of pH-sensitive proteo-liposomes, the voxels with highest Gd(III) DTPA release co-localized with the voxels with lowest pH (Fig. **3A** and **3C**). The pH-insensitive proteo-liposomes, on the other hand, showed significantly smaller contrast agent release independent of the tumor extracellular pH, consistent with the basal leakage previously detected *in vitro* in the fluorescence-dequenching assay. Finally, panels **3E** and **3H** show the relationship between the extracellular pH (pH_e) and the relative ΔSI_{mean} values as determined by ^1H MRSI and T_1 weighted MRI in the same tumor voxels, respectively. A clearly negative correlation between extracellular pH and drug release can be observed when using the pH-sensitive proteo-liposomes (**Fig. 3D**), and virtually no correlation can be detected when using the pH-insensitive preparation (**Fig. 3H**).

We repeated this experiment in four animals receiving pH-sensitive proteo-liposomes and seven animals receiving pH-insensitive proteo-liposomes. In spite of intrinsic variations between animals and tumors within animals, all animals receiving the pH-

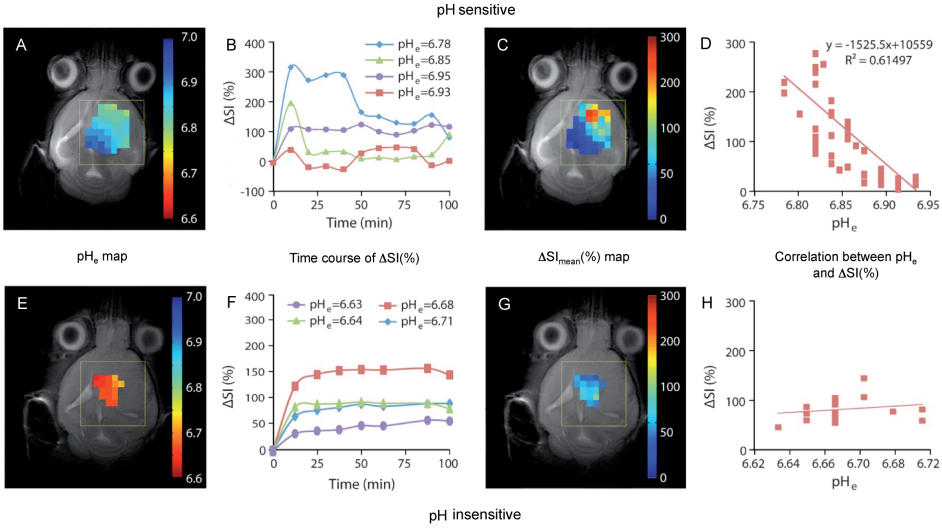

Figure 3. Extracellular pH triggered drug release from pH-sensitive and pH-insensitive proteo-liposomes *in vivo*. The top panels show a representative study with pH-sensitive proteo-liposomes, whereas the bottom panels depict representative results obtained with pH-insensitive proteo-liposomes. A,E) The pH maps obtained *in vivo* with ISUCA. B,F) The SI evolution over time in different tumor voxels, indicating the pH_e of the voxel. C,G) The mean change in signal intensity (ΔSImean) in all tumor voxels due to contrast agent release from the liposomes. D,H) The correlation between the pH values and the ΔSImean in a voxel by voxel manner, for all tumor voxels investigated. **Inserts**: Parameter values for the linear regression analysis.

sensitive proteo-liposomes showed a negative linear regression (r^2>0.6) and a high Pearson's correlation coefficients (>0.75) between pH_e and ΔSI_{mean} (**Table 1**). This finding reveals that the release of intraluminal content increases as the extracellular pH decreases and *vice versa*. On the other hand, the seven animals receiving pH-insensitive proteo-liposomes showed poor linear regressions between pH and ΔSI (r^2<0.2) and much lower Pearson's correlation coefficients (<0.5). This indicates that there is no significant correlation between the extracellular pH of the tumor and the amount of contrast agent released from the pH-insensitive proteo-liposomes. Taken together, these results are consistent with those obtained *in vitro* with the same proteo-liposomal preparations (**Fig. 1B**), revealing that, the intraluminal content of pH-sensitive proteo-liposomes is effectively released under the mildly acidic pH_e conditions prevailing *in vivo*, while no pH_e dependent release occurs from the pH-insensitive preparations.

Table 1. Summary of pH_e dependent release of Gd(III)DTPA from pH-sensitive and pH-insensitive liposomes into C6 tumors *in vivo*.

Animal ID	Type of liposomes	Extracellular pH range	Number of voxels	Pearson's correlation coef.	Linear regression (r^2)
1	pH senstive	6.75-6.95	44	-0.7842	0.615
2	pH senstive	6.5-6.9	7	-0.9205	0.8479
3	pH senstive	6.6-6.8	51	-0.7758	0.6018
4	pH senstive	6.6-6.7	15	-0.8315	0.7434
5	pH insenstive	6.6-6.7	17	0.1971	0.0149
6	pH insenstive	6.7-6.8	9	-0.2205	0.0293
7	pH insenstive	6.6-6.8	13	0.1578	0.0559
8	pH insenstive	6.6-6.7	13	0.3178	0.0865
9	pH insenstive	6.65-6.8	25	0.4387	0.1924
10	pH insenstive	6.75-6.85	22	-0.4593	0.211
11	pH insenstive	6.45-6.55	14	0.1051	0.0111

CONCLUSION

Here we demonstrate the ability of engineered ion-channels to transform stealth liposomes into sensitive pH_e-responsive drug-carriers that can detect mild, physiologically relevant pH_e differences and release the drug selectively in the low pH_e areas of the tumor *in vivo*. The use of an engineered ion channel as a sensory component is advantageous over alternative pH-sensitive liposomal formulations that need to contain high amounts of negatively charged lipids, polymers, or unsaturated lipids, which make liposomes prone to fast clearance from the blood, affect their pharmacokinetic properties and may cause incompatibilities with drug encapsulation (Drummond, 2008). Ion channels, conversely, are membrane proteins, which can be

sensitized to different triggers; their opening/closing properties can be conveniently manipulated and fine-tuned by small chemical modulators. In addition, ion channels react fast to an external stimulus and only a small number of channels per liposome are needed to release efficiently the intraluminal content, thus presenting minimal interference with the physicochemical properties of the hosting liposome and have minimal physiological consequences for the animal.

The engineered ion-channel based pH-sensitive liposomes implemented herein may serve as sensitive image-guided drug delivery devices, useful for improving the performance of chemotherapeutic regimes, helping to decrease undesired systemic toxicity and drug resistance responses (Drummond, 2000).

REFERENCES

Allen TM & Cullis PR (2004) Drug delivery systems: entering the mainstream *Science* **303**: 1818-1822

Bae KH, Chung HJ, & Park TG (2011) Nanomaterials for cancer therapy and imaging *Mol Cells* **31**: 295-302

Birkner JP, Poolman B, & Kocer A (2012) Hydrophobic gating of mechanosensitive channel of large conductance evidenced by single-subunit resolution. *Proc Natl Acad Sci U S A* **109**: 12944-12949

Blount P, Sukharev SI, Schroeder MJ, Nagle SK, & Kung C (1996) Single residue substitutions that change the gating properties of a mechanosensitive channel in Escherichia coli. *Proc Natl Acad Sci U S A* **93**: 11652-11657

Drummond DC, Noble CO, Hayes ME, Park JW, & Kirpotin DB (2008) Pharmacokinetics and in vivo drug release rates in liposomal nanocarrier development *J Pharm Sci* **97**: 4696-4740

Drummond DC, Zignani M, & Leroux J (2000) Current status of pH-sensitive liposomes in drug delivery *Prog Lipid Res* **39**: 409-460

Egusquiaguirre SP, Igartua M, Hernandez RM, & Pedraz JL (2012) Nanoparticle delivery systems for cancer therapy: advances in clinical and preclinical research *Clin Transl Oncol* **14**: 83-93

Fojo T & Coley HM (2007) The role of efflux pumps in drug-resistant metastatic breast cancer: new insights and treatment strategies *Clin Breast Cancer* **7**: 749-756

Gabizon AA (2001) Pegylated liposomal doxorubicin: metamorphosis of an old drug into a new form of chemotherapy *Cancer Invest* **19**: 424-436

Garcia-Martin ML, Herigault G, Remy C, Farion R, Ballesteros P, Coles JA, Cerdan S, & Ziegler A (2001) Mapping extracellular pH in rat brain gliomas in vivo by 1H magnetic resonance spectroscopic imaging: comparison with maps of metabolites *Cancer Res* **61**: 6524-6531

Gatenby RA, Gawlinski ET, Gmitro AF, Kaylor B, & Gillies RJ (2006) Acid-mediated tumor invasion: a multidisciplinary study *Cancer Res* **66**: 5216-5223

Gatenby RA & Gillies RJ (2008) A microenvironmental model of carcinogenesis *Nat Rev Cancer* **8**: 56-61

Gerweck LE, Kozin SV, & Stocks SJ (1999) The pH partition theory predicts the accumulation and toxicity of doxorubicin in normal and low-pH-adapted cells *Br J Cancer* **79**: 838-842

Guzman LM, Belin D, Carson MJ, & Beckwith J (1995) Tight regulation, modulation, and high-level expression by vectors containing the arabinose PBAD promoter. *J Bacteriol* **177**: 4121-4130

Hennig J & Friedburg H (1988) Clinical applications and methodological developments of the RARE technique. *Magn Reson Imaging* **6**: 391-395

Hennig J, Nauerth A, & Friedburg H (1986) RARE imaging: a fast imaging method for clinical MR. *Magn Reson Med* **3**: 823-833

Higgins CF (2007) Multiple molecular mechanisms for multidrug resistance transporters. *Nature* **446**: 749-757

Kallinowski F & Vaupel P (1988) pH distributions in spontaneous and isotransplanted rat tumours *Br J Cancer* **58**: 314-321

Kocer A, Walko M, Bulten E, Halza E, Feringa BL, & Meijberg W (2006) Rationally designed chemical modulators convert a bacterial channel protein into a pH-sensory valve. *Angew Chem Int Ed Engl* **45**: 3126-3130

Kocer A, Walko M, & Feringa BL (2007) Synthesis and utilization of reversible and irreversible light-activated nanovalves derived from the channel protein MscL. *Nat Protoc* **2**: 1426-1437

Lee ES, Gao Z, & Bae YH (2008) Recent progress in tumor pH targeting nanotechnology *J Control Release* **132**: 164-170

Northfelt DW, Dezube BJ, Thommes JA, Miller BJ, Fischl MA, Friedman-Kien A, Kaplan LD, Du Mond C, Mamelok RD, & Henry DH (1998) Pegylated-liposomal doxorubicin versus doxorubicin, bleomycin, and vincristine in the treatment of AIDS-related Kaposi's sarcoma: results of a randomized phase III clinical trial *J Clin Oncol* **16**: 2445-2451

O'Connor R (2007) The pharmacology of cancer resistance *Anticancer Res* **27**: 1267-1272

Ou X, Blount P, Hoffman RJ, & Kung C (1998) One face of a transmembrane helix is crucial in mechanosensitive channel gating. *Proc Natl Acad Sci U S A* **95**: 11471-11475

Park JH, von Maltzahn G, Xu MJ, Fogal V, Kotamraju VR, Ruoslahti E, Bhatia SN, & Sailor MJ (2010) Cooperative nanomaterial system to sensitize, target, and treat tumors *Proc Natl Acad Sci U S A* **107**: 981-986

Pinedo HM & Giaccone G (1997) Chemotherapy *Lancet* **349 Suppl 2**: SII7-9

Provent P, Benito M, Hiba B, Farion R, Lopez-Larrubia P, Ballesteros P, Remy C, Segebarth C, Cerdan S, Coles JA, & Garcia-Martin ML (2007) Serial in

vivo spectroscopic nuclear magnetic resonance imaging of lactate and extracellular pH in rat gliomas shows redistribution of protons away from sites of glycolysis *Cancer Res* **67**: 7638-7645

Raghunand N, He X, van Sluis R, Mahoney B, Baggett B, Taylor CW, Paine-Murrieta G, Roe D, Bhujwalla ZM, & Gillies RJ (1999) Enhancement of chemotherapy by manipulation of tumour pH *Br J Cancer* **80**: 1005-1011

Stewart LA (2002) Chemotherapy in adult high-grade glioma: a systematic review and meta-analysis of individual patient data from 12 randomised trials *Lancet* **359**: 1011-1018

Stubbs M, McSheehy PM, & Griffiths JR (1999) Causes and consequences of acidic pH in tumors: a magnetic resonance study *Adv Enzyme Regul* **39**: 13-30

Torchilin VP (2005) Recent advances with liposomes as pharmaceutical carriers *Nat Rev Drug Discov* **4**: 145-160

Vaupel P (1997) Vascularization, blood flow, oxygenation, tissue pH, and bioenergetic status of human breast cancer *Adv Exp Med Biol* **411**: 243-254

Wike-Hooley JL, Haveman J, & Reinhold HS (1984) The relevance of tumour pH to the treatment of malignant disease *Radiother Oncol* **2**: 343-366

Wike-Hooley JL, Van der Zee J, van Rhoon GC, Van den Berg AP, & Reinhold HS (1984) Human tumour pH changes following hyperthermia and radiation therapy *Eur J Cancer Clin Oncol* **20**: 619-623

Wojtkowiak JW, Verduzco D, Schramm KJ, & Gillies RJ (2011) Drug resistance and cellular adaptation to tumor acidic pH microenvironment. *Mol Pharm* **8**: 2032-2038

Yatvin MB, Kreutz W, Horwitz BA, & Shinitzky M (1980) pH-sensitive liposomes: possible clinical implications *Science* **210**: 1253-1255

Yoshimura K, Batiza A, & Kung C (2001) Chemically Charging the Pore Constriction Opens the Mechanosensitive Channel, MscL. *Biophys J* **80**: 2198-2206

CHAPTER 5

Functional studies of liposome-embedded MscL on nanochip at single channel resolution

Nobina Mukherjee[1], Michael Urban[2], Alexander Kleefen[2], Barbara Windschiegl[3], Patrick Seelheim[3], Marc vor der Brüggen[3], Robert Tampé[2,4‡], Armağan Koçer[1]

[1]Department of Biochemistry Groningen Biomolecular Sciences and Biotechnology Institute, University of Groningen, Groningen, The Netherlands
[2]Institute of Biochemistry, Biocenter, Goethe-University Frankfurt, Germany
[3]Nanospot GmbH, Münster, Germany;
[4]Cluster of Excellence – Macromolecular Complexes, Goethe-University Frankfurt, Germany

This chapter has been published as part of the NanoLetters paper "Highly Parallel Transport Recordings on a Membrane-on-Nanopore Chip at Single Molecule Resolution" by Urban *et al*, 2014, 14(3): 1674-80

ABSTRACT

With the advent of high resolution electrical and optical signal detection methods, ion channels can be designed to be the future detection modules for sensory devices. Our goal here was to have suitable platforms to reconstitute the mechanosensitive channel of large conductance (MscL) in lipid bilayer for potential use in sensory high-throughput applications. For this purpose, we have successfully employed a nanofabricated chip platform for studying multiple flux events in parallel through MscL in suspended lipid bilayers (SLB). The nano-fabricated silicon-based chip contains 250,000 cylindrical cavities enclosed by a silicon dioxide top layer with well-defined apertures in the nanometer range. Large-unilamellar vesicles harboring functionally-reconstituted membrane protein, MscL, are fused and spread on the nanopore-chip surface. More than hundreds of import and export events of single MscL channels can be recorded simultaneously via real-time detection of multi-spectral fluorescence signals. The presented nanochip platform combines highly parallel, semi-automated analysis and small sample consumption with ultrahigh sensitivity at single-channel resolution, creating the first step towards a miniaturized high-throughput sensory device.

INTRODUCTION

Detection of a single molecule by selective, efficient biosensors comprising of biological channels embedded in lipid membrane on a robust platform is an attractive but challenging concept. The channel proteins form temporary pores upon being stimulated by electrical, mechanical or chemical triggers (Hille, 2001 a, b) and allow the passage of 10^6 to 10^9 ions/s (Hamil, 1981 a, b; Neher and Sackmann, 1976). Upon the passage of an analyte, the signature ionic current of the channel changes, which can be detected as an electrical signal. The attractive attributes of using bio-nanopores as sensors are their sensitivity towards a trigger and/or their selectivity for a given analyte and their ease of manipulation. The primary challenge is to incorporate the ion channel into a lipid bilayer (a compatible environment which serves as a robust support for the channel) on a device platform, like a silicon chip, so that it is functional in a sensory device. Important contributions have been made towards realizing this goal (Janshoff, 2006; Bally, 2010; Stava, 2012). A conventional approach is to form suspended bilayer lipid membranes (BLM) with reconstituted membrane protein over a micro-aperture in an electrically insulated platform (Mueller, 1962). The BLM forms two separate aqueous compartments connected to electrodes to record current signals through the membrane protein. Although lipid membranes (BLMs) have been used for measurement of channel activity or binding assays (Bayley, 2001; Howorka, 2001; Sackmann, 1996), it still is not an appropriate setup for sensory devices. The reason being, in the conventional BLM setup the free-standing lipid bilayer (around 5-20 nm thick) remains unsupported and tends to be fragile over a large aperture dimension (50-100 μm). This makes the bilayer more sensitive to external mechanical and electrical stimuli and noises, which can break it easily. To overcome this challenge, apertures with sub-10 μm diameter can be an alternative (Schmidt, 2000; McGeoch, 2000), but the fabrication method and material often poses problems (Halza, 2012). Another solution for attaining stability of membranes is to use a supported lipid bilayer (Tamm, 1985; Sackmann, 1996), native vesicle arrays (Stamou, 2003) or tethered bilayers (Wagner, 2000; Naumann, 2002). These surface-based model systems present a promising tool for incorporation of ion channels to efficiently study them by techniques like surface plasmon resonance (SPR), nuclear magnetic resonance (NMR) and X-ray, neutron scattering (Kjaer, 1987, Reimhult, 2008; Suzuki, 2008; Janshoff, 2006). But the sensitivity of signal detection can be low due to inefficient bilayer membrane sealing in the mega ohm resistance range and difficulty in recording channel activity due to fast accumulation of ions in a very short space between the bilayer and the supporting material (Tanaka and Sackmann, 2005).

The next necessary feature for the use of ion channels as sensors is to find an efficient detection system. Detection of analyte can be achieved by transforming the gated ion channel like MscL into "on/off" switches, sensitive to different stimuli. The conventional method of signal detection is by electrical measurement like patch clamp, where signals in the time resolution of microseconds are detected (Hille, 1992 a, b). Although electrical

detection is a very sensitive method, parallelization of electrical measurements as a high throughput read-out of signal can be difficult (Lemay, 2009; Osaki, 2009). Recent advances in imaging techniques have made it possible to circumvent this problem and follow biochemical interactions by fluorescence techniques like confocal laser scanning microscopy (Moerner, 2007; Peters, 2003).

The goal of this chapter is to reconstitute the channel protein, MscL, in a lipid environment on a multi-structured nanochip, so that they - (i) form functional channels, (ii) can be optically detected, and (iii) perform as a high throughput bio-hybrid platform. MscL has been previously incorporated into a polymer-lipid hybrid nanocontainer. It comprised of a lipid bilayer patch with inserted channels and covering a nanostructure on a polymer scaffold (Dudia, 2008). The authors showed that MscL channels were functional and could fill the nanocontainer upon activation. In a recent study, a stable sensory chip was developed using functional MscL in a lipid bilayer on a Si/SiO_2 chip with a single 3μm pore aperture (Halza, 2012). Electrical activity of the channel was reported in a micro meter sized bilayer lipid membrane setup on a Si/SiO_2 chip.

The development of chip arrays consisting of individual, spatially-confined compartments combines the desired features of high sensitivity, parallel analysis and small sample consumption in a single platform (Howorka, 2009; Dekker, 2007). Considerable efforts have been made in this field using silicon (Buchholz, 2008; Kleefen, 2010) or aluminum oxide substrates (Hennesthal, 2002; Venkatesan, 2011), but chip production is both labor and cost intensive, and reproducible fabrication quality at the nanoscale is not always ensured. We use a chip fabricated by Nanospot, featuring nanometer-sized apertures. We present a method to incorporate MscL in the suspended lipid bilayer and detect the high throughput translocation events through MscL channels optically. The advantages of this system are manifold: (i) the membrane formation is unaided and is accomplished by self-organized MscL-liposome fusion and spreading, (ii) the membrane system forms an organic solvent-free suspended lipid bilayer (SLB) (Richter, 2006), (iii) preparation of protein-Giant Unilamellar Vesicles (GUVs) are not required (GUVs, which are difficult to form, are conventionally used to cover the chip), (iv) high efficiency coverage of the nano structures with membrane bilayers, and (v) the nanopores can be individually accessible for analysis of flux events. This makes the platform compatible for parallel analysis of flux events through MscL channels on a single molecule level.

The high throughput sensory platform, with multi-well nanochip can be used to study the fundamental properties of a channel protein in a lipid environment. It is important to gain insight into the functioning of membrane proteins because 60% of all known drug targets are membrane proteins (Bakheet, 2009; Yildirim, 2007). It has been estimated that the human genome codes for up to 6,000 membrane proteins (Wallin, 1998; Fagerberg, 2010; Kozma, 2013). Despite their ubiquitous abundance in cells, they evaded detailed analysis due to the lack of suitable techniques and major challenges relating to their properties. Notable developments generated necessary insight into membrane protein structure,

dynamics and function (Catherman, 2013; Helbig, 2010; Bill, 2011; Alguel, 2010; Shadiac, 2013), but research in this field still represents a challenging undertaking. Several studies have reported innovative techniques to elucidate the function of various channels; some of them have become commercially available (Dunlop, 2008; Milligan, 2009). But they are not yet able to combine highly parallel semi-automated analysis, small sample consumption, high sensitivity and a single protein resolution. Thus, multiplexed nanochip can serve as a perfect system for studying the membrane proteins at a single molecule level.

MATERIALS AND METHODS

Strain and cell growth

Escherichia coli (E. coli) strain PB104 (ΔmscL::Cm) (Blount, 1996) was used to host the p1BAD G22C-His expression constructs containing *mscL*G22C from *E.coli* (Sukharev, 1994; Birkner, 2012). Chemically competent *E. coli* PB104 cells were transformed with p1BAD G22C-His and were grown in Luria broth (LB) supplemented with 10 μg/mL chloramphenicol and 100 μg/mL ampicillin. Cells were grown in a bioreactor at pH 7.5, temperature 37 °C, and oxygen control (dissolved oxygen >70%), using a complex medium [12 g/L Bacto-Tryptone (BD), 24 g/L yeast extract (BD), potassium phosphate (17 mM KH_2PO_4 and 72 mM K_2HPO_4) (pH 7). The medium was supplemented with chloramphenicol and ampicillin. At the early and mid-log phases, 10 ml of 40% (vol/vol) glycerol/L medium were added as an additional carbon source. The protein expression was induced in the late logarithmic phase by adding L-arabinose at 0.1% (wt/vol). Upon induction, another 10 ml 40% (vol/vol) glycerol was added, and cultivation was continued for 90 min.

Membrane vesicle preparation

Bacterial cells were harvested by centrifugation and suspended in ice-cold 25 mM Tris·HCl, pH 8.0, to a final OD_{600} of 100–150. Subsequently, DNAse (0.5 mg/mL, final concentration), RNAse (0.5 mg/mL, final concentration), and 5 mM $MgSO_4$ were added, and cells were broken using a cell disrupter (Type TS/40; Constant Systems) at 1.7 kbar at 4 °C. Cellular debris was removed by centrifugation for 30 min at 18,460 g at 4°C. Supernatant was ultra-centrifuged at 145,400g for 90 min at 4 °C. The supernatant was discarded, and the remaining membrane vesicles were re-suspended and homogenized in ice-cold 25 mM Tris·HCl (pH 8.0) to 0.7 g (wet weight)/ml, corresponding to about 30 mg of protein/ml. Membrane vesicles were frozen in liquid nitrogen and stored at −80 °C.

Protein isolation

MscL-his tagged proteins were purified by nickel-nitriloacetic acid (Ni-NTA) affinity column chromatography, as explained before (Kocer, 2007). Briefly, membrane vesicles were solubilized at 5 mg/ml in 50 mM sodium phosphate (pH 8.0), 300 mM NaCl, 1%

(vol/vol) Triton X-100, and 35 mM imidazole (solubilization buffer) for 30 min at 4 °C. After ultracentrifugation at 267,000g for 20 min at 4°C, the supernatant was applied to pre-equilibrated Ni-NTA agarose resin (Qiagen) [30 mg membrane protein/mL per 50% (wt/vol) matrix slurry] and incubated under mild agitation for 30 min at 4 °C, enabling binding of his-tagged proteins to the matrix. Unbound material was collected as flow through and analyzed when appropriate. The column was washed consecutively with 15 column volumes (CV) wash buffer [50 mM sodium phosphate (pH 8.0), 300 mM NaCl, 0.2% (vol/vol) Triton X-100, 35 mM imidazole]. The non-specific proteins were washed off the affinity column with 7.5 CV L-histidine wash buffer [50 mM sodium-phosphate (pH 8.0), 300 mM NaCl, 0.2% (vol/vol) Triton X-100, 50 mM histidine]. His-tagged proteins were eluted by addition of 15× 0.5 CV Ni-NTA elution buffer [50 mM sodium phosphate (pH 8.0), 300 mM NaCl, 0.2% (vol/vol) Triton X-100, 235 mM L-histidine]. The protein content of the fractions was checked with the Bradford assay. The total yield of protein was 3-4 mg at an average concentration of ca 0.5 mg/ml MscL. Protein was aliquoted and frozen in liquid nitrogen and stored at −80°C.

Preparation of liposomes

Large unilamellar vesicles (LUVs) were prepared as described elsewhere (Reeves, 1969, Kocer, 2007). In brief, lipids (azolectin, *E.coli* polar lipids, DOPC; Avanti Polar Lipids Inc.) dissolved in chloroform were dried in a round-bottomed flask in a rotary evaporator for 2 h under vacuum while rotating the flask at maximum speed at room temperature. The lipid film was rehydrated in buffer (20 mM Tris, 150 mM NaCl, pH 8.0) for 45 min at 50°C to a final concentration of 20 mg/ml, followed by brief sonication for 4 min in a water bath sonicator at room temperature. Subsequently, seven freeze-thaw cycles were performed with rapid freezing in liquid nitrogen, and thawing in a water bath at 50 °C, respectively. Aliquots of 1 ml were stored at -80 °C (Castile, 1999).

Protein reconstitution into liposomes

G22C MscL was reconstituted into azolectin liposomes by a detergent mediated reconstitution method (Kocer, 2007). Briefly, the liposome mixture was thawed and extruded through a 400 nm filter (11 times). Liposomes were destabilized by the addition of a final concentration of 0.25% Triton-X (Affymetrix). MscL and detergent-saturated liposomes were mixed at a 1:20 weight ratio, respectively, and incubated for 30 minutes at 50°C in a water bath. Subsequently, a buffer solution (10 mM sodium-phosphate pH 8.0, 150 mM NaCl) with (200 mM) was added to liposome-MscL mixture in a 1:1 volume ratio and supplemented with 16 mg (wet weight) Biobeads (SM-2 Absorbents) per µl detergent (Triton-X). For detergent removal, the sample was incubated overnight (~16 hours) at 4 °C on a rotating plate. Proteoliposomes with an average diameter of 120nm were formed (as determined by Dynamic Light Scattering, DLS). Fluorescence dequenching assay was used to determine protein activity after reconstitution as described before (Kocer, 2007).

Design of nanopores and femtoliter cavities

Here we discuss briefly, the design of the silicon oxide nanochip used for high throughput studies. 5 inch silicon-on-insulator (SOI) wafers were prepared with photolithography for the processing of approximately 1,150 individual chips (Fig. 5a, b). The SOI chips were subsequently structured by reactive ion etching (RIE) resulting in arrays of 250,000 uniform cylindrical cavities in the silicon (diameter: 0.95 µm; depth: 10 µm; volume: 6.5 fL; Fig. 5c). The cavities are arranged in a rectangular pattern on each chip with a center-to-center distance of 4 µm (Fig. 5d). In a third step, a silicon dioxide top layer is formed by chemical vapor deposition, narrowing the cavity opening to a pore in the nanometer range (Fig. 5e). Importantly, the chip features an optically non-transparent top layer and a transparent glass support. After wafer dicing, the cleaned chips were integrated into an 8-well sample holder (Ibidi) for use on inverted fluorescence microscopes. Nanopore chips were analyzed by atomic force microscopy (AFM) and scanning electron microscopy (SEM). For AFM studies, a Nanowizard II (JPK Instruments) was used in contact mode. The surface roughness of the silicon dioxide top layer of the chips was determined as the root-mean-squared roughness (Rq) from multiple AFM scans (n = 40). Sample areas of 2 x 2 µm2 were analyzed.

Pore-spanning solvent-free suspended lipid bilayers

Nanopore biochips, made by Nanospot BV, were treated with air plasma for 5 min. The cavities were pre-wetted with ethanol for 20 min. Ethanol was gradually exchanged for buffer (20 mM Tris, 150 mM NaCl, 5 mM $CaCl_2$ pH 8.0). Liposomes or proteoliposomes were added to a final concentration of 0.5 mg/ml, along with non-encapsulated fluorescent dyes and incubated for 1 h at room temperature. Excess of non-fused liposomes and fluorescent dye were removed by washing the biochip with calcium-free buffer.

Fluorescence recovery after photobleaching

FRAP was performed on a Leica DMRE upright microscope (Leica Microsystems) equipped with a Leica HCX APO L 63×/0.90 water-immersion objective, a Leica TCS SL confocal scanner and an argon ion laser (488 nm, 25 mW). Images with an edge length of 59.5 µm and a resolution of 0.116 µm/px were acquired at 10% laser power every 346 ms. After recording ten pre-bleach images, a central rectangular region of 7.4×7.4 μm^2 was bleached for 346 ms (1 frame) at 100 % laser power, and 180 post-bleach frames at intervals of 346 ms were acquired. Data analysis was performed as explained before (Goehring, 2010).

MscL efflux experiments

Before liposome fusion to the wells, the cavities were prefilled with buffer containing 10 µM of Atto 488 or Oy647 (Luminartis) as efflux substrate. Also, 5 µM of OregonGreen-labeled Dextran 70 kDa (Life Technologies) was used as a non-permeable substrate, i.e. one that

cannot pass through the channel protein, MscL. Proteoliposomes were supplemented with 0.1 mol% Atto390-labeled DOPE (Atto-Tec) during liposome preparation. Efflux of the fluorescent substrate was initiated by activating MscL with the addition of cysteine–specific, positively-charged reagent, MTSET (3 mM). Labeling of the 22nd amino acid position of MscL with MTSET is sufficient to activate the channel (Yoshimura, 2001). Images were recorded every 10 s over a period of 90 min. Data processing of the images was performed using ImageJ. Transport kinetics were analyzed and fitted using the Nanocalc software (Nanospot GmbH) and Gaussian fits calculated using Origin 8.6 Pro.

High throughput efflux experiments were followed by a NyONE microscope (SynenTec GmbH) equipped with a 20x Olympus air objective (Olympus UPlan SApo 20x/0.75). Additional experiments were carried out with a DMI6000 TIRF microscope (Leica Microsystems) equipped with a 40x Leica air objective (Leica HCX PL FLUOTAR 40x/0.60 CORR). For AFM studies, a Nanowizard II (JPK Instruments) was used. Nanoparticle tracking analysis was carried out with a NanoSight LM10 (Nanosight).

RESULTS

MscL as a model bio-nanosensor

In order to study and have control over the flux through the nanopore, we used MscL as a part of the hybrid system that comprises a lipid bilayer with embedded channels. For the initial characterization studies, we used a silicon nitride chip fabricated with 24 arrays of nanopores. An individual array contained 2025 (45x45) nanopores with 30 fL volume (Kleefen, 2010). The top layer of the chip was formed from 50 nm thick silicon nitride (Si_3N_4) layer, which is thin enough to ensure transmission of light through the whole surface of the nanopore. The primary aim was to optimize the process of reconstitution of MscL in a lipid bilayer and attain maximum coverage of the nanochip. For this purpose we used MscL-containing large unilamellar vesicles (LUVs). The self-organized pore-spanning lipid bilayers formed by spontaneous fusion and subsequent spreading of the vesicles has advantages in comparison to creating bilayer lipid membranes. Bilayer lipid membrane (BLM) strategy often utilizes the organic solvents for aiding the membrane formation. This may disrupt the native structure and function of membrane proteins and are therefore less feasible for mechanistic studies. Fusion of giant unilamellar vesicles (GUVs) is able to seal nanopore openings and is organic solvent free (Buchholz, 2008; Kleefen, 2010), but reconstitution of membrane proteins, in particular mammalian proteins, into GUVs is very challenging (Doeven, 2005). LUVs in comparison offer the advantage that they are easily formed and there are established techniques for the reconstitution of membrane proteins without the loss of their native structure and function in LUVs. In our study, different lipids and lipid mixtures were tested for their ability to form stable pore-spanning lipid bilayers. Vesicles consisting of soy bean lipids or a mixture of *E.coli* polar lipids and DOPC in a

ratio of 70:30 (w/w) yielded the best results. Apart from proteoliposomes, subcellular vesicles with comparable sizes to LUVs, such as microsomes and lysosomes, can directly be applied to the chip for SLB formation.

The principle of the study is based on the optical detection of flux of a fluorescent dye, Atto 488, across the lipid bilayer through the MscL channels, upon triggered opening, through confocal laser scanning microscopy (Fig.1). Incubation of the nanochip with MscL-liposomes (LUVs) along with Atto 488 resulted in spreading of the LUVs on the pores and 60 to 70% sealing of the nanopores was observed. Upon sealing, the dye, Atto 488 which was pre-incubated with the liposomes was trapped inside the compartments. Each nanopore with trapped dye inside gave a clear optical signal (Fig.2). As shown previously, addition of MTSET transfers five positive charges to the pore, which activates the MscL channel opening and releases the dye (Yoshimura, 2001). Hence, the signal decreases (Fig.2-2). In some cases, if extra dye was added to the bulk solution, refilling of the cavities with the dye from the external bulk was observed (Fig.2-3). Addition of 1mm DTT cleaved the disulphide bond between MTSET and MscL, and closed the channel. Excess DTT and dye was washed off. Upon re-addition of MTSET, efflux of dye was observed for the second time (Fig.2-4).The decay constant, τ, of the flux of the dye molecule through the MscL channel was calculated from the following equation:

$$\tau \approx \frac{V}{4rD} + \frac{L^2}{2D} \qquad \text{Eq(1)}$$

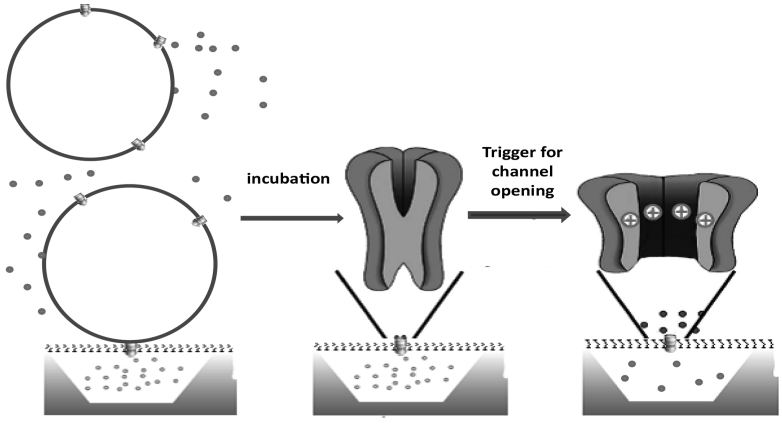

Figure 1. The principle of membrane sealing and MscL activity: Single dye experiment. At first the nanochip is incubated with MscL-liposome vesicles and the fluorescent analyte, Atto 488 (left panel). The nanopore is sealed by the spontaneous collapse of the MscL-liposomes on it. The fluorophore is trapped upon sealing of the chip cavities by the lipid bilayer, resulting in an optical signal (Atto488), which is detected by a confocal laser scanning microscopy (CLSM) (middle panel). Now, upon activation of MscL by MTSET, the channel opens up and releases the fluorophore which is recorded by the microscope.

Where, V is the volume of the cylinder (assuming the MscL pore to be a cylinder), D is the diffusion coefficient, r is the radius of the MscL, L is the length of the protein. Taking into account, a MscL pore diameter of 4 nm, τ was calculated to be 13.4 s for a single MscL channel and 6.3 s for 2 MscL channels. The results are summarized in figure 3.

From figure 2, it is evident that MscL was successfully inserted in the suspended lipid bilayer and the efficiency of coverage of the nanopores was about 60%.

To better analyze these refilling events, and particularly to distinguish channel-induced release from release through any possible lipid bilayer defects, we designed another experiment in which the dye used inside the cavities was PEGylated (Oyster 488-PEG). PEG increased the molecular weight of the dye to 25 kDa and made the dye bulky. MscL allows passage of molecules upto 6.5 kDa (van den Bogaart, 2007; Mika, 2012). Therefore, the PEGylation ensures that even if MscL opens up, the trapped dye cannot escape. So, even after MTSET addition, there should be no decrease in signal except if there is a membrane rupture. Subsequently, a second dye, Atto 532, was added to the bulk. If the channels were open, the second dye would enter the pore, thus giving a co-localized signal, as depicted in Figure 4. The result illustrates that co-localization of signal (yellow, marked in circle) is seen in some nanopores, which implies that influx

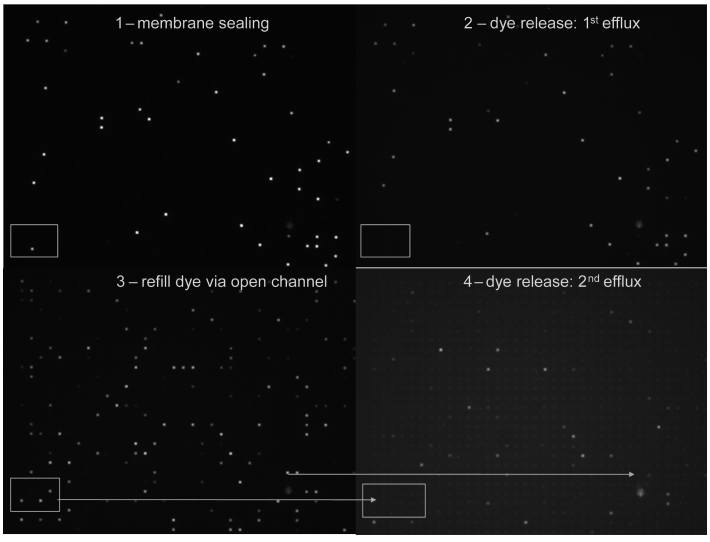

Figure 2. Membrane sealing and MscL activity: Single dye experiment. 1) Fluorophore, Atto 488 is trapped upon sealing of the chip cavities by the lipid, resulting in optical signal (here Atto488 only). Excess dye is washed off. 2) MTSET activates the opening of MscL and the trapped dye is released. 3) Atto488 is again added to the bulk, cavities get refilled. Addition of DTT cleaves the disulphide bond and closes the channels. Excess dye and DTT is washed off. 4) By adding MTSET again to the external solution, MscL is triggered open for the second time, leading to efflux of the entrapped dye. The box represents an area with nanopores where all the above events are visible. The arrow represents the corresponding nanopores where efflux occurs. Scale bar = 10 μm.

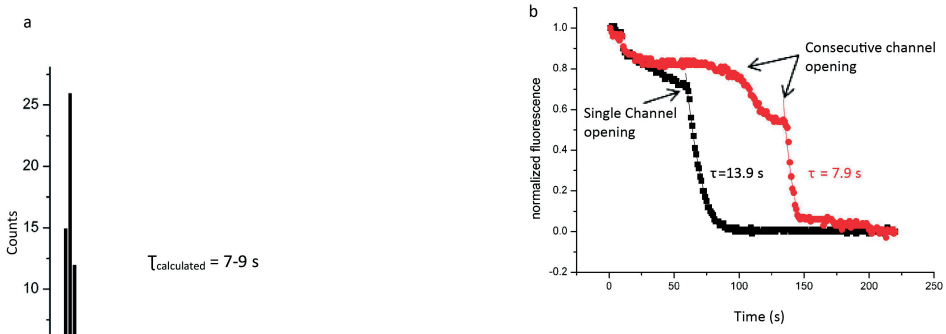

pore	calculated τ (s)
MscL (d=4nm)	13.4
2x MscL	6.3
nanopore (d=15 nm)	0.3
nanopore (d=120 nm)	2.3

Figure 3. Decay Constant, τ of flux of dye through MscL. a) Graph of number of events vs time constant of efflux of dye through a single MscL channel (Atto488). b) Graph of normalized fluorescence signal vs time from a candidate nanopore showing the decay constant of efflux of the entrapped dye either through a single or two MscL channels. Inset showing the value of decay constant, τ given the diameter of the channel or the nanopore of specific size. Scale bar = 10 μm.

of Atto 532 (red) into these cavities occurred through the functional MscL channels, whereas Oyster 488-PEG (green) did not escape. Thus, the bilayer was intact and contained functional MscL channels. The sole green spots signify that the cavities are covered by intact lipid bilayer but do not contain MscL (or in some cases MscL may not have been functionally inserted into the membrane or be inserted in an inside-out direction). The red spots indicate that the pores are covered by bilayer and Atto 532 dye entered the cavities through the opening of MscL channels; in these cavities Oyster 488-PEG dye did not get trapped. The nanopores with no signal signify that either they are not covered with bilayer or the bilayer is ruptured.

Taken together, these experiments proved that the channels were functional and that release via MscL could be differentiated from non-specific release through the lipid bilayer itself. Next, we aimed for a scale-up of the whole setup in order to obtain a high-throughput detection chip. For this, we used a nanochip designed by Nanospot, which allows multiplexing of flux events. This is discussed in the following section.

The design of nanopores with femtoliter cavities

Her we introduce the silicon oxide nanochip used for the high throughput studies. The nanochip was fabricated by Nanospot from a 5-inch silicon-on-insulator (SOI) wafer by reactive-ion etching, creating cylindrical cavities of approximately 1 μm in diameter and 10 μm in depth. A silicon-oxide top layer was formed by chemical vapor

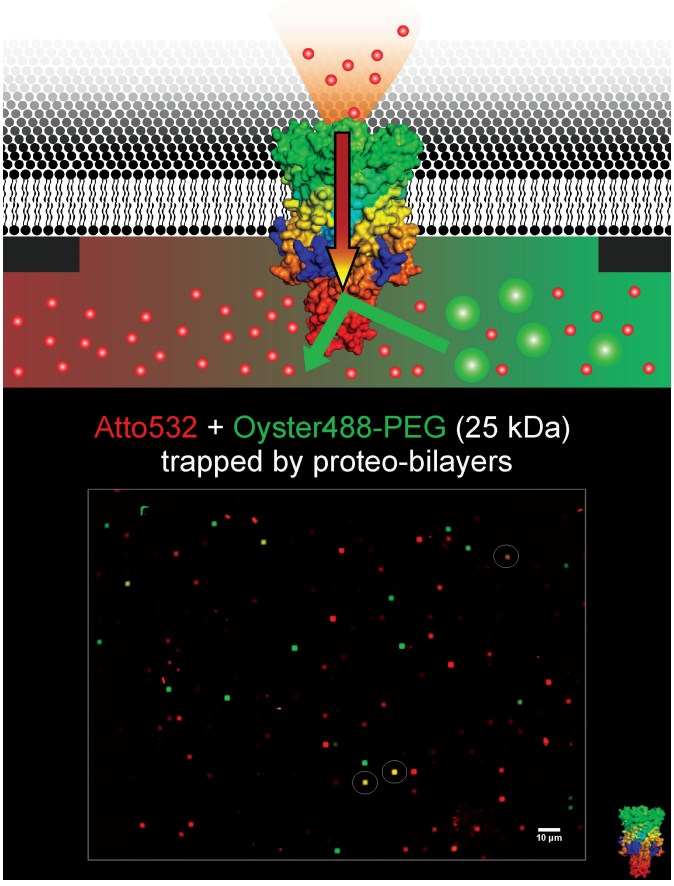

Figure 4. MscL-mediated influx of dye: Dual colour experiment in CLSM. Top-A graphic representation of engineered MscL channel through which the first dye, Oyster 488-PEG (green) cannot diffuse out upon channel opening, but a second dye, Atto 532 (red) can diffuse in, when added to the bulk. This is visible in the colocalization of the signals (yellow). Bottom-Upon addition of MTSET, the MscL channel opens and the entrapped dye cannot diffuse out of the cavity. At the same time, another dye, Atto 532 just diffuses inside the nanopore through the channel, thus showing colocalization of two dyes, marked as circle (yellow).

deposition, narrowing the cavity opening to a pore in the nanometer range. Pore sizes ranging from 70 - 120 nm were created with an enclosed cavity volume of about 6.5 femtoliter (Fig. 5c). Each wafer resulted in approximately 1,000 individual chips of identical quality (5a), with each chip consisting of around 250,000 homogeneous nanopores and cavities arranged in a rectangular pattern, with the possibility to address each cavity individually by fluorescence readout. In addition, the chip possesses an optically opaque top layer and a transparent glass bottom. The presented nanopore chip is compatible with standard inverted epifluorescence microscopes operating with air objectives widely used in life sciences and easy to automatize.

Chips processed as described above were analyzed by atomic force microscopy (AFM) and scanning electron microscopy (SEM). Figure 5d shows an AFM image of an imaged chip with perfectly ordered arrays of nanopores with a pitch of 4 µm between individual pores. A surface roughness of *Rq* = 3.6 nm was estimated by AFM (n = 40). The accurate fabrication of the cavities and nanopore diameters was confirmed via SEM for several chip cross-sections (n=5) (Fig.5e). In conclusion, the nanopore design offers a high throughput analysis of single transport events by simple fluorescence read-out.

Formation of suspended membranes on nanopores by vesicle fusion and spreading

In this new set up, we again covered the wells with a lipid bilayer by spreading the large unilamellar liposomes over the chip surface. The nanochip was incubated with liposomes and a fluorescent dye, Atto 488. Spontaneous spreading of the liposomes resulted in

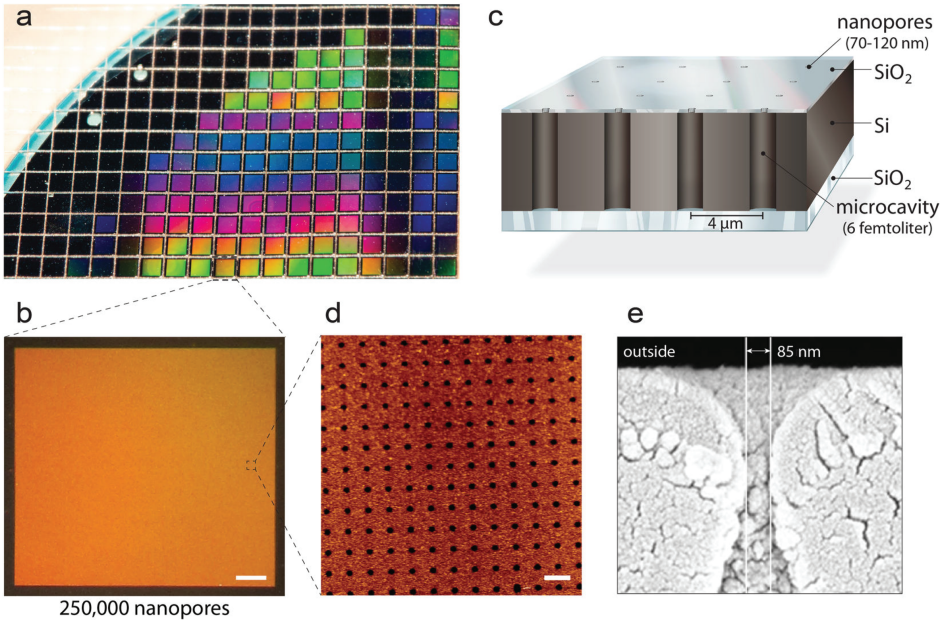

Figure 5. Design of multiplexed nanopore chip. a) A silicon-on-insulator (SOI) wafer is structured by reactive-ion etching. Approximately 1000 individual chips are fabricated from each wafer with identical properties and quality. b) Each chip comprises 250,000 individual nano-cavities. Scale bar: 200 µm, c) Each cavity is addressable via multi-spectral fluorescence read-out. Fluorescent signals from the buffer reservoir are blocked by a non-transparent silicon dioxide top layer making the nanochip compatible with inverted microscopes, d) Atomic Force Microscopy (AFM) image shows regularly arranged pore opening, with optimal surface property for vesicle spreading. The surface roughness of the silicon dioxide layer was 3.6nm (n =40) Scale bar: 5 µm, e) Scanning electron microscopy (SEM) images show a cross-section through the nanocavities embedded inside the silicon chip.

formation of suspended lipid bilayers with entrapped dye. Lipid vesicles consisting of Soy lecithin (azolectin) yielded best results. Membranes created by these vesicles are stable for up to 20 hours on the chip (Fig. 6a) and seal up to 94% of the cavities, occluding small and large solutes, such as free fluorophores (0.7 kDa) or fluorescently-labelled dextran (10 kDa). Vesicle fusion and spreading to the chip surface was aided by the addition of 5 mM $CaCl_2$ prior to LUV application, increasing the adherence of LUVs to the silicon dioxide chip surface. The size distribution of the liposomes was examined via nanoparticle tracking analysis. Liposomes must be monodisperse to avoid lipid contaminations inside the cavities and to achieve optimal suspended lipid bilayer (SLB) formation.

The coverage as well as the fluidic properties of the membranes covering the nanopore chip were examined by Fluorescence Recovery After Photobleaching (FRAP). Liposomes supplemented with 0.1 mol% Bodipy-PE were fused and spread on the chip surface, resulting in a homogenous bilayer (Fig.6). A region of interest (7.4 x 7.4 μm2) was bleached by using an argon laser (488 nm, 25 mW/cm^2). Notably, 90% fluorescence recovery was observed, demonstrating that the suspended lipid bilayer is intact, mostly homogeneous and fluid on the chip surface (Fig. 6b). The lateral diffusion constant for independent FRAP experiments was 2.0 ± 0.7 $\mu m^2 s^{-1}$ (n=49) with an immobile fraction of 6.0 ± 3.0 %. This result is in agreement with the lateral diffusion coefficient of 1 - 3 $\mu m^2 s^{-1}$ for lipid molecules on SiO_2 surfaces (Venkatesan, 2011). If the liposome concentration applied to the chip was too low, the fluorescent recovery was impaired, leading to mostly ill-defined membrane patches or free vesicles on the SiO_2 interface. These results thus demonstrate that fluid lipid bilayers are properly assembled on nanopore chips.

Nanopore-spanning membranes separate the cavities from the bulk compartment

To investigate if the bilayer is stable and its formation leads to proper compartmentalization, we designed a dual fluorophore assay. The principle is that the chip cavities are easily accessible to fluorophores if no lipid bilayer is present (Fig. 7a), resulting in complete co-localization of two dyes, Atto 488 and Atto 594 inside the cavities. In contrast, complete separation of fluorescent solutes is observed if a lipid bilayer seals the nanopore (Fig. 7b). Prior to bilayer formation, a fluorescent analyte (e.g. Atto 488) is added to the buffer reservoir, when all cavities are freely accessible. After bilayer formation and buffer exchange, the cavities get sealed and the analyte is entrapped. In all non-sealed cavities, the fluorophore is diluted out (Fig. 7b).

In a subsequent step, a differently labelled analyte is added (Atto 594) to the bulk. Atto 594 cannot enter cavities sealed by the SLB, demonstrating the complete retention of small fluorophores by the bilayer. Disruption of the SLB by the addition of detergent results in a rapid efflux of the entrapped solute. Simultaneously, the second analyte from the external reservoir entered the cavities, leading to Atto 594 signal (Fig. 7c). With time, this signal also decreases due to diffusion of the dye. In summary, the

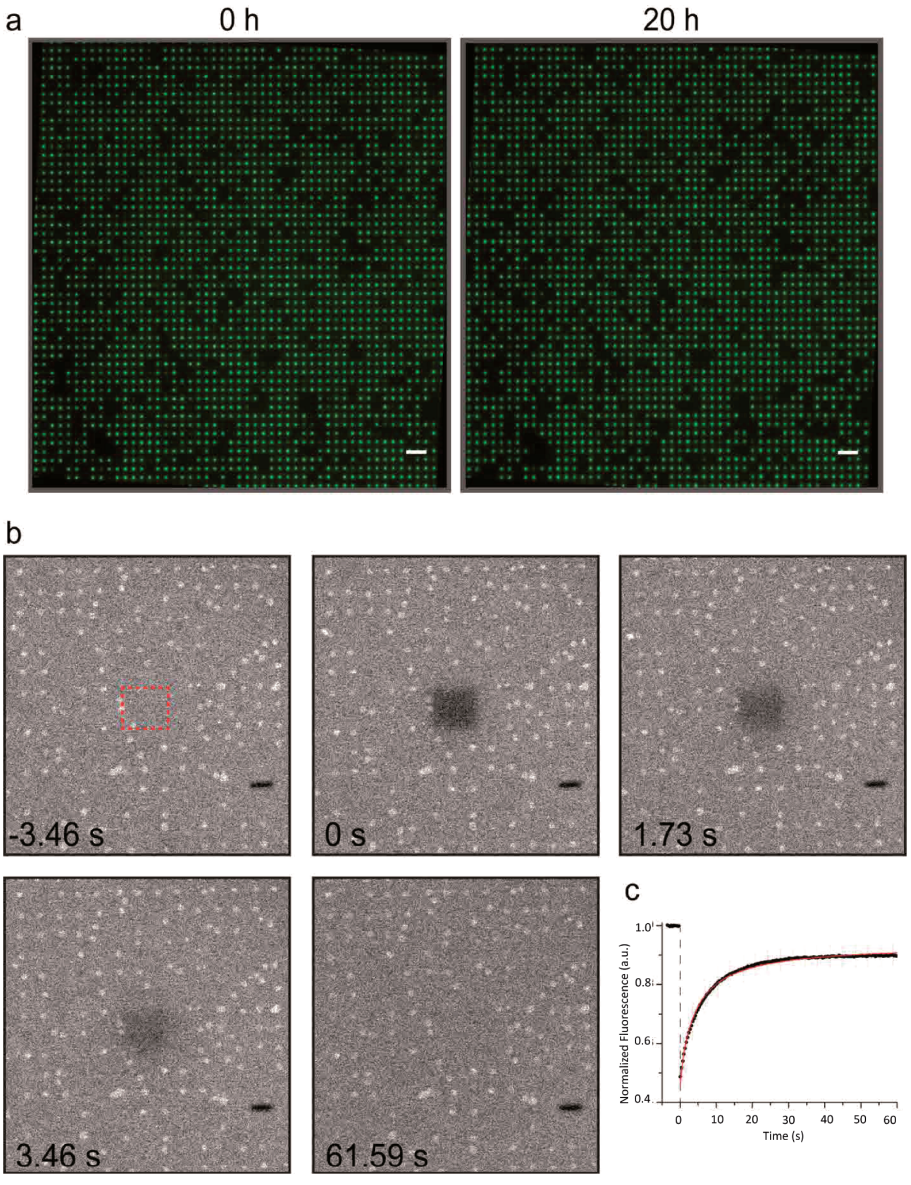

Figure 6. Membrane stability and fluidity. a) Small fluorescent dyes (e.g. Atto488) can be trapped inside the nanocavities by suspended lipid bilayer (SLB) formation. All cavities that are sealed off from the outside buffer reservoir by an intact lipid bilayer show a fluorescent signal, whereas all non-sealed cavities appear black. SLBs are stable for up to 20 h. Scale bar = 10 µm. b) LUVs (SoyPC20 + 0.1 mol% Bodipy-PE) spread and fused to the nanopore chip were studied by FRAP. A square of 7.4 x 7.4 µm^2 was bleached with an Argon laser (488 nm, 25 mW) and the recovery of the fluorescence was observed over time. Within 60 s, 90% recovery of the bleached area can be observed. c) The normalized recovery curves provide a diffusion constant of 2.0 ± 0.7 µm^2 s^{-1} (n=49) with an immobile fraction of 6 ± 3%, being in perfect agreement with previously reported values for silicon-oxide. The shown images are 60 x 60 µm^2.

results show that nanopore-suspended lipid bilayers form stable impermeable barriers for small, hydrophilic solutes, and their efflux is mediated by MscL.

Multiplexed single channel recordings

Here we demonstrate MscL-mediated multiple parallel efflux events across the membrane. Following the procedure optimized in the above section, MscL was reconstituted into liposomes composed of Soy lecithin (azolectin) and protein activity after reconstitution was verified by an ensemble assay, i.e. fluorescence dequenching assay, as described in methods. Using the same conditions as previously shown with silicon nitride chips, proteoliposomes were allowed to spontaneously fuse to the nanopore chip by incubating them with the chip and a fluorescent dye. Sealing rates up to 84% were achieved for protein-containing proteoliposomes. In this set up we used Oy647 dye as a reporter for efflux events. Oy647 was entrapped inside the cavities prior

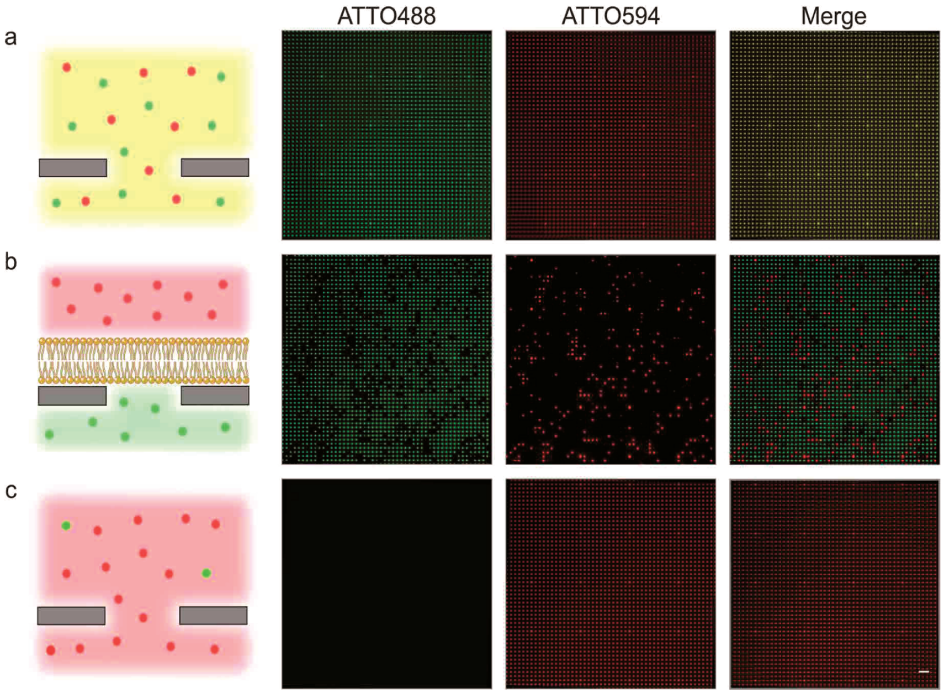

Figure 7. Compartmental separation by SLB. a) Fluorophores easily access chip cavities if no SLB is present, resulting in perfect co-localization, when e.g. two dyes are added to the buffer reservoir (here Atto488 and Atto594). b) Lipid bilayers spanning the nanopores retain small hydrophilic fluorophores inside the nanocavities, sealing them off from the above buffer reservoir and thus forming an impermeable barrier. If a second fluorophore is added after SLB formation, co-localization is not observed. c) By adding detergents, the SLB is totally disrupted, leading to efflux of the entrapped dye, the second dye from the bulk buffer reservoir will gradually fill the cavity. Scale bar = 10 µm.

to SLB formation; Oregon Green Dextran (70 kDa) was used as a channel impermeable control substrate. Atto390-labeled DOPE was incorporated into the lipid bilayer to monitor membrane integrity during the experiment. Upon MTSET-triggered opening of the MscL channel, Oy647 efflux was observed for cavities, where MscL was located in the pore spanning SLB region (Fig. 8a). Several hundred of these events were recorded in each experiment. The three fluorescence readout channels could be classified and discriminated from each other (Fig. 8b-d). This permits for unbiased data selection. Only the events showing mono-exponential efflux kinetics in the Oy647 channel (red) and constant signals for the control solute (green) as well as the lipid channel (violet) were chosen for final data analysis (Fig.8). Selected Oy647 efflux curves were subsequently analyzed. In a single experiment, hundreds of MTSET mediated efflux events were recorded (Fig. 9). Determination of the translocation rate constant revealed events in two Gaussian populations, representing either one (k_{efflux} = 1.36 10^{-3} s^{-1}; 68% of all events) or two MscL channels per well (k_{efflux} = 3.33 $10^{-3}s^{-1}$).

From all sealed cavities analyzed in this study (n = 9,046), approximately 8% showed efflux activity. By multi-spectral decoding, these flux events can be classified into four categories: (i) mono-exponential efflux events (Fig. 8b), (ii) complex kinetics, (iii) membrane rupture (Fig. 8c), and (iv) lipid intrusion into the cavities (Fig. 8d). 50% of all efflux events are mono-exponential with stable signals for the lipid probe. In contrast, complex efflux events are defined by exponential efflux of the translocated substrate, but displaying unsteady signals for the control and/or the membrane dye. They are therefore not considered for final data analysis. Likewise, lipid intrusion events are discarded, where the lipid bilayer enters cavity space and reduces the cavity volume by displacing the entrapped dye. Overall, the data show the potential of the technique to resolve single flux events. Thus, by combining a membrane-embedded channel protein, MscL, with a nanochip, we have successfully established a high throughput bio-hybrid sensor.

DISCUSSION

We have established a procedure for coating the nanopores on a solid support with lipid membranes reconstituted with functional MscL. Further, we have demonstrated controlled permeability of cargo through the channel protein in the membrane coated nanochip, which is an ideal biohybrid system for studying membrane protein functions. Also, it can be used for semi-automated high throughput assays for screening of drugs and binding partners of channel proteins. The important features of the nanocontainer system are: i) high coverage efficiency of the nanochip with MscL-LUVs, ii) simultaneous detection of flux events in thousands of wells, (iii) the controlled opening and closing of the channel protein, (iv) the interior of each nanopore is individually accessible for detection, and (v) optical detection of the passage of distinct fluorescent dyes (cargo molecules) at real time.

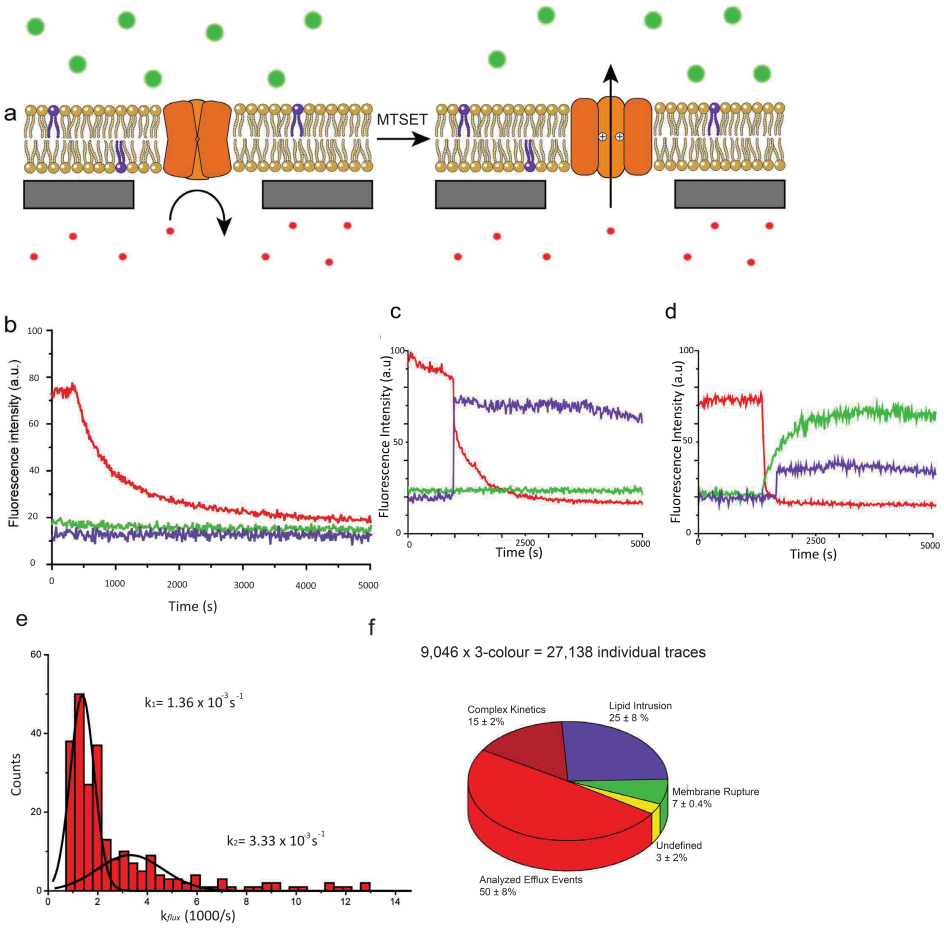

Figure 8. MscL-mediated substrate translocation. a) Proteoliposomes containing functionally reconstituted MscL were fused and spread on the chip surface. Small solutes like a fluorophore are neither able to pass through the channel nor the lipid bilayer. Upon addition of 3 mM MTSET, the MscL channel opens and the entrapped dye can diffuse out of the cavity, leading to a decrease in fluorescence intensity. Oy647 (red curves) was entrapped inside the cavities as translocation reporter, while OregonGreen Dextran (10 kDa, green) was added as channel impermeable control substrate. LUVs were supplemented with 0.1 mol% Atto390 – DOPE (purple) to follow the integrity of the SLB during the experiment. Different events can be discriminated like, (b) most frequently being efflux events of Oy647 dye through the MscL pore, (c) lipid invasion into the cavities and, (d) unspecific membrane rupture. The multi-color fluorescence read-out enables unbiased data selection. e) Rate constants for translocation events (n = 242) cluster into two Gaussian populations, demonstrating the ability of the system to discriminate between single- and multi-channel transport. f) Pie diagram of statistical analysis of 9046 sealed chip cavities. 8% of all analyzed cavities show exponential efflux events. Red: efflux of translocated analyte, green: rupture of bilayer, violet: lipid intrusion into the cavities.

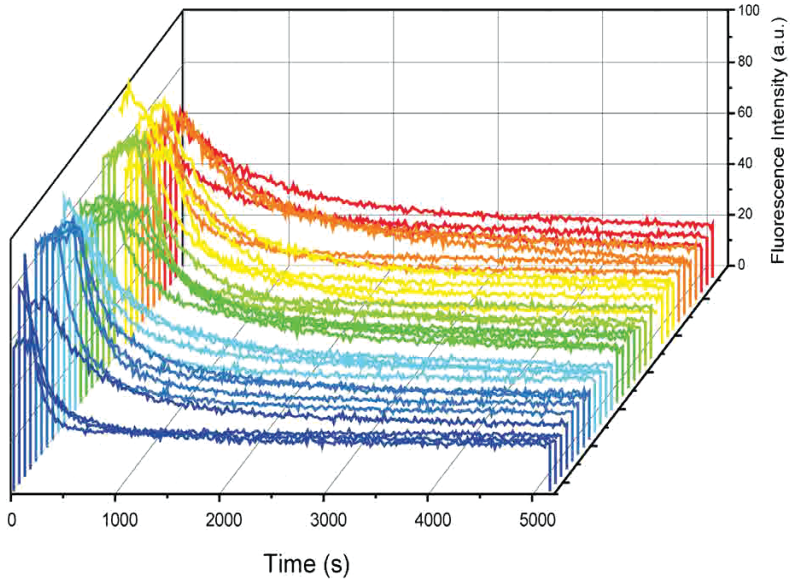

Figure 9. MscL efflux curves. Shown are 24 curves of MscL efflux assays representing 10% of randomly selected events in this study. MTSET (3 mM) was added at time point 0. As soon as the positively charged MTSET labels the constriction site of MscL, the channel opens, and releases the entrapped dye.

These novel features allow control and optical visibility of the cargo moving in or out of the nano-compartments and makes the system applicable for carrying out biochemical reactions in parallel. Previously many biochemical studies were performed with self inserting, pore forming peptides, like α-hemolysin or OmpF, which remain permanently open after inserting in the membrane (Kleefen, 2010; Okumus, 2009; Broz, 2006). Even though these peptides insert very easily into the membrane bilayer, they don't have an "off" state: the molecules smaller than the pore size freely diffuse and generate current signals. However, if an "on/off" switch is desired, other strategies are required. For example, thermodynamic properties of lipids are utilized for generating temporary "on/off" pores (Cisse, 2007). A characteristic property of phospholipid membranes is development of temperature-triggered lipid packing defects at the phase transition temperature. In this case, the number and dimension of pores can vary and is dependent on the ambient temperature. As a solution to attain external control over permeability through nanopores, Dudia et al applied engineered MscL as an on/off switch (Dudia, 2008). They used optical readout to follow loading of the polystyrene scaffold though triggered opening of MscL embedded in a membrane patch. In another application, MscL-containing suspended bilayer is used to coat a 3 μm microaperture in Si/SiO_2 chips (Halza, 2012). They used both the self-inserting peptide alamethicin and the ion channel MscL in a stable bilayer lipid membrane (BLM) setup. In our system, we

employ MscL-bilayer to seal nano chip cavities of 100nm and achieve parallelization of thousands of flux events through the nanopores. Further, we could obtain efficient coverage rate (~80%) of nanopores by stable membrane due to the smaller nanopore dimension. Taken together, we use a more sophisticated multiplexed nanochip and utilize engineered MscL to generate a stable and externally controlled nanopore, which could lead to nanochip-based sensory platform.

CONCLUSION

After establishing the proper conditions for reconstitution and coverage of nanopores with MscL-lipid bilayer, using a comparatively simpler silicon oxide nanochip (2025 nanopores), we scaled-up the setup to silicon nitride nanochip (250,000 nanopores) for high throughput studies. Optical detection of individually accessible nanopores, led to acquizition of information from thousands of flux events occuring parallely in a real-time analysis. This ensured statistically relevant data with minimal sample consumption. Silicon-on-insulator (SOI) based nanochips, featuring cylindrical cavities and pore apertures below 100 nm, are compatible for spontaneous collapse and fusion of liposomes to nanopores. The channel protein MscL used in this study demonstrates the capability of the system to analyze gated ion channels. In future, this technology can be used as a high-throughput sensory device for studying fundamental properties like diffusion through channels and can be also applied for screening of a broad spectrum of therapeutic drug targets.

REFERENCES

Alguel Y, Leung J, Singh S, Rana R, Civiero L, Alves C, & Byrne B (2010) New tools for membrane protein research. *Curr Protein Pept Sci* **11**: 156-165

Bakheet TM & Doig AJ (2009) Properties and identification of human protein drug targets. *Bioinformatics* **25**: 451-457

Bally M, Bailey K, Sugihara K, Grieshaber D, Voros J, & Stadler B (2010) Liposome and lipid bilayer arrays towards biosensing applications. *Small* **6**: 2481-2497

Bayley H & Cremer PS (2001) Stochastic sensors inspired by biology. *Nature* **413**: 226-230

Bill RM, Henderson PJ, Iwata S, Kunji ER, Michel H, Neutze R, Newstead S, Poolman B, Tate CG, & Vogel H (2011) Overcoming barriers to membrane protein structure determination. *Nat Biotechnol* **29**: 335-340

Birkner JP, Poolman B, & Kocer A (2012) Hydrophobic gating of mechanosensitive channel of large conductance evidenced by single-subunit resolution. *Proc Natl Acad Sci U S A* **109**: 12944-12949

Blount P, Sukharev SI, Moe PC, Schroeder MJ, Guy HR, & Kung C (1996) Membrane topology and multimeric structure of a mechanosensitive channel protein of Escherichia coli. *EMBO J* **15**: 4798-4805

Broz P, Driamov S, Ziegler J, Ben-Haim N, Marsch S, Meier W, & Hunziker P (2006) Toward intelligent nanosize bioreactors: a pH-switchable, channel-equipped, functional polymer nanocontainer. *Nano Lett* **6**: 2349-2353

Buchholz K, Tinazli A, Kleefen A, Dorfner D, Pedone D, Rant U, Tampe R, Abstreiter G, & Tornow M (2008) Silicon-on-insulator based nanopore cavity arrays for lipid membrane investigation. *Nanotechnology* **19**: 445305-4484/19/44/445305.

Castile JD & Taylor KM (1999) Factors affecting the size distribution of liposomes produced by freeze-thaw extrusion. *Int J Pharm* **188**: 87-95

Catherman AD, Li M, Tran JC, Durbin KR, Compton PD, Early BP, Thomas PM, & Kelleher NL (2013) Top down proteomics of human membrane proteins from enriched mitochondrial fractions. *Anal Chem* **85**: 1880-1888

Cisse I, Okumus B, Joo C, & Ha T (2007) Fueling protein DNA interactions inside porous nanocontainers. *Proc Natl Acad Sci U S A* **104**: 12646-12650

Dekker C (2007) Solid-state nanopores. *Nat Nanotechnol* **2**: 209-215

Dudia A, Kocer A, Subramaniam V, & Kanger JS (2008) Biofunctionalized lipid-polymer hybrid nanocontainers with controlled permeability. *Nano Lett* **8**: 1105-1110

Dunlop J, Bowlby M, Peri R, Vasilyev D, & Arias R (2008) High-throughput electrophysiology: an emerging paradigm for ion-channel screening and physiology. *Nat Rev Drug Discov* **7**: 358-368

Fagerberg L, Jonasson K, von Heijne G, Uhlen M, & Berglund L (2010) Prediction of the human membrane proteome. *Proteomics* **10**: 1141-1149

Goehring NW, Chowdhury D, Hyman AA, & Grill SW (2010) FRAP analysis of membrane-associated proteins: lateral diffusion and membrane-cytoplasmic exchange. *Biophys J* **99**: 2443-2452

Halza E, Bro TH, Bilenberg B, & Kocer A (2013) Well-defined microapertures for ion channel biosensors. *Anal Chem* **85**: 811-815

Hamill OP, Marty A, Neher E, Sakmann B, & Sigworth FJ (1981) Improved patch-clamp techniques for high-resolution current recording from cells and cell-free membrane patches. *Pflugers Arch* **391**: 85-100

Hamill OP & Sakmann B (1981) Multiple conductance states of single acetylcholine receptor channels in embryonic muscle cells. *Nature* **294**: 462-464

Helbig AO, Heck AJ, & Slijper M (2010) Exploring the membrane proteome--challenges and analytical strategies. *J Proteomics* **73**: 868-878

Hennesthal C, Drexler J, & Steinem C (2002) Membrane-suspended nanocompartments based on ordered pores in alumina. *Chemphyschem* **3**: 885-889

Hille B (1992) G protein-coupled mechanisms and nervous signaling. *Neuron* **9**: 187-195

Hille B (1992) Pumping ions. *Science* **255**: 742

Howorka S & Siwy Z (2009) Nanopore analytics: sensing of single molecules. *Chem Soc Rev* **38**: 2360-2384

Janshoff A & Steinem C (2006) Transport across artificial membranes-an analytical perspective. *Anal Bioanal Chem* **385**: 433-451

Kjaer K, Als-Nielsen J, Helm CA, Laxhuber LA, & Mohwald H (1987) Ordering in lipid monolayers studied by synchrotron x-ray diffraction and fluorescence microscopy. *Phys Rev Lett* **58**: 2224-2227

Kleefen A, Pedone D, Grunwald C, Wei R, Firnkes M, Abstreiter G, Rant U, & Tampe R (2010) Multiplexed Parallel Single Transport Recordings on Nanopore Arrays. *Nano Lett*

Kocer A, Walko M, & Feringa BL (2007) Synthesis and utilization of reversible and irreversible light-activated nanovalves derived from the channel protein MscL. *Nat Protoc* **2**: 1426-1437

Kozma D, Simon I, & Tusnady GE (2013) PDBTM: Protein Data Bank of transmembrane proteins after 8 years. *Nucleic Acids Res* **41**: D524-9

Lemay SG (2009) Nanopore-based biosensors: the interface between ionics and electronics. *ACS Nano* **3**: 775-779

McGeoch JE, McGeoch MW, Carter DJ, Shuman RF, & Guidotti G (2000) Biological-to-electronic interface with pores of ATP synthase subunit C in silicon nitride barrier. *Med Biol Eng Comput* **38**: 113-119

Mika JT, Birkner JP, Poolman B, & Kocer A (2013) On the role of individual subunits in MscL gating: "all for one, one for all?". *FASEB J* **27**: 882-892

Milligan CJ, Li J, Sukumar P, Majeed Y, Dallas ML, English A, Emery P, Porter KE, Smith AM, McFadzean I, Beccano-Kelly D, Bahnasi Y, Cheong A, Naylor J, Zeng F, Liu X, Gamper N, Jiang LH, Pearson HA, Peers C et al (2009) Robotic multiwell planar patch-clamp for native and primary mammalian cells. *Nat Protoc* **4**: 244-255

Moerner WE (2007) New directions in single-molecule imaging and analysis. *Proc Natl Acad Sci U S A* **104**: 12596-12602

Mueller P, Rudin DO, Tien HT, & Wescott WC (1962) Reconstitution of cell membrane structure in vitro and its transformation into an excitable system. *Nature* **194**: 979-980

Naumann C, Prucker O, Lehmann T, Ruhe J, Knoll W, & Frank CW (2002) The polymer-supported phospholipid bilayer: tethering as a new approach to substrate-membrane stabilization. *Biomacromolecules* **3**: 27-35

Neher E & Sakmann B (1976) Single-channel currents recorded from membrane of denervated frog muscle fibres. *Nature* **260**: 799-802

Okumus B, Arslan S, Fengler SM, Myong S, & Ha T (2009) Single molecule nanocontainers made porous using a bacterial toxin. *J Am Chem Soc* **131**: 14844-14849

Osaki T, Suzuki H, Le Pioufle B, & Takeuchi S (2009) Multichannel simultaneous measurements of single-molecule translocation in alpha-hemolysin nanopore array. *Anal Chem* **81**: 9866-9870

Peters R (2003) Optical single transporter recording: transport kinetics in microarrays of membrane patches. *Annu Rev Biophys Biomol Struct* **32**: 47-67

Reeves JP & Dowben RM (1969) Formation and properties of thin-walled phospholipid vesicles. *J Cell Physiol* **73**: 49-60

Reimhult E & Kumar K (2008) Membrane biosensor platforms using nano- and microporous supports. *Trends Biotechnol* **26**: 82-89

Richter RP, Berat R, & Brisson AR (2006) Formation of solid-supported lipid bilayers: an integrated view. *Langmuir* **22**: 3497-3505

Sackmann E (1996) Supported membranes: scientific and practical applications. *Science* **271**: 43-48

Schmidt C, Mayer M, & Vogel H (2000) A Chip-Based Biosensor for the Functional Analysis of Single Ion Channels. *Angew Chem Int Ed Engl* **39**: 3137-3140

Shadiac N, Nagarajan Y, Waters S, & Hrmova M (2013) Close allies in membrane protein research: cell-free synthesis and nanotechnology. *Mol Membr Biol* **30**: 229-245

Stamou D, Duschl C, Delamarche E, & Vogel H (2003) Self-assembled microarrays of attoliter molecular vessels. *Angew Chem Int Ed Engl* **42**: 5580-5583

Stava E, Choi S, Kim HS, & Blick RH (2012) On-chip stochastic resonance of ion channel systems with variable internal noise. *IEEE Trans Nanobioscience* **11**: 169-175

Sukharev SI, Blount P, Martinac B, Blattner FR, & Kung C (1994) A large-conductance mechanosensitive channel in E. coli encoded by mscL alone. *Nature* **368**: 265-268

Suzuki H & Takeuchi S (2008) Microtechnologies for membrane protein studies. *Anal Bioanal Chem* **391**: 2695-2702

Tamm LK & McConnell HM (1985) Supported phospholipid bilayers. *Biophys J* **47**: 105-113

Tanaka M & Sackmann E (2005) Polymer-supported membranes as models of the cell surface. *Nature* **437**: 656-663

van den Bogaart G, Krasnikov V, & Poolman B (2007) Dual-color fluorescence-burst analysis to probe protein efflux through the mechanosensitive channel MscL. *Biophys J* **92**: 1233-1240

Venkatesan BM, Polans J, Comer J, Sridhar S, Wendell D, Aksimentiev A, & Bashir R (2011) Lipid bilayer coated Al(2)O(3) nanopore sensors: towards a hybrid biological solid-state nanopore. *Biomed Microdevices* **13**: 671-682

Wagner ML & Tamm LK (2000) Tethered polymer-supported planar lipid bilayers for reconstitution of integral membrane proteins: silane-polyethyleneglycol-lipid as a cushion and covalent linker. *Biophys J* **79**: 1400-1414

Wallin E & von Heijne G (1998) Genome-wide analysis of integral membrane proteins from eubacterial, archaean, and eukaryotic organisms. *Protein Sci* **7**: 1029-1038

Yildirim MA, Goh KI, Cusick ME, Barabasi AL, & Vidal M (2007) Drug-target network. *Nat Biotechnol* **25**: 1119-1126

Yoshimura K, Batiza A, & Kung C (2001) Chemically charging the pore constriction opens the mechanosensitive channel MscL. *Biophys J* **80**: 2198-2206

CHAPTER 6

Towards formation of biomimetic vesicles using GUVs

Ilja Kusters[2], Nobina Mukherjee[1], M. R. de Jong[3], S. Tans[4], Armağan Koçer[1], A.J.M. Driessen[2]

[1]Department of Membrane Enzymology,
[2]Department of Molecular Microbiology Groningen
Biomolecular Sciences and Biotechnology Institute,
Zernike Institute for Advanced Materials University of Groningen,
Groningen, The Netherlands
[3]BiOMaDe Technology Foundation, Groningen, The Netherlands
[4]AMOLF Institute, Amsterdam, The Netherlands

This chapter has been published as part of the *PLoS ONE* paper "Taming membranes: Functional immobilization of biological membrane in hydrogels" 2011, 6(5): e20435

ABSTRACT

In this study we aim to imitate how a living cell communicates with its environment. The encapsulation of the transcription and translation machineries in lipid vesicles and the synthesis of protein from DNA template within a liposomal container have been demonstrated before (Nomura, 2003; Ishikawa, 2004; Noireaux, 2004; Ota, 2009). One of the major components of a cell is the lipid bilayer embedded membrane proteins, which ensure proper communication of the cell with its environment. For instance the channel and transport proteins ensure controlled influx of nutrients and other molecules for growth, proliferation and survival. However, the designs of most of the present day artificial cells lack the functionality of controlled communication and solute fluxes across the cell membrane. So, our aim is to add a membrane protein, the mechanosensitive channel of large conductance (MscL) in an artificial cell as a possible solution for transmembrane communication and transport. Here, we show that MscL controls the influx of a dye molecule, calcein, into giant unilamellar vesicles (GUVs). The triggered opening of MscL is followed in real time. MscL-GUVs are trapped in hydrogels, composed of nano-scaled fibers, as a generally applicable tool to immobilize biological membrane vesicles. Importantly, MscL immobilized in the hydrogel is fully functional.

INTRODUCTION

A significant amount of research is dedicated towards bioinspired materials, functioning as a nano bioreactor, and enabling the entrapment of biomolecules like enzymes and nucleic acid (Meier, 2009). Vesicle encapsulation of biological macromolecules offers an alternative method for studying their function. The design of these vesicles is inspired by biological membranes which are ubiquitous in all living cells. This method of confining the biomolecules inside the vesicles provides a native environment compared to tethering of biomolecules by agarose gels, silicate glass, polyacrylamide etc (Cisse, 2007). The only caveat is that the lipid bilayer itself is impenetrable and acts as a barrier for solute exchange with the surroundings. In order to overcome this limitation, previously 1,2-Dimyristoyl-*sn*-Glycero-3-Phosphocholine (DMPC) was used for making the membrane porous (Cisse, 2007; Nourian, 2012). But the use of lipids for making transient pores in the membrane does not allow control over the system. So, inspiration is drawn from the cell membrane, which harbors a unique set of membrane proteins. These proteins play a crucial role in cellular and physiological processes such as nutrient transport, signaling, and energy-transduction. About 60% of the human druggable targets are membrane proteins (Bakheet, 2009). Thus, including membrane proteins in the design of artificial cells is essential. Previous studies have incorporated bacterial membrane proteins like α-hemolysin or OmpF in the vesicles (Okumus, 2009; Meier, 2009). Although insertion of these proteins was an elegant solution and could establish transmembrane transport, there was no real time control over the opening and closing of the channels. The mechanosensitive channel of large conductance (MscL) from *E. coli* has been engineered to allow real time control over transmembrane transport. MscL forms a 3nm wide non-selective pore in the fully open state and allows the passage of upto 6.5 kDa molecules (Cruickshank, 1997; van den Bogaart, 2007; Mika, 2012). In this section, we optimized the formation of giant unilamellar vesicles (GUVs), reconstituted with MscL and we achieved control over the influx of fluorescent dye, calcein, into the GUVs. A glycine residue at the 22nd position of MscL was converted to cysteine, such that a positively charged sulphahydryl reagent MTSET could be attached to the protein. Addition of charge in the pore of MscL led to the opening of channel (Yoshimura, 2001). This provided greater control over transmembrane fluxes of nutrients as compared to α-hemolysin, which is continuously open. We carried out a proof of concept study by tracking the influx of calcein into the GUVs via MscL by fluorescence microscopy.

To be able to follow the influx of dye into a particular vesicle, the vesicle has to remain in the observation area of a microscope for a substantial period of time, requiring immobilization of the entire vesicle. Immobilization of biological membranes without affecting their functionality is a major challenge due to the fragility of the lipid bilayer. Therefore, new immobilization techniques are needed to facilitate detailed investigations of membrane protein in cellular systems. Due to their big size (5-50 μm) GUVs have a low curvature and their membrane surface appears practically planar

in the observation area of a confocal microscope. In addition, transport processes across the membranes of these giant vesicles can be investigated by high-resolution fluorescence imaging. However, the same property, their large size, makes the surface immobilization of GUVs very challenging as they have a large area that can interact with the surface. In most cases direct attachment of GUVs to a surface via surface modifications results in rupture and collapse of the vesicles (Hamai, 2007).

In this study we present, hydrogels composed of organic gelators for the functional immobilization of membrane protein in synthetic lipid environments. Hydrogels composed of self-assembling units of low-molecular-weight gelators, based on 1,3,5-cyclohexyltricarboxamide, form networks of nano-scaled fibers that are an attractive way to immobilize membrane vesicles (Brizard, 2008) . The di-ethylene glycol functionalization of the gelator creates a low interacting fiber surface that minimizes surface interactions with biological molecules (Figure 1). Moreover, as fiber-fiber interactions are weak, the local mesh size of the gel is adjusted by the vesicles, allowing them to form their own cavity. Importantly, the vesicles are completely surrounded by an aqueous environment and the self-adapting mesh size of the gel allows the free diffusion of macromolecules such as proteins, yet restricts the movement of the membrane vesicle. The fibers of hydrogelators from the same family of gelators were previously shown to immobilize bilayer liposomes composed of zwitterionic synthetic lipids without interacting at the molecular level (Brizard, 2008). Here, we demonstrate that hydrogels based on 1,3,5-cyclohexyltricarboxamide effectively immobilize micron-sized GUVs composed of a synthetic lipid mixture. The integrity of the lipid bilayer of the different vesicles remains intact during the immobilization procedure. Importantly, the embedded membrane protein, MscL is fully active. Since these hydrogels are optically transparent, they allow fluorescent investigations of the activity of the membrane proteins and processes at the membrane interface.

MATERIALS AND METHODS

Hydrogels

Gelator 1 (Figure 1) was synthesized as described by Brizard et al. Preformed hydrogels were obtained by solubilising 1.3 % (w/v) gelator 1 in buffer (50 mM Hepes-KOH, pH 7.5, 30 mM KCl, and 2 mM MgCl2) by heating to 130°C using an oil bath. After cooling to <100°C, the hot suspension was aliquoted to 50µl and cooled down to room temperature (RT) upon which the gels formed. Incorporation and immobilization of GUV was achieved by adding one volume GUV containing buffer to one volume of hydrogel.

Formation of GUVs containing MscL channels

Phosphatidylcholine (DPhPC, 1,2-Diphytanoyl-sn-Glycero-3-Phosphocholine) and POPG (PG, 1-Palmitoyl-2-Oleoyl-sn-Glycero-3-[Phospho-rac-(1-glycerol)], Sodium salt) were

purchased from Avanti polar lipids. Cholesterol (3β-Hydroxy-5-cholestene, C27H46O) was obtained from Sigma. MTSET ([2-(trimethylammonio)ethyl]methanethiosulfonate and bio-beads (Bio-Beads SM-2 adsorbents) were from Anatrace and Bio-Rad Laboratories B.V., respectively. Giant unilamellar vesicles (5-20μm) were formed from PLs (150nm) by electroformation as described previously (Girard, 2004). Briefly, first MscL was reconstituted into DPhPC:POPG:cholesterol liposomes (70:25:5 weight ratio) by a detergent-mediated reconstitution method as described before(Kocer, 2007). The resulting proteoliposomes (PLs) were used to obtain a thin lipid film on the surface of conductive glass slides (ITO). Droplets of 2 μl containing 0.8 mg/ml PLs in 2 mM MOPS-Tris buffer pH 7.0 were applied to the glass surface, followed by overnight partial dehydration in a vacuum desiccator at 4 °C. After the PL film was obtained, an electroformation chamber was prepared in Nanion Vesicle Prep Pro (Nanion Technologies GmbH, Munich, Germany). The chamber was filled with 250mM sucrose. An AC voltage was applied for 4 hours across the cell unit with stepwise increases from 0.1 to 1.1 V at 12 kHz frequency. At the end, in order to detach the glass-bound giant unilamellar liposomes, the frequency was lowered to 4 kHz and the voltage raised to 2 V for 30 min. Vesicles formed in this way had a diameter of 10-15 μm. In order to image the GUVs, a fluorescent lipid analog DiD (650 nm/670 nm, excitation/emission) was added to the vesicles after they were formed. Calcein (497 nm/516 nm, excitation/emission) was used as an external dye for uptake by the GUVs.

Fluorescent measurements

Immobilized GUVs were imaged in a dual-color laser scanning confocal microscope (LSCM) that is described in details elsewhere (van den Bogaart, 2007; Arkowitz, 1993). The two laser beams (488 nm, argon ion laser; 633 nm, He-Ne laser) were aligned to a high degree of spatial overlap and moved simultaneously with a galvanometer optical scanner through the sample. Two confocal images (30 × 30 μm) of the blue and red fluorescence channels were recorded simultaneously. Hydrogel immobilized GUVs and calcein were imaged in a Confocor3 confocal microscope (Zeiss) using the 488 nm argon ion laser and the 633 nm He-Ne laser.

RESULTS

The membrane integrity of hydrogel immobilized GUVs is maintained

Hydrogelator molecules based on 1,3,5-cyclohexyltricarboxamide self-assemble into nano-scaled fibers that form a three-dimensional interpenetrating network with defined mesh size (Brizard, 2008). Here, we obtained hydrogels (Figure 1A) by cooling a hot solution of 1.3 % gelator 1 in buffer to room temperature. Immobilization of the GUV vesicles was achieved by short vortexing of the hydrogel suspension and then mixing the GUVs in a 1:1 ratio with the preformed gel. Subsequently, the gel with GUVs was applied onto a microscopic cover slip, followed by a resting phase in which

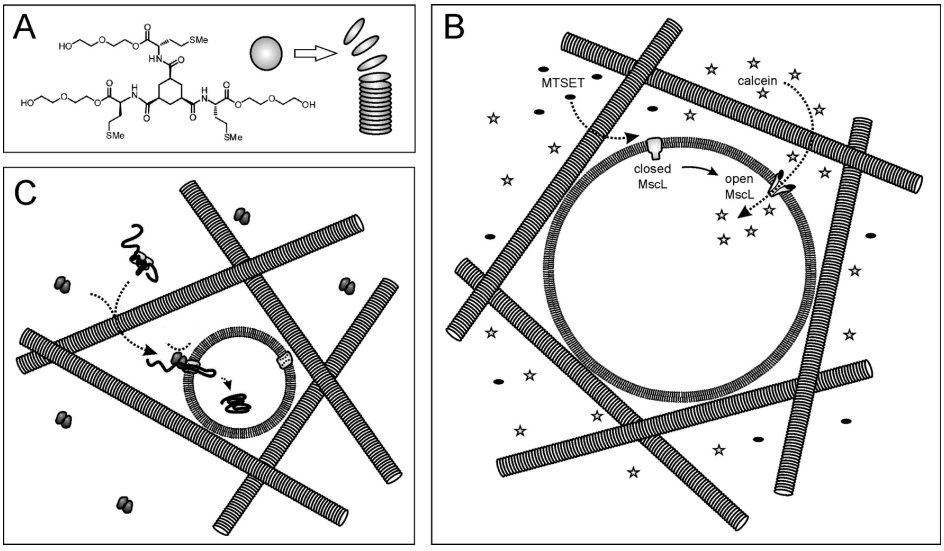

Figure 1. Hydrogels composed of self-assembling organic gelators immobilize membrane vesicles. (A) Gelator molecule 1 is based on 1,3,5-cyclohexyltricarboxamide and self-assembles into fibers of 20-100nm. (B) Schematic representation of a hydrogel immobilized GUV with embedded MscL channel. The lipid bilayer is impermeable for the soluble fluorophore calcein when MscL occupies the closed conformation. Addition of MTSET triggers the opening of genetically engineered MscL and allows influx of calcein into the lumen of the GUV. Molecules in (B) are not drawn in scale. (C) Schematic representation of hydrogel immobilization of Large Unilamellar Vesicle (LUVs).

the gel "heals", i.e. cross-links between fibers are re-formed leading to a network with incorporated liposomes. The immobilized vesicles were imaged in the gel using a dual-color laser-scanning confocal microscope. In contrast to the GUVs in suspension which moved while taking the image, the location of the GUVs in the hydrogel was entirely stable within the confocal plane (Figure 2 A). Moreover, the fluorescent signal of calcein entering the GUVs was clearly visible, due to the transparency of the hydrogel.

GUVs with inserted mechanosensitive channel of large conductance (MscL) can communicate with the environment in a controlled manner

To investigate whether MscL helps to establish communication across the bilayer membrane of the GUVs, we prepared several micron-sized GUVs and tested them for membrane integrity and membrane protein activity in the gel. The performance of a hydrogel as described in the previous section was tested for GUV immobilization and monitoring of membrane protein activity. The Loss-of-Function mutant of the mechanosensitive channel of large conductance, MscL-G22C, from *E. coli* was reconstituted into liposomes, and the resulting proteoliposomes (PL) were used to generate DiD-labelled GUVs (Girard, 2004). We activated MscL-G22C by labeling the

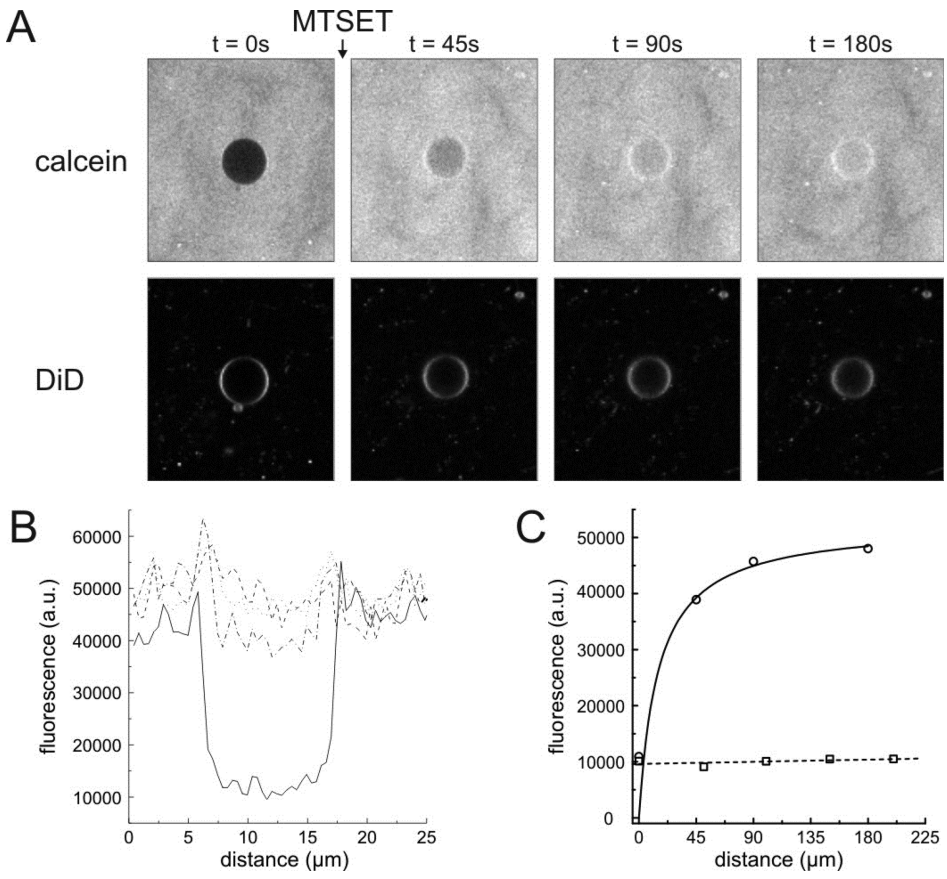

Figure 2. Opening of the MscL channel monitored on a single hydrogel-immobilized GUV, containing the fluorescent lipid analogue DiD. (A) Addition of MTSET to the top of the hydrogel causes opening of the membrane embedded MscL channel, whereupon the soluble fluorophore calcein diffuses into the lumen of the GUV. (B) Calcein fluorescence inside and outside of the GUV quantified by cross-sections through the center of the GUV depicted in (A) at different time points; t = 0s (straight line), 45s (dash-dot), 90s (dot), 180s (dash). (C) Calcein fluorescence at the center of the GUV (A) at the indicated time points (straight line). Background fluorescence inside a GUV (as shown in Fig 3) did not change upon addition of buffer (dashed line).

cysteine at position22 with the charged molecule MTSET. This covalent modification results in the opening and closing of the channel in the absence of its native trigger, i.e. membrane tension (Yoshimura, 2001; Sukharev, 1994). The performance of MscL, embedded in hydrogel immobilized GUVs, was tested by following the triggered influx of a fluorescent dye (calcein) into GUVs through MscL, using confocal microscopy. Due to their fragile nature, DiD-labelled GUVs containing MscL were embedded in a hydrogel of gelator 1 by first liquefying the preformed hydrogel by vortexing it for 1 min and mixing the hydrogel afterwards with 0.5 volume of GUVs at room temperature. This

mixture was applied onto a cover slip and incubated for about 10 minutes to ensure gel healing. The DiD-stained membrane of an approximately 10 μm-sized MscL-GUV was imaged by a two-dimensional scan using a dual-laser confocal microscope (Figure 2A, lower panel). Calcein is added to the hydrogel prior to imaging without disturbing the setup (Figure 2A, upper panel, first picture). Since MscL was not activated at this point, it stayed closed and calcein could not enter the GUV, demonstrating the membrane integrity, hence the dark interior of the GUV. Upon the addition of the membrane-impermeable channel activator, MTSET, the channel opened and the gradual, time-dependent filling up of the GUV was observed (Figure 2A-C). The concentration of calcein inside and outside of the GUV was quantified by analyzing a one-dimensional cross-section through the center of the GUV at the different time points, illustrating MscL channel opening (Figure 2B). Time-dependent influx of calcein into the GUV was quantified by measuring the calcein fluorescence at the center of the GUV resulting in a kinetic saturation curve (Figure 2C). Equilibration of the calcein concentration inside and outside of the GUV was reached after about 180 s (Figure 2C), in accordance with the results obtained with PLs in solution. As a control, buffer without MTSET was added to MscL GUVs in another gel (Figure 3). No influx of calcein into the GUV was observed (Figure 3A and 3B), demonstrating the stability of the GUV and the closed state of the MscL channel. Taken together, this data demonstrate that MscL, a mechanosensitive membrane protein, allows influx of small molecules into GUVs. Also, the MscL-GUVs are not affected by the hydrogel. This method of vesicle immobilization ensures membrane integrity even of fragile, micron-sized vesicles.

DISCUSSION

Our system offers a rational solution for both communication and compartmentalization in biomimetic vesicles. It provides tunability of pore openings and allows passage of cargo across the GUV membranes, which can be used to carry out biological or chemical reactions in a confined space. This simplified model will help us to address various biological processes, which in their native environment are challenging to study. Our results show that MscL facilitates influx of cargo inside the GUVs. On the other hand, when there are no channels inserted in the GUVs, the cargo cannot enter the vesicles. To follow a single GUV, the vesicle should be static. In solution the GUVs are usually mobile and it is very difficult to study the kinetics of influx of cargo. So, to immobilize GUVs, a new method employing hydrogels composed of self-assembling low molecular weight gelators was investigated. Here, we demonstrate that the nano-scaled fibers of hydrogels based on 1,3,5-cyclohexyltricarboxamide are efficiently immobilizing vesicles from synthetic lipid mixtures without disturbing the membrane integrity. This is evident as calcein is unable to penetrate hydrogel immobilized GUVs containing a closed MscL channel. In a previous study, the pore-

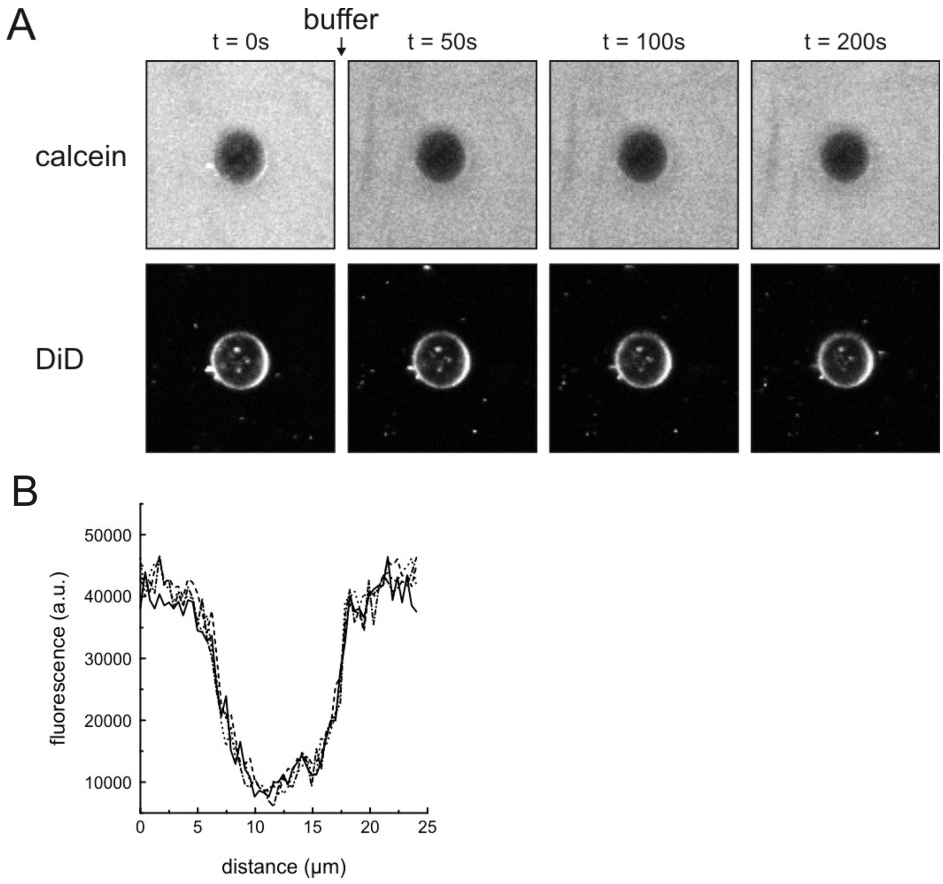

Figure 3. The MscL channel remains in its closed state in the absence of a trigger. A) MscL-containing and DiD-stained GUV at various time points after addition of buffer. B) Calcein fluorescence outside and inside the GUV was quantified by cross-sections through the center of the GUV depicted in A at different time points: t = 0s (straight line), 50s (dash-dot), 100s (dot), 200s (dash).

forming mechanism of the antimicrobial peptide melittin was studied by following the leakage of fluorescently-labelled glutathione from liposomes (Arkowitz, 1993) and leakage of fluorescently labelled size marker was used to estimate the pore size of the mechanosensitive channel MscL (van den Bogaart, 2007). Thus, if membrane integrity had been compromised during liposome or GUV immobilization, significant leakage would have been observed.

Hydrogels composed of nano-scaled fibers are a generally applicable immobilization tool for a wide range of native and synthetic membrane systems. Importantly, the biological activity of (folded) proteins in the gel is sustained and macromolecules can diffuse freely in the gel due to its large mesh size. The transparency of the hydrogel

allows the application of optical microscopy and processes at the membrane interface or within can be quantitatively assessed at the single vesicle and single molecule level.

The hydrogels presented in this study are inert to environmental factors such as pH, salts and temperature, allowing immobilization of membrane vesicles over a wide range of physiologically-relevant conditions. As the mesh size of the gel fibers is adjusted by the dimensions of the encapsulated particles, membrane vesicles of various sizes can be incorporated. Importantly, the biological activity of embedded membrane proteins in hydrogel immobilized membrane vesicles is preserved. Thus, the hydrogels are to a high degree biologically orthogonal. The fast and easy gel immobilization further allows high throughput sample preparation and single molecule measurements without time consuming surface preparations. Several strategies can be employed to incorporate molecules and vesicles in the gel. While small membrane vesicles and molecules can be vortexed with the gel, immobilization of fragile GUVs is accomplished by first liquefying the gel following by mild mixing with the GUV containing suspension. Furthermore, small molecules can diffuse uniformly throughout the gel. This is evident by the presented triggered opening of the MscL channel upon addition of the activator MTSET. Influx of the soluble fluorophore calcein into single GUVs was followed in time by confocal microscopy. Hydrogel immobilization of GUVs is possible and allows measurements without interference from surfaces, as molecules can diffuse freely in the gel.

CONCLUSION

In summary, the results show that a cargo can enter the GUVs through the channel protein, MscL, which is opened by an external trigger that is added *in situ*. The channel proteins embedded in the lipid vesicles are functional and they do not lose their functionality upon immobilization by hydrogels. Further, we show that when the trigger is absent but all the other conditions are identical, the channel remains tightly closed. In the future we aim to develop a minimal cell based on this system and utilize MscL for influx or efflux of candidate molecules.

REFERENCES

Arkowitz RA, Joly JC, & Wickner W (1993) Translocation can drive the unfolding of a preprotein domain. *EMBO J* 12: 243-253

Bakheet TM & Doig AJ (2009) Properties and identification of human protein drug targets. *Bioinformatics* 25: 451-457

Brizard A, Stuart M, van Bommel K, Friggeri A, de Jong M, & van Esch J (2008) Preparation of nanostructures by orthogonal self-assembly of hydrogelators and surfactants. *Angew Chem Int Ed Engl* 47: 2063-2066

Cisse I, Okumus B, Joo C, & Ha T (2007) Fueling protein DNA interactions inside porous nanocontainers. *Proc Natl Acad Sci U S A* 104: 12646-12650

Cruickshank CC, Minchin RF, Le Dain AC, & Martinac B (1997) Estimation of the Pore Size of the Large-Conductance Mechanosensitive Ion Channel of Escherichia coli. *Biophys J* 73: 1925-1931

Girard P, Pécréaux, J.Lenoir G, Falson P, Rigaud J-, & Bassereau P (2004) A new method for the reconstitution of membrane proteins into giant unilamellar vesicles. *Biophys J* 87: 419-429

Grzelakowski M, Onaca O, Rigler P, Kumar M, & Meier W (2009) Immobilized protein-polymer nanoreactors. *Small* 5: 2545-2548

Hamai C, Cremer PS, & Musser SM (2007) Single giant vesicle rupture events reveal multiple mechanisms of glass-supported bilayer formation. *Biophys J* 92: 1988-1999

Ishikawa K, Sato K, Shima Y, Urabe I, & Yomo T (2004) Expression of a cascading genetic network within liposomes. *FEBS Lett* 576: 387-390

Koçer A, Walko M, & Feringa BL (2007) Synthesis and utilization of reversible and irreversible light-activated nanovalves derived from the channel protein MscL. *Nat.Protoc.* 2: 1426-1437

Mika JT, Birkner JP, Poolman B, & Kocer A (2012) On the role of individual subunits in MscL gating: "All for one, one for all?" *FASEB J*

Noireaux V & Libchaber A (2004) A vesicle bioreactor as a step toward an artificial cell assembly. *Proc Natl Acad Sci U S A* 101: 17669-17674

Nomura SM, Tsumoto K, Hamada T, Akiyoshi K, Nakatani Y, & Yoshikawa K (2003) Gene expression within cell-sized lipid vesicles. *Chembiochem* 4: 1172-1175

Nourian Z, Roelofsen W, & Danelon C (2012) Triggered Gene Expression in Fed-Vesicle Microreactors with a Multifunctional Membrane. *Angewandte Chemie International Edition* 51: 3114-3118

Okumus B, Arslan S, Fengler SM, Myong S, & Ha T (2009) Single molecule nanocontainers made porous using a bacterial toxin. *J Am Chem Soc* 131: 14844-14849

Ota S, Yoshizawa S, & Takeuchi S (2009) Microfluidic formation of monodisperse, cell-sized, and unilamellar vesicles. *Angew Chem Int Ed Engl* 48: 6533-6537

Sukharev SI, Blount P, Martinac B, Blattner FR, & Kung C (1994) A large-conductance mechanosensitive channel in E. coli encoded by mscL alone. 368: 265-268

van den Bogaart G, Krasnikov V, & Poolman B (2007) Dual-color fluorescence-burst analysis to probe protein efflux through the mechanosensitive channel MscL. *Biophys J* 92: 1233-1240

Yoshimura K, Batiza A, & Kung C (2001) Chemically Charging the Pore Constriction Opens the Mechanosensitive Channel, MscL. *Biophys J* **80**: 2198-2206

CHAPTER 7

Summary and Future Perspectives
Nederlandse Samenvatting
Acknowledgement

Nobina Mukherjee

SUMMARY AND FUTURE PERSPECTIVE

"Equipped with his five senses, man explores the universe around him
and calls the adventure science."- E.P. Hubble

Using the five senses we have achieved tremendous breakthroughs in science but ironically very little is known about how some of these senses are actually sensed. For example, the molecular mechanism behind the sensation of touch and hearing still remains to be uncovered. The key elements behind these sensations are the mechanosensitive (MS) channels, which sense mechanical perturbations in the environment. These channels are stimulated through a process called mechanotransduction. Mechanotransduction is the mechanism of conversion of mechanical energy, exerted on the cellular membrane into electrical or chemical energy and is transduced via the conformational changes of a membrane protein. In order to unravel the underlying principle of stress sensation and mechanotransduction in the MS channels, firstly, there is a need to generate force in the membrane to activate the channel; secondly to follow in real-time the structural changes occurring in the protein in response to the activation; and lastly, to relate how these structural changes lead to mechanotransduction.

We have used a candidate MS channel, MscL, to find and characterize a suitable alternative trigger, other than mechanical stress, for channel activation. The ultimate aim is to subsequently utilize the channel for diverse applications such as drug delivery and sensing in a nanochip. MscL is an appropriate candidate as it is one of the best understood MS channels and is ubiquitously present in bacterial membranes. MscL plays an important role in bacterial osmoregulation. During hypoosmotic shock, there is a build-up of turgor, which exerts stress onto the membrane. Mechano-gated MscL responds to this stress through 'sensing' the tension in the membrane and opening the gate. This jettisons out solutes through a non selective pore of 30 to 40 Å and helps to lower the turgor pressure and prevent cell rupture.

This thesis aims to answer: "how can MscL be activated by non-natural triggers?" and "how can we use this extrinsically-activated channel for different applications?" Based on these questions, the thesis is broadly divided into two parts. In the first part, I present studies on the activation of MscL through the bilayer membrane and by chemically modifying the channel. In the second part, the modified channel has found application in a candidate drug delivery device and as a sensory module in a nanochip, and it has been used to study the influx of a dye molecule into lipid vesicles.

Converting a mechano-gated channel into a nano-valve

The motivation for the first part was to examine whether we could convert this mechano-gated channel into a nanovalve, whose gating could be triggered with precision by activators from the membrane and the protein-pore side.

In chapter 2, MscL is activated by interfering with its interaction with the lipid bilayer by inserting the inverted cone-shaped amphiphile, LPC asymmetrically into the lipid bilayer. The goal of this study was to find whether LPC, as an alternative trigger, is equivalent to and can replace tension in the membrane as an activator of MscL. This is necessary to know because conventional patch clamp methods allow application of tension but can only detect the passage of the ions through the channel and does not probe the initial structural changes in the protein. Spectroscopic techniques allow observation of the initial conformational changes that the protein undergoes during gating. Unlike, patch clamp, controlled generation of mechanical force in the membrane is not possible with current spectroscopic set ups. Hence, alternative triggers that can activate MS channel like MscL are needed. We characterized activation of MscL by LPC and concluded that, although LPC triggers MscL gating, the results are not totally comparable to tension-induced MscL gating. Previous studies and our study indicate that the initiation of the conformational changes in the channel and the sensitivity of the channel to different triggers are different. So, when we are replacing tension with other channel activators, care should be taken in the interpretation of how initial conformational changes lead to mechanotransduction.

In chapter 3, MscL is modified by attaching thiol reactive agent to the channel pore. The aim of this study was to gain fine-tuned control of MscL reconstituted in liposomes. This is possible by a two-step activation process. In this process, the secondary trigger primes the system for activation by the primary trigger. Here, the primary trigger is the ambient pH sensed by the pH modulator attached to MscL. Attaching an azide moiety to the pH modulator made it insensitive to pH, and the channel remained closed irrespective of the pH. Upon reaction of the azide group with triphenylphosphine (the secondary trigger), the amine version of the pH modulator is generated, which is sensitive to the ambient pH. Modified MscL thus became responsive to the ambient pH and the channel opened when the pH dropped below the pK_a of the modulator. Since all the molecules involved are bio-compatible, in the future this system could be translated to a drug delivery device, in which the release of drug at the target site can be properly controlled.

Utilization of extrinsically activated nano-valve for different applications

Not only is it necessary to learn about mechanotransduction but also to utilize nature's amazing 'portals' for innovative applications. Nature applied the channel proteins as portals to establish communication across the lipid bilayer. Taking a cue from nature, we made an effort to use MscL as a portal in systems where translocation of solutes and cargo is a prerequisite. For this purpose, MscL is converted into an extrinsically controlled nanovalve.

MscL was functionalized with a chemically modified pH-sensitive label and used in a liposomal drug delivery system, as described in chapter 4. The presence of MscL in the liposomes ensures that the portal will open and release the drug, only upon

reaching the target site. We converted MscL into a pH-actuated valve, because, in many disease conditions, the pH becomes acidic locally around the afflicted tissue, compared to the normal situation. Taking advantage of this phenotype, our aim was to design the delivery device such that it could sense the acidic ambient pH and release the drug at the target site, minimizing side-effects due to uptake of the drug by healthy tissue. The study showed that the engineered channel detects the low pH of the tumor microenvironment, and release the liposomal luminal content into implanted C6 glioma tumors in a mouse model. There was a good correlation between the amount of release of drug and the pH, i.e. lower the pH, the higher the release and *vice versa*.

In another application, MscL is used as a valve inserted in lipid bilayer, which compartmentalizes a nanocontainer in a chip platform. In chapter 5, the goal was to study multiple flux events in parallel, using the pore of MscL and the protein embedded in a suspended lipid bilayer. Here, we used a silicon-based chip containing 250,000 cylindrical cavities with well-defined apertures in the nanometer range, which are individually accessible for detection. Hundreds of import and export events through single MscL channel are recorded simultaneously via real-time detection of multi-spectral fluorescence signals. This nanochip platform combines highly parallel, semi-automated analysis and small sample consumption with ultra-high sensitivity at single-channel resolution. Based on these results we aim to optimize the system as a miniaturized high-throughput sensory device. In the future, this chip platform can be used to analyze and characterize other membrane channels and transporters. The semi-automated multiplexed setup, small sample consumption and high sensitivity provided by the system will improve the high throughput characterization of new pharmaceuticals against membrane proteins that serve as drug target. Apart from drug screening, the setup can be also used as a nanoreactor for bioengineered production processes.

Chapter 6 portrays an attempt to employ MscL as a nanovalve for loading of cargo in giant unilamellar vesicles (GUVs). The presence of MscL in the vesicles allows control over the influx of a model dye, calcein, into the GUVs. Our effort was to implement MscL in the design of biomimetic lipid vesicles to establish control over translocation of solutes and solvents across the lipid bilayer. Control over the efflux and influx of cargo through the nanovalve, into and out of lipid vesicles, can improve the existing design of a minimal artificial cell. In this chapter we also provide a solution to immobilize membrane proteins embedded in lipid vesicles in nanoscale hydrogel fibres. Hydrogels are ideal environment for the immobilization of membrane proteins as they can support a variety of biological membranes without inhibiting the functioning of the membrane-embedded proteins, and at the same time they allow single molecule fluorescence measurements. Having, all the tools in place, in the future we may be able to design an artificial cell with encapsulated genetic material, where the influx and efflux of molecules will occur through MscL.

Perspectives

This thesis was an endeavour to characterize non-natural triggers of the mechanosensitive channel MscL and to apply the extrinsically-gated nano-valve for controlling solute fluxes across the lipid bilayer. Through our work, we have gained insight into how a non-natural trigger can activate MscL. Combining this knowledge with sophisticated techniques like EPR and patch clamp, we can get closer to answering the question: how mechanosensitive channels 'sense' mechanical stress in the membrane. And whether there is a unifying principle for sensing mechanical stress in mechanosensitive channels.

Based on the large body of fundamental research done on MscL, we could find sufficient scope for utilizing the protein in micro-/nano-devices. Engineering of MscL into an extrinsically-controlled nanovalve makes it possible to tune the permeability of closed vesicular systems. Through our work, we could substantiate that MscL can be converted into a sensory response element that controls the influx or efflux of cargo into different micro/nano compartments. The findings outlined in this thesis will possibly contribute towards the advancement of liposomal delivery systems by streamlining the side-effects and enhancing the therapeutic effectiveness of drugs. It will also have an impact on the design of high throughput nanochip platform for screening of drugs or the creation of artificial cells.

Nature has provided a repertoire of solutions to address some of the scientific problems that we face. Sometimes instead of inventing a 'novel' idea, it can be more effective to get inspiration from nature.

"Look deep into nature, and then you will understand everything better."
- Albert Einstein

NEDERLANDSE SAMENVATTING

Wij wetenschappers worden voortdurend geïnspireerd door de natuur om ons heen. De enorme hoeveelheden aan informatie die de natuur ons brengt wekt regelmatig verbazing en enthousiasme op. Overal maken we gebruik van vondsten uit de natuur voor vele wetenschappelijke toepassingen.

Ons onderzoek laat zich ook inspereren door de natuur. Veel mensen om me heen en ik zelfs richten hun interesse daarbij voornamelijk op bacteriën. Bacteriën zijn eencellige organismen, heel goed aangepast aan rare levensomstandigheden, maar net zoals de mens volgen ook bacteriën de fundamentele levensprocessen zoals beweging, groei, reproductie, consumptie, en uitscheiding. Daarnaast hebben ook bacteriën te maken met een vijandige omgeving. En dat begint heel simpel, nemen wij bijvoorbeeld regen: bij regen vind vochtophoping plaats, en vochtophoging leidt ertoe dat de bacteriën opzwellen. Als bacteriën te veel zwellen zullen ze barsten en sterven. De druk die bij het zwellen ontstaat wordt turgor genoemd, het barsten heet ook wel lyses. Maar als elke keer dat het regent alle bacterien barsten, dat zit de wereld dik in de problemen. Om dit te voorkomen heeft de evolutie de bacterien die de toename in turgor en lysis met behulp van speciale eiwitten/kanalen wisten te ontsnappen laten doorgroeien. Deze portwachters regelen de druk en transport van moleculen welke de bacterie in- en uitgaan. Deze eiwitten/kanalen bevinden zich in membraan van de bacteriën. Dit is de buitenste laag van de bacteriën, welke bestaat uit vele kleine gerangschikte vetmoleculen. Deze vetmoleculen worden ook wel lipiden genoemd. Als de druk/turgor binnen in de cel toeneemt, laten de kanalen

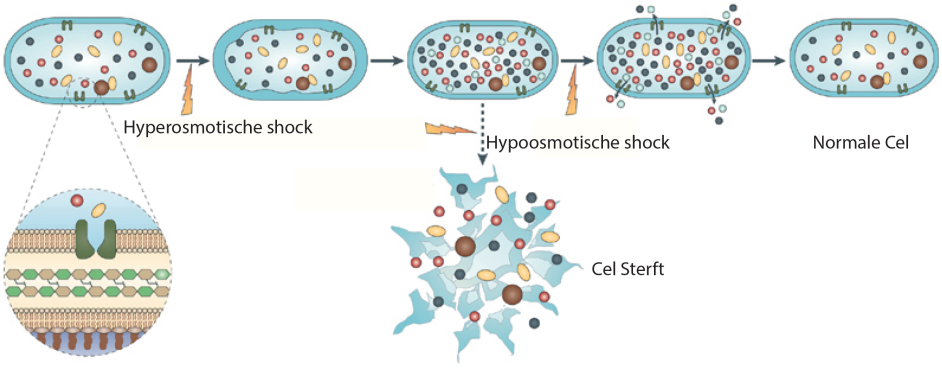

Figuur 1. Bij hyperosmotische schok verliezen cellen water en krimpen. Ze herstellen volledig door de accumulatie van opgeloste stoffen (licht blauwe cirkels). Verdunning van de cellen in een omgeving met lage osmolariteit (hypo-osmotische shock) leidt tot de snelle intrede van water samen met de onmiddellijke activering van het MS kanalen, wat resulteert in het verlies van zouten maar het behoud van grote eiwitten en opgeloste stoffen (bruine cirkels en ovalen geel). Indien de kanalen afwezig of niet openen, genereert de instroom van water een hoge turgor, wat leidt tot de lysis van de cel wanneer de druk boven de mechanische sterkte van de celwand komt. Aangepast van Booth *et al.*, 2007: Mechanosensitive channels in bacteria: signs of closure? *Nat Rev Microbiol* 5: 431-440.

zouten los vanuit de bacterie, hierdoor wordt de druk op het membraam minder en zal de bacterie overleven. Kanalen (Figuur 1) die gevoelig zijn voor druk en kracht rondom en in het lipide membraan, heten mechanosensitive kanalen.

Deze familie van mechanosensitive kanalen voelen de kracht en spanning in het lipide membraan en vormen de portalen voor communicatie binnen en buiten de cel. Niet alleen bacteriën, maar (vrijwel) alle andere organismen, inclusief de mens hebben deze stress gevoelige kanalen. In ons zijn ze betrokken bij het tast, gehoor, in zenuwstelsel en regulatie van de bloeddruk.

Verhaal van een poortwachter

In dit proefschrift gebruiken we één van de mechanosensitive kanalen van bacteriën, genaamd mechanosensitive channel of large conductance (MscL). De doelstellingen van dit proefschrift zijn het zoeken naar manieren om kanalen op een gecontroleerde manier te activeren, met het oog op toepassingen zoals de toediening van medicijnen op nano niveau.

Om MscL te gebruiken als kanaal of nanopoort moeten we eerst MscL van buiten af kunnen openen of sluiten met behulp van activatiesignalen. Hetzij door middel van omringende lipiden, anderzijds door gebruik te maken van een molecuul gekopeld aan het eiwit MscL als activatiesleutels . Deze activatie sleutels zijn moleculen die reageren in een selectieve omgeving en vervolgens het kanaal kunnen openen.

In hoofdstuk 2 hebben we geprobeerd om de lipide omgeving van MscL te veranderen om opening van het kanaal te bewerkstellingen. De lipiden membraan bestaat uit een binnen- en buitenlaag van lipiden. Deze twee lagen liggen boven op elkaar met de hydrofobe (waterschuwe) staarten van elke laag naar elkaar toe gericht. De hydrofiele koppen richten zich naar buiten tot de binnenkant van de twee lagen. Door genoeg speciale lipide (LPC) met één staart en kegelachtige vorm in te brengen in de buitenste laag van het membraan kunnen we stress creëren die wordt gedecteerd door MscL, welke als gevolg hiervan opent.

Vervolgens hebben we onderzocht of we kanalen kunnen laten openen door de zuurgraad te veranderen (Hoofdstuk 3). Hiervoor hebben we een mutatie moeten toepassen op MscL om de juiste activatiesleutel te kunnen bevestigen. De gevoeligheid van MscL op de pH concentratie kan worden gecontroleerd door het toevoegen van extra groepen aan de activatiesleutel en/of veranderen van chemische moleculen van de activatie sleutel. Hoofdstuk 4 wordt gebruik gemaakt van deze pH gevoelige activatie van MscL bij de toediening van medicijnen op nano niveau (als “drug delivery agent”).

Bij veel aandoeningen zoals kanker en ontstekingen worden lactaten geproduceerd, dit komt voornamelijk door een te hoge stofwisselingsactiviteit en glycolyse. Als gevolg verlaagt de pH van de omgeving op deze plaatsen ten opzichte van de rest van het lichaam. Ons doel is om gebruik te maken van de pH eigenschappen van deze

aandoeningen en ons kanaal dusdanig te ontwerpen dat deze niet opent wanneer het zich in fysiologische (normale) pH van het lichaam bevind, maar wel op plaatsen die zijn betroffen door de ziekte. Hierdoor zijn we in staat om onnodige bijwerkingen zoveel mogelijk te voorkomen en de effectiviteit van de behandeling te verbeteren.

Met dit als doel hebben we besloten om het pH-gevoelige MscL te gebruiken in een drug vehikel genoemd liposomen. (Figuur 2) Hierbij wordt pH-gevoelige MscL ingebracht in de lipiden bilaag van de liposomen. Om deze liposomen te volgen zijn ze gevuld met een kleurstof. De pH-gevoelige liposomen zijn getest op muizen met een hersentumor. De regio waar de tumoren zich bevinden bevatten een lagere pH, en uit de beelden is duidelijk waarneembaar dat hoe lager de pH des te meer kleurstof wordt afgegeven door de liposomen. Als controle groep hebben wij liposomen getest op deze muizen welke niet pH-gevoelig zijn. In dit geval is geen afgifte van kleurstof te zien in en rondom de tumor. In de toekomst zal deze methode veel belovend zijn voor doelgerichte therapie en het gericht toedienen van geneesmiddelen.

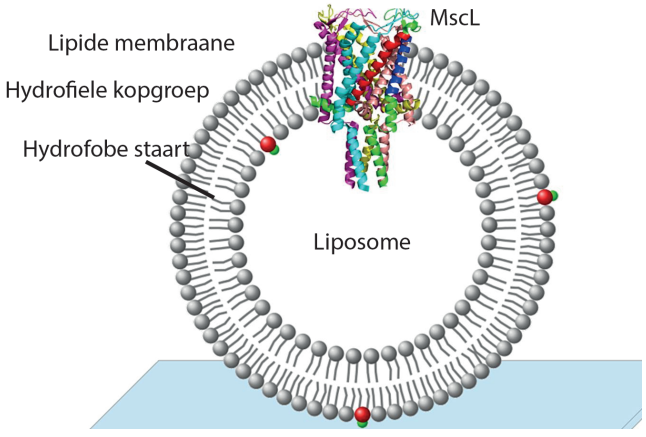

Figuur 2. Liposoom met een MscL kanaal. Het bestaat uit twee lipiden lagen (bilaag) met de lipide kopgroepen van elke laag naar buiten en lipide staarten naar binnen.

Zo zijn wij, geïnspireerd door de natuur, van een klein kanaaltje dat een cel gebruikt om in een drukke situatie niet te barsten, tot een ingenieuze methode gekomen om medicijnen specifiek op de juiste plek te brengen. Dit zou in de toekomst de kwaliteit van het leven weer een stukje verbeteren als men getroffen is door een ernstige aandoening en geneesmiddelen benodigd die eigenlijk niet goed zijn voor onze eigen lichaam, zoals bijvoorbeeld een chemotherapie bij kanker.

In hoofdstuk 5 gebruikten we nog een keer een aangepast variant van MscL. Nu hebben wij MscL dusdanig met een chemische groep verandert, dat het kanaal opent na

toevoeging van een chemisch middel MTSET in plaats van detectie van de pH. Deze chemisch gemodificeerde variant van MscL werd in liposomen gebruikt op een silicium nano-chip. De silicium nano-chip heeft talloze holtes. De liposomen binden nu aan de chip en sluiten de holtes af, zo dat volledig geïsoleerd compartimenten met ongeveer een femtoliter inhoud ontstaan. Uitwisseling van opgeloste stoffen en oplosmiddelen in de compartimenten kan alleen gebeuren door het openen van MscL.

Dit systeem maakt kans voor zeer belangrijke toepassingen, zoals screening van drugs of geneesmiddelen die werken op deze kanalen. 60% van de medicijnen die wij vandaag slikken zij gericht op het beïnvloeden van kanalen en andere eiwitten in biomembranen. Een chip, zoals de nano-chip door ons gebruikt, heeft 250.000 holtes. Dat betekend, dat je makkelijk verschillende geneesmiddelen tegelijkertijd kunt testen. Daardoor versnelt men de karakterisering van kandidaat geneesmiddelen en dat helpt enorm bij de ontwikkeling van nieuwe geneesmiddelen.

De hierboven beschreven liposomen hebben een doorsnee van ongeveer 150 nm, ongeveer honderd keer kleiner dan de giant unilamellar vesicles (GUVs) welke ca. 15 tot 50 μm in diameter zijn. In hoofdstuk 6 is het chemisch gemodificeerde MscL bestudeerd in GUVs, dus grotere bolletjes. In dit hoofdstuk hebben wij het geleidelijke vullen van de GUVs met een kleurstof via de MscLs gevisualiseerd. In de natuur wordt MscL alleen gebruikt om stoffen van binnen de cel kwijt te raken, maar wij hebben het nu zo onder controle, dat we het ook andersom kunnen gebruiken, dus de passage van opgeloste stoffen en oplosmiddelen in de GUVs kan worden geregeld via de activering van MscL. GUVs zijn groot genoeg om genetisch materiaal te bevatten en kunnen functioneren als een soort minimale cel. Als men GUVs als minimale cel gebruikt, dan hebben zij tegenover de klassieke omgeving, namelijk reageerbuizen wel een grote voordeel, zij lijken veel beter op een levende cel dan het reageerbuisje. Na de juiste optimalisering, dan zou dit systeem een goed alternatief bieden voor de studie van vele fundamentele biologische processen.

Het middenpunt van alle studies hierboven vermeld is een bacteriële kanaal eiwit, MscL. Het is verbazingwekkend om te zien hoe een natuurlijk eiwit kan worden aangepast en gebruikt kan worden in verschillende toepassingen. Maar wat je ook doet, in alle gevallen blijft zijn functie hetzelfde, namelijk van een kanaal, die toegang biedt tot communicatie tussen beide zijden van een lipide membraan. Vergelijkbaar met een poortwachter die bij de ingang van een huis staat en ervoor zorgt dat alleen de juiste mensen op het juiste moment het huis in en uit kunnen lopen.

THANK YOU FOR BEING A PART OF THIS JOURNEY

Groningen, March 2014

Few years ago I started as a PhD student. It turned out to be life's experience taught by a small protein. Words cannot summarize the days spent in the lab with my fellow scientists and friends, the joy when something worked out for the first time, the hope for good results and the sadness and tiredness of each failed attempt.

This thesis is a testimony to the labour of love and passion. In this journey, many people have contributed, personally and professionally. I cannot find a better way of thanking all, than to dedicate this thesis as a humble gesture of gratitude. If you have experienced the trials and tribulations of science, this thesis is an ode of thanks to you.

I would like to start off with my co-promoter. Dear *Armagan*, this book is as much yours as it is mine. You have infused in me the passion for the 'small protein' MscL. It has been an absolute pleasure to be a part of your young and dynamic group. The out-of-the-box ideas have given me a new perspective to science. The interdisciplinary projects that we have undertaken have helped me to grow as a scientist. Your smile and enthusiasm is infectious. Thank you for being a very supportive and innovative mentor.

Bert, thank you for accepting me in your group. It all started way back as a master's project. I fell in love with the stimulating environment of the group and never left it after that (until now!). I am amazed how you recall all the literature from different fields, so effortlessly. And, of course the famous calculations on a piece of paper.

I extend my heartfelt thanks to the members of the reading committee, *Prof. Sebastian Cerdan*, *Prof. Adriaan J. Minnaard* and *Prof. Siewert-Jan Marrink* for offering thorough and excellent feedback on the thesis. *Prof. Cerdan,* thank you for accepting to be a part of the defense committee. Also, I would like to thank you and *Jesus* for the wonderful collaboration, which has resulted in a chapter in this thesis.

Collaborations are important in science and have played an important part in this thesis. I am thankful to all my collaborators- *George Robillard, Marc Robillard, Siewert-Jan, Helgi, Clement, Robert Tampe, Alexander Kleefen, Michael Urban, Ilja, Menno, Sander Tans, A.J.M. Driessen*.

Dirk-Jan, Liesbeth, Fabrizia, Eric Geertsma for your scientific acumen and constructive discussions in the meetings. I was really lucky to have Eric as my supervisor for my master's project.

Jan Peter, my unofficial first supervisor in PhD. Thank you for welcoming me at the start of my PhD and taking me under your wings when Armagan was on leave. You were a year old PhD student then but you gave an impression of a senior post-doc! I remember how we grew a 10 L fermentor in the first week and I was breaking cells till 9 p.m. Thank you for your comic reliefs and being the comedian of our lab. On a serious note, I have always appreciated the thoroughness of your work. For example, I was

really impressed by your MscL-diary/dictionary. Also on the last day of my PhD, I will be proud to have you by side (but no more growing fermentor).

Randy, thank you for everything. You are an amazing person and I am inspired by your principles (even if sometimes they are self-effacing). Yes, I remember, the first time we met in the lift! Then there were long discussion about politics, science, philosophy, music. I never expected you to play piano so well. And, your amazing culinary skill was a big surprise to me. Getting to know you has been a pleasure for me. You have taught me to break out of my comfort zone and reach out, as only 'sky is the limit'. Thanks for the amazing trips we made; seeing nature through your eyes have enriched me. Thank you for all your support. You should go ahead with your idea about 'Science Int' website. We need something like that in science. Thank you for the amazing cover art of the thesis and the background designs of the posters. I am honored to have you as my paranymph.

Pranav, my dearest friend and closest colleague. I cannot even imagine that we are graduating on the same day. Congrats, we made it! It felt safe to be in the same boat with you- you were the boatman cum anchor. To you I could vent out my frustrations, especially in the last year of PhD. Those afternoon coffee breaks were therapy sessions for me. Your support-I cannot put in words how much it meant to me. And, thanks for the Gran Canaria trip. It was one of the most amazing trips. After you went to Amsterdam, I almost do not have afternoon coffee anymore. Wish you success in life and career. By the way, when you launch your company, do consider me also.

MscL group members (present and former): *Jan Peter, Mac Donald, Erik, Martin, Anna, Helgi* and *Duygu*. The first thing that comes to my mind is the Monday morning sub-group meetings, where all of us would be done in thirty minutes, while Jan Peter and Anna will take up the rest of the morning till lunch-time. Though, the meetings were very helpful in getting good feedbacks, exchanging ideas, designing new projects. I learned a lot from our insightful and detailed discussions. *Martin*, you are an inspiration to me. *Mac Donald*, thanks for the discussion and inputs for the LPC manuscript. Your hard work and dedication is exemplary. Wish you the best for your PhD. *Duygu* it seems that you started yesterday, now you are almost at the end. Wish you the best with your collaborations and a wonderful PhD. Jan Peter, Mac Donald, Helgi, Anna, Martin- thanks for your contribution to LPC project, we could make a nice story.

'Poolman Group' members (former and present): I thank all the lab members for their support and making my stay in this group memorable.

Ria and *Gea,* thanks for all the support in the lab and in the office. You have a great responsibility of keeping the lab up and running.

Siva, Ronnie, Josy, Andreja, Adeline, Ravi, Jacek, Tejas, Geert, Guus, Akira, Anne, Inga- You were a great bunch and since you all left, it is like a change of an era.

Jeanette, I know you since almost my first days here. We have shared so many ups and downs together, that I have lost count. I followed you to 'Poolman lab' and then we started PhD

together. You were also my officemate, all these years. This office feels different without you and I miss you. Hope to be here during your defense. Wish you, Cesar and Andre all the best.

Nadia, over the years you become one of the closest friends in the group. Your hard work and patience is an example to me. I expect a great career and life for you, Tanweer and Hunain.

My office-mates: *Ria, Rianne, Joury*, you provided me a perfect environment for writing. Rianne, thanks for your inputs to Dutch Summary.

The "yeast team" consists of fun loving people with a red couch in the office-*Gemma, Dusan, Frans, Stephanie* and *Ryan* (newest person in lab and have inherited my lab-space). *Gemma,* Bio-Business Summer School was a great week. I will not forget that Thursday evening. Thanks for all the brownies and tortilla-de-patatas. Wish you and *Edu* best in Amsterdam. *Dusan,* as I told you- Dusan is an idea. *Frans*, thanks for occupying the whole bench with your flasks and stuff. You have been a great bench-mate.

The "ECF group": *Marysia*, *Dorith, Raj, Sonja, Lotteke, Michael, Albert, Katja, Wieronika. Marysia*, we started PhD around the same time and it was a great journey for you. You really believe that "the kitchen is a laboratory" and it reflects in both. *Raj*, thanks for the instant dinners and wish you all the best with the crystal structure. *Dorith*, thanks for the coffee corner talks and help with 'feuerzangenbowle', wish you good luck with job search. *Sonja* and *Lotteke*, the wall of your office will be full of solved structures by the time you leave!

All the other members: *Faizah, Arnold, Jonas, Ruslan, Paul, Giorgios, Franz, Boqun, Hallie*. *Faizah* you have tremendous perseverance and will have great results for it. Wish you the best for PhD. *Arnold*, your motivation for science is impressive. Thanks for the tips about UK. Looking forward to joining your former lab.

Lastly, the 'ERIBA team': *Anton, Justyna, Astri, Petra, Annemarie*. *Anton*, we still miss you here. I was proud to inherit your lab-bench. *Justyna*, you are fun-loving person and we made quite good "Gemma clones"; good luck with finishing your PhD. *Astri*, *Annemarie* and *Petra* wish you good luck too.

I am grateful to all the administrative staff, *Karlien, Durkje, Margriet* for practical support throughout my PhD.

My life outside the lab in Groningen cannot be complete without my family and friends. *Vaishali* (the really better half of Pranav), I have seen all the shades of emotion in our friendship. Ours is a time-tested one, thanks to the 'bridge'. I count on you. You will have a great PhD defense. *Dipayan*, thanks to GISA we got to know each other. Your easy-going, calm and composed nature really soothed me, when I was in hyper states. You have been a great friend. You should write a recipe book someday. *Hansie*, you have been an inspiration. Wish you and *Sangeeta* the best. *Vinod*, I had a great time in the lab course that you supervised. You opened up my horizons. Thanks to you I applied and got a call for interview from ETH. You and *Kalyani* make a perfect couple. Wish your family all the happiness. *Samta*, you are another person, I look up to. It was great interacting with you

and *Ilja*. Wish you both a bright future in Boston. *Vinay* and *Anil*, thanks for all the help during the initial years. *Gaurav, Subir* and *Saurabh*, it was great knowing you guys. We had an amazing time during the badminton practice sessions. Wish you all the best in life. *Tamalika* di, you will always be a source of inspiration. *Arpita* you are the champion. You deserve the best in life. Thanks for your friendship. Wish you and *Bedabrata*, all the best. As a member of Groningen Indian Student Association (GISA), I learned a lot and had an opportunity to meet many nice people. Among them I would like to mention, *Ashish, Reema, Suresh babu, Vineet, Nilesh, Ekta, Tiziana, Andrea, Matea, Milon*.

Hanneke, thanks for all the care, support and advice. You are a wonderful mother. Wish you peace and happiness in life. *Linh*, my first roomie in Groningen. We have shared some funny, crazy moments of our student life. After we graduated, we became busy with our lives but the bond is still there. I always will treasure your friendship. Thanks. *Fred*, after our first meeting, I never expected to be friends with you. But now I am happy that it happened. *Tlu* and *Shiela*, you know how special you are! *Vineet,* a friend from school with whom I have never lost contact. Thanks for coming here for my defense. Talking to you is always a journey down the memory lane. I cherish those moments of fun and laughter.

Last but not the least, I convey my gratitude to my family and cousins here: thank you for your endless support. *Wieska jethima*, you were a wonderful and very helpful person. *Tante Fook*, thank you for all the help and support. *Ulco* and *Hendrike*, thank you for all the paper works and support in the difficult days. Thank you for letting me stay at your place. Wish you both, *Hanna* and *Heleen*, lots of happiness. A special thanks to *Anneke* did*i* and her family, *Rani* didi and her family, *Mon*i didi and her family.

Finally, my family back home in India, my rock and anchor of my life. *Baba, Ma, Pallavi* (my sister) - thank you for your love, support, and unwavering faith in me. Without you, I would not be the person I am today. I am eternally grateful for your encouragement and belief in me, even when I doubted myself. You are the biggest of all my strengths. Baba and Ma, I cannot thank enough for the opportunities that you have given me and for always being there. I am very fortunate to have parents like you, who are supportive and motivating in equal measures. Thank you for helping me and my sister to take baby step in science. I wish I could relive the moments when we discussed science. My grandmother, thanks for your unconditional love. I admire the determination in you. *Jethima* I cannot tell you, how lucky I feel to have your love and affection. Both my grandfathers would have been happy to see me graduate. I am proud that through my parents, I could inherit some of their values in life.

As my journey comes to an end, I want to share few things I have learned during these years. These years have taught me how to think. Finding imaginative solution to a problem is a step towards realizing it. We should have the courage to imagine and dream- nothing is absurd. With this, I am ready to dive into the exciting ocean of science.

- Nobina